

EUROGRAPHICS 2001

Simulation of Light Interaction with Plants

Tutorial Notes

by

Gladimir V. G. Baranoski

Jon G. Rokne

September 2001

Contents

Abstract	9
1 Introduction	11
2 Selected Topics on Physically-Based Rendering	15
2.1 Optics Concepts	15
2.2 Radiometric Terms and Properties	18
2.3 Absorption in a Homogeneous Medium	20
2.4 Rendering Equation	21
2.5 Monte Carlo Techniques for Directional Sampling	22
2.5.1 Importance Sampling and Warping Transformations	23
2.5.2 Probability Density Functions	23
2.5.3 Warping Functions	25
3 Measurement Procedures	29
3.1 Virtual Spectrophotometry	30
3.1.1 Characteristics of Actual Spectrophotometers	30
3.1.2 Formulation of Virtual Spectrophotometers	31
3.2 Virtual Goniophotometry	32
3.2.1 Characteristics of Actual Goniophotometers	32
3.2.2 Formulation of Virtual Goniophotometers	33
4 Biological Issues	35
4.1 Structural Description of a Plant Leaf	35
4.2 Factors Affecting the Propagation of Light	36
4.2.1 Internal Structure and Thickness	36
4.2.2 Surface Features	37
4.2.3 Pigments Composition, Concentration and Distribution	37
4.2.4 Water Content	38
4.3 Scattering Profile of Plant Leaves	38
5 Review of Models for Botany and Remote Sensing Applications	41
5.1 Plate Models	41
5.2 K-M Theory Based Models	42
5.3 Ray Tracing Based Models	43
5.4 Radiative Transfer Theory Based Models	44
6 The H-K Multiple-Layer Scattering Model	47
6.1 Overview	47
6.2 Scattering Simulation	47
6.3 Evaluation and Implementation Issues	48
6.4 Strengths and Limitations	49

7	The Algorithmic Reflectance and Scattering Model	51
7.1	Overview	51
7.2	Scattering Simulation	52
7.3	Absorption Simulation	54
7.4	Implementation Issues and Summary of Parameters	55
7.5	Evaluation Issues	56
7.6	Strengths and Limitations	57
8	The Foliar Scattering Model	61
8.1	Overview	61
8.2	Scattering Simulation	61
8.3	Implementation Issues and Summary of Parameters	62
8.4	Evaluation Issues	63
8.5	Strengths and Limitations	66
9	What Next?	71
9.1	Accuracy Issues	71
9.1.1	Surface Reflectance	71
9.1.2	Anisotropy	71
9.1.3	Geometrical Representation of Veins	72
9.1.4	Environmental Factors	72
9.1.5	Spectral Dependency	72
9.1.6	Wave Optics Phenomena	73
9.2	Efficiency Issues	73
9.3	Extensions	73
9.3.1	Simulation of Senescence	73
9.3.2	Scattering Profile of Petals and Stems	73
9.3.3	Near-Infrared and Infrared Applications	73
9.4	Radiative Transfer in Regions of Vegetation	74
10	Conclusion	77
	References	78

List of Tables

7.1	Parameters used in the testing of the <i>ABM</i>	57
7.2	Chromaticity coordinates and wavelength values.	60
8.1	Comparison of accuracy vs. performance gain.	67

List of Figures

2.1	Geometry for light incident at an interface between different materials.	16
2.2	Reciprocity of the BDF.	19
2.3	Loss of light at wavelength λ in a medium of thickness h	21
2.4	Geometry for computing L_p as an integral over all the surfaces within the environment.	22
2.5	Geometry for computing L_p in terms of all directions visible to a point x	22
3.1	Sketch of a virtual spectrophotometer.	31
3.2	Sketch of a goniophotometer (redrawn from [88]).	33
4.1	Typical cross-section of foliar tissues.	35
4.2	Artist’s conception of a typical epidermis tissue. Redrawn from [10].	36
4.3	Photographs of venation systems of different plant leaves. On the left the parallel venation system of a <i>hosta</i> leaf, and, on the right a reticulate venation system of a <i>magnolia</i> leaf. Redrawn from [26].	37
4.4	Photograph of soybean leaves showing the three components of the BDF of foliar tissues: surface reflectance, subsurface reflectance and transmittance.	38
4.5	Curves of reflectance and transmittance of a soybean leaf obtained using the ABM (Chapter 7) at a wavelength of $550nm$ and considering the front (adaxial epidermis) of the leaf towards the light source.	39
4.6	Photograph of soybean leaves showing the reflectance differences between the adaxial and abaxial surfaces.	39
5.1	Sketch of the geometry used by the “plate model”.	41
5.2	Sketch of the geometry used by the “generalized plate model”.	42
5.3	Four flux approach used by the <i>SAIL</i> model.	43
5.4	Three-dimensional model of the internal cellular structure of various leaf tissues used by <i>Raytran</i> . Redrawn from [86].	44
5.5	Sketch of the geometry used by the model proposed by Ma <i>et al.</i> [104].	45
6.1	Sketch of the scattering geometry used in the <i>H-K</i> multiple-layer model.	48
6.2	Leaf model used by Hanrahan and Krueger. On the left is the albedo image, and on the right is a thickness image in which white indicates increased thickness. Redrawn from [75].	49
6.3	Images of a cluster of leaves under different lighting conditions which were generated using the <i>H-K</i> multiple-layer model. Back lit images on the left, and front lit images on the right. Redrawn from [75].	49
7.1	Interfaces and tissues considered by the <i>ABM</i>	52
7.2	Perturbations performed by the <i>ABM</i> on the rays distributions at the four interfaces in the upwards and downwards directions of propagation considering the adaxial surface on the top and the abaxial surface on the bottom. a) Interface 1. b) Interface 2. c) Interface 3. d) Interface 4.	53
7.3	<i>Mesophyll loop</i> . a) Ray coming from outside interacts with interface 1. b) Refracted ray from interface 1 interacts with interface 2. c) Reflected ray from interface 2 interacts with interface 1. d) Ray coming from interface 3 interacts with interface 2.	54
7.4	Absorption spectra of chlorophylls $a + b$ used in the testing of the <i>ABM</i>	57

7.5	Comparison of spectral curves of a soybean leaf computed with the <i>ABM</i> with measured spectral curves provided by <i>LOPEX</i> , for an angle of incidence of 8° and 10^6 rays. a) Absolute spectral reflectance. b) Absolute spectral transmittance.	58
7.6	Spectrophotometric curves of a soybean leaf obtained using the <i>ABM</i> and from its front surface (adaxial surface) towards the light and its back surface (abaxial surface) towards the light, for an angle of incidence of 8° and 10^6 rays. a) Absolute spectral reflectance. b) Absolute spectral transmittance.	58
7.7	BDF of a soybean leaf at a wavelength of $550nm$ (which corresponds approximately to the reflectance and transmittance peaks), for angles of incidence of 15° , 30° and 45° , in the plane given by the incidence direction and the normal of the specimen, 10^7 rays, and the collector sphere divided into 20 patches along its latitude and 40 patches along its longitude.	59
7.8	Number of interactions per ray and per wavelength for 10^4 rays. a) Graph for zero to fifty interactions per ray, b) Zoom in of the region with high frequency of interactions per ray.	59
7.9	Image generated using the <i>ABM</i> . On the left back lit, on the right, front lit.	60
8.1	Scattering distribution performed by the <i>FSM</i> to represent the three components of a foliar specimen's SPF: a) surface reflectance b) subsurface reflectance and c) transmittance.	62
8.2	Graphs corresponding to the entries of the table of absolute spectral reflectances and transmittances for a soybean leaf.	64
8.3	Graphs corresponding to the entries of the table of absolute spectral reflectances and transmittances for the veins of a soybean leaf.	65
8.4	BDF curves for a front lit leaf obtained at the wavelengths associated with the RGB channels (Table 6.1). a) and c) Using the <i>ABM</i> . b) and d) Using the <i>FSM</i>	66
8.5	Top row: front lit leaves (1^{st} set) using the <i>ABM</i> (a) and the <i>FSM</i> (b). Middle row: back lit leaves (2^{nd} set) using the <i>ABM</i> (c) and the <i>FSM</i> (d). Bottom row: Images with ambient light only (3^{rd} set) and using the <i>ABM</i> (e) and the <i>FSM</i> (f). For all three scenes we used $\varsigma_c = 0.01$	68
8.6	Convergence graphs for: a) 1^{st} set, b) 2^{nd} set and c) 3^{rd} set, showing the percentage of rays that still need to be propagated after each depth of propagation.	69
8.7	Number of rays propagated at each depth of propagation for: a) 1^{st} set, b) 2^{nd} set and c) 3^{rd} set.	70
9.1	Shadowing and masking.	71
9.2	Photograph showing the veinlets of a <i>privet</i> leaf. Redrawn from [26].	72

Abstract

The visual simulation of plants involves two major areas of computer graphics research: geometrical modeling and lighting modeling. Clearly, the first step to visualize a plant is to geometrically model its shape and structural characteristics. The next step is to simulate its interaction with light in order to determine appearance attributes such as color, glossiness and translucency. This step corresponds to the main stage of the rendering pipeline. After all, our perception of any object depends on how it scatters or absorbs light. Viewed in this context, the understanding of the natural processes involved in light interaction with plants is not only central to the simulation of their appearance, but it is also essential for the simulation of their growth and their interaction with the surrounding environment. In this tutorial the main physical and biological aspects involved in the processes of reflection, transmission and absorption of light by plants are addressed. The formulation of virtual measurement devices used to verify the accuracy of reflectance and scattering models is also presented. Computer graphics models of light interaction with plants are examined in detail to allow their implementation and incorporation into rendering frameworks by computer graphics researchers and skilled practitioners. Finally, open problems and current trends in this area are discussed. The focus of this discussion will be on the generation of more realistic images of natural scenes through the use of more comprehensive and efficient reflectance and transmittance models for plants.

Chapter 1

Introduction

The interaction of light with different materials is of fundamental importance in computer graphics. It determines the two attributes that define the appearance of objects: namely their color and surface finish. For instance, two spheres of same radius, one made of silver and the other made of plastic, have very different appearances. The color attribute is determined by the spectral energy distribution of the scattered light, measured in terms of reflectance and transmittance, and the surface finish attribute is determined by the spatial distribution of that light, measured in terms of the bidirectional surface-scattering distribution function (BSSDF or simply BDF). The term BDF represents a combination of the bidirectional reflectance distribution function (BRDF) and the bidirectional transmittance distribution function (BTDF).

The rendering community has developed several models that can be applied to simulate the interaction of light with a wide range of inorganic materials. Only recently, however, have researchers in this field started to look more closely at the interaction of light with plants. It is possible to create a very realistic scene composed of inorganic materials, either dielectrics like glass or conductors like gold. It is more difficult to create a realistic scene containing organic materials, such as plants, since the non-realistic traits of a synthetic plant are easily perceived despite the sophisticated geometrical plant models available in the computer graphics literature. This happens largely because relevant biological factors are usually not considered in the rendering of plants relying instead on coarse approximations of foliar optics.

This tutorial discusses the recent advances in the biologically and physically-based rendering of plants. In particular, it concentrates on light transport by leaves, which are the most important plant surfaces interacting with light. Many of the issues discussed in this tutorial can, however, be extended to other plant surfaces, such as stems and petals, since they present similar optical and structural characteristics. Participants in this course will be briefed on the main biological aspects involved in the reflection, transmission and absorption of light by plant leaves and will learn the concepts behind the current computer models used to simulate these natural phenomena. The tutorial also aims to provide enough information on these models so that researchers may incorporate them in their rendering framework.

The course notes are organized into 10 chapters. Chapter 1 discusses biologically and physically-based rendering within the general context of the simulation of light transport through rendering algorithms and examines how this approach can improve the accuracy and efficiency of the current methods of image synthesis for biological systems. It concludes with an outline of the organization of these notes. The remaining chapters are divided into two groups. In the first group (Chapters 2-5) a concise background for the development and validation of computer models of light interaction with plants is provided, while in the second group (Chapters 6-10) models of light interaction with plants available in the computer graphics literature are described noting their limitations.

Chapter 2 introduces the relevant aspects of physically-based rendering that are used throughout these course notes. Physically-based rendering involves the simulation of the propagation of light, starting from light sources, traveling through the environment, interacting with different object and materials, and finally reaching the viewer. Generally speaking reflectance and scattering models are used to describe how light interacts with various materials. The expression reflectance model is restrictive since there are reflectance models that handle transmittance as well. We will retain this term in this abstract for consistency with the graphics literature, explicitly mentioning the transmittance components when they become relevant. The term scattering model refers to models used to compute BDFs. In this chapter the laws of optics commonly used in reflectance and scattering models are briefly described along with the definition of relevant radiometric terms and their physical properties. Besides reflection and transmission, the absorption of light by pigments is also a relevant natural phenomenon to be considered in the rendering of foliar tissues. For this reason the absorption mechanisms commonly involved in the absorption of light

by pigments are also reviewed in this chapter. From a global point view, reflectance and scattering models form the kernel of the rendering equation. This equation, also known as the transport equation, unifies the discussion of the global illumination methods used to determine the appearance of an environment by simulating the transport of light within it. The formulation of this equation is examined in this chapter along with the Monte Carlo techniques that are often applied to solve it.

It is important to evaluate the accuracy of a reflectance or a scattering model before including it in a rendering pipeline since the comparison of the readings given by these models with actual measured data provides a valuable insight into their quantitative and qualitative accuracy. Reflectances and transmittances are measured using a device known as spectrophotometer and BDFs are measured using a device known as goniophotometer. Computer simulations of these devices, known as virtual measurement devices, can be used to evaluate the accuracy of reflectance and scattering models. These virtual devices can also be used to obtain data from previously validated models through spectral and spatial measurements. In Chapter 3 the differences between these two groups of measurements are highlighted. Moreover, the main characteristics of real measurement devices are outlined to provide a substrate for the derivation of the formulation of the virtual devices. Their formulation is presented with a level of detail to allow their straightforward implementation by researchers and skilled practitioners.

The understanding of foliar optics issues is essential to improve the rendering of plants. For instance, we intuitively associate plants with the color green. However, there are many different shades of green in nature and these may vary considerably according to the viewing and illuminating geometry of the incident light. One could design a scattering model for these materials in which the spectral data that define their color is incorporated into the model as input parameters. The main question is where to find this data since this spectral information is only available in the literature for a limited number of species and viewing and illuminating geometries. The development of accurate and reliable reflectance and transmittance models for foliar tissues is, therefore, a requisite to perform a biologically-based rendering of these materials. In order to design such models one shall focus on the factors that directly affect the transport and absorption of light within foliar tissues, such as surface features, differences in the internal arrangement of cell layers, differences in thickness, water content and pigments composition, concentration and distribution. These factors and their effects on light transport and absorption within the foliar tissues are described in Chapter 4. The manifestations of these effects, namely the spectral and spatial characteristics of the scattering profile of real plant leaves, are also examined in this chapter.

Many researchers from areas like botany and remote sensing have proposed reflectance and scattering models for leaves where the goal is to understand the physiological processes that relate foliar optical properties to biophysical characteristics. These models present different levels of complexity and propose different techniques to describe and simulate light transport and absorption within the foliar tissues. Although we have different goals in computer graphics, some concepts, as well as data provided by these models, can be incorporated in the design of models aimed at rendering applications. For this reason an overview of the most relevant models and approaches used in these areas is presented in Chapter 5. In this overview the models are divided into four groups: plate models, Kubelka-Munk theory based models, ray-tracing based models and radiative transfer theory based models. As one can observe in this classification, these models apply methods which are also used by the computer graphics community. Some of them, however, were developed long before their application became pervasive in rendering. Other models were developed fairly recently and took advantage of enhancements performed on these methods by computer graphics researchers. This aspect also illustrates how advantageous a symbiosis between fields with a mutual interest, such as the simulation of natural processes of light interaction with plants, can be. This symbiosis is also present in the simulation of radiative transfer processes in vegetation. Although most of the research on this topic has been restricted to remote sensing applications, the fundamental aspects involved in these processes are also relevant for the rendering of natural scenes. Not surprisingly global illumination methods used in rendering applications have been incorporated by remote sensing researchers in their studies of radiative transfer in plant canopies. For this reason, in this chapter it is also provided an overview of global illumination applications for radiative transfer in regions of vegetation such as forest canopies and crops.

The tutorial now focuses on the specific models for light interaction with plants tissues available in the computer graphics literature. In Chapter 6 the *H-K* multiple-layer scattering model [75, 60] is described. This model can be used to simulate light interaction with a wide range of materials appearing in nature. Its description in the tutorial is tailored to application to plant leaves. Reflectance and transmittance of foliar tissues are not computed by this model, but incorporated as input data. This model simulates the light scattering by objects that can be represented by a series of layers, an intuitive idea that has appeared previously in physics and remote sensing. It computes the BDF using concepts of linear transport theory and Monte Carlo techniques. Its formulation is concisely reviewed in this chapter and its strengths and limitations are examined within the context of biologically and physically-based rendering. This model assumes that the reflection component of the scattering profile has two terms. One arises due to surface reflection and the other due to subsurface volume scattering. It also assumes that

the transmission component has two terms. One represents the amount of light transmitted through a layer without scattering inside the layer, but accounting for absorption, and the other is due to scattering in the volume. The mechanisms of light absorption by foliar pigments, such as chlorophyll, are not account for by this model.

Chapter 7 describes the first reflectance and scattering model specifically designed for foliar tissues presented in the computer graphics literature, namely the *ABM* [10, 8]. It is also the first model of this kind in computer graphics to have the accuracy of its results verified against actual experimental data. The scattering simulation performed by this model accounts for the three components of light transport in plant tissues, namely surface reflection, subsurface reflection and transmission. This simulation is performed stochastically using standard Monte Carlo techniques and it is described in detail in this chapter. In contrast to many standard scattering models used in computer graphics, this model does not rely on the input values of reflectance and transmittance. In other words, the reflectances and transmittances for different viewing and illuminating geometries are computed by the model itself through the simulation of the process of light absorption by foliar pigments. This means that besides its on-line applications this model can be used off-line in order to generate spectral curves of reflectance and transmittance required as input parameters by other models such as the ones presented in Chapters 6 and 8. The simulation of light absorption by foliar pigments is performed stochastically using standard Monte Carlo techniques. The procedures involved in this simulation are also described in this chapter. Implementations issues, such as the adjustments performed in the spectral curves of absorption of the pigments to account for intensification factors, are also examined. A summary of the strengths and limitations of this model within the context of biologically and physically-based rendering concludes this chapter.

Chapter 8 presents the *FSM* [8, 12], an efficient scattering model for foliar tissue. This model aims to provide a balance between two seemingly conflicting goals, namely accuracy and efficiency. Like the multiple-layer model, this model only accounts for the spatial distribution of the propagated light measured in terms of the BDF. The reflectances and transmittances are incorporated into this model as input data. They are used as scale factors in the stochastic simulation of the scattering profile of plant leaves. This approach replaces the random walk process used by the previous model to simulate the randomization and absorption of light within the foliar tissues. This in turn, reduces the computational time required to achieve a desired accuracy level of the results. The main characteristics of this model and its formulation are described in this chapter. Implementation issues, such as the selection of scale factors according to the position of the light source with respect to the foliar specimen and the selection of cutoff attenuation threshold, are also discussed. This chapter closes with a summary of the strengths and limitations of this model within the context of biologically and physically-based rendering.

The models of light interaction with plant leaves available in the literature are isotropic, *i.e.*, the reflected light intensity at a given point is independent of the surface orientation along this normal at this point. Plant leaves are, however, anisotropic, *i.e.*, if an element of such a biological surface is rotated around its normal while the light and the viewer directions remain unchanged, the light intensity reflected to the viewer will vary. In order to develop models capable of capturing the anisotropic behavior of foliar tissues, it would be necessary to account for the characteristics of their venation systems. Unfortunately, as of today, very few publications have presented experiments and data regarding this topic. This issue is examined in Chapter 9. Other issues associated with the accuracy of these models are also briefly discussed. Among these issues are the shadowing of the incident light and the masking of the scattered light by surface features, polarization effects and environmental factors such as the deposition of inorganic materials, *e.g.*, water, dust or chemicals. Obviously, the efficiency of models for light interaction with plant leaves becomes even more important when one uses these models in applications involving a large number of foliar primitives. Strategies to improve the efficiency of the existing models and guidelines to developed more efficient models are discussed along with extensions to allow the simulation of other relevant natural phenomena, such as the senescence of plant leaves, which is characterized by their change of colors, the optical properties of other plant surfaces, namely petals and stems, and the processes of scattering and absorption of the incident light in the near-infrared and infrared regions of the light spectrum. Chapter 9 closes with a brief overview of applications involving global illumination methods in the simulation of radiative transfer processes in vegetation.

Chapter 10 summarizes the main aspects of the modeling of light interaction with plants that are presented in this tutorial. Moreover, applications involving the models described in the second part of this tutorial are discussed within and outside the scope of computer graphics, *e.g.*, in remote sensing and in environmental design fields. Finally, current trends on biologically-based rendering are briefly examined.

In this tutorial light propagation is described in terms of geometrical optics. From a practical point of view, it is more efficient to model light as rays rather than waves. We can think of a wave as just a ray with an energy, and the wavelength of light, a physical optics parameter important for rendering applications, can be included in geometrical optics by associating a wavelength with each ray [133]. Furthermore, as pointed out by Shirley [133] and Arvo [7], in many situations physical optics

effects are not visually important, and do not dominate the scenes that we commonly wish to simulate. For instance, the light sources commonly used in rendering applications are usually incoherent, and effects related to phase, such as interference, are usually masked [7]. Also, diffraction phenomena are noticeable for long wavelength radiation, but have a fairly small effect for visible light [133].

In addition, in the experiments presented in this tutorial we will assume that the energies of different wavelengths are decoupled. In other words, the energy associated with some region of the space, or surface, at wavelength λ_1 is independent of the energy at another wavelength λ_2 [60]. We will also assume that objects within an environment exchange energy directly with no atmospheric attenuation. since atmospheric effects over tens of meters are insignificant under normal circumstances as noted by Arvo [7].

Chapter 2

Selected Topics on Physically-Based Rendering

In this chapter we will concentrate on the fundamental aspects of physically-based rendering that will be used throughout this tutorial. Physically-based rendering involves simulating the behavior of light, starting from luminaires, *i.e.*, area light sources, traveling through the environment, interacting with different objects, and finally reaching the viewer. Reflectance and transmittance models are used to describe how the light interacts with different objects. These models must satisfy certain physical requirements to avoid excluding important physical effects and to maintain the energy consistency needed for global illumination calculations [155]. These issues will also be examined in this chapter.

2.1 Optics Concepts

Throughout this tutorial we will use the following terminology suggested by Meyer-Arendt [114]. Terms ending in *-ion*, such as reflection, transmission and absorption, describe a process. Terms ending in *-ivity*, such as reflectivity, transmissivity and absorptivity, refer to a general property of a material. Terms ending in *-ance*, such as reflectance, transmittance or absorptance, refer to properties of a given object or surface.

Reflection is the process in which light at a specific wavelength incident on a material is propagated outward by the material without a change in wavelength. Similarly, transmission is the process in which light at a specific wavelength incident on the interface between materials passes through the interface and into the other material without a change in wavelength [60].

Hall [70] suggested that reflection and transmission can be broken into two components, a coherent component and an incoherent or scattered component [15]. The coherent component is reflected using the law of reflection and transmitted using the law of refraction, which are described later. The incoherent component is reflected and transmitted in all directions based upon a statistical probability function associated with surface properties (Section 2.5).

Absorption is a general term for the process by which the light incident on a material is converted to another form of energy, usually to heat. All of the incident light is accounted for by the processes of reflection, transmission and absorption [6].

The reflection and transmission (refraction¹) of light at the smooth surfaces of pure materials is described by the Fresnel equations [60, 78, 133]. Before getting to the specifics of the Fresnel equations, however, we shall review some relevant physical parameters, definitions and laws.

Materials such as conductors (metals), semi-conductors and dielectrics are characterized by their complex index of refraction, $N(\lambda)$, which is composed of a real and an imaginary term. The real term corresponds to the real index of refraction (refractive index, for short), which measures how much an electromagnetic wave slows down relative to its speed in vacuum [60]. The imaginary term corresponds to the extinction coefficient, which represents how easily an electromagnetic wave can penetrate into the medium [60]. The resulting expression for $N(\lambda)$ is given by:

¹Refraction, or the coherent component of transmission, can be defined as the bending or the change in the direction of the light rays as they pass from one medium to another [82]. This bending is determined by the change in the velocity of propagation associated with the different indexes of refraction of the media [48].

$$N(\lambda) = \eta(\lambda) + j\mu(\lambda) \quad (2.1)$$

where:

- λ = wavelength,
- $\eta(\lambda)$ = real index of refraction as a function of λ ,
- $\mu(\lambda)$ = extinction coefficient as a function of λ ,
- j = imaginary unit ($j = \sqrt{-1}$).

Semi-conductors are conductors with a small extinction coefficient. Dielectrics are essentially non-conductors whose extinction coefficient is by definition zero [133]. For notational simplicity, we will remove the explicit dependency on λ in the remaining equations presented in this section.

When light hits a smooth surface, the reflection direction, represented by the vector \vec{r} (Figure 2.1), for light incident at an interface is obtained using the law of reflection [78]. This states that the angle of the reflection direction, θ_r , is equal to the angle of incidence, θ_i , and will be in the same plane as the incident direction, represented by the vector \vec{i} , and the surface normal, represented by the vector \vec{n} :

$$\theta_r = \theta_i \quad (2.2)$$

where the angle θ_i can be obtained using the following equation:

$$\theta_i = \arccos \left(\frac{\vec{n} \cdot \vec{i}}{|\vec{n}| |\vec{i}|} \right) \quad (2.3)$$

Considering the geometry described in Figure 2.1 and applying the law of reflection stated above, the reflection direction, \vec{r} , is given by:

$$\vec{r} = \vec{i} + 2\vec{n} \cos \theta_i = \vec{i} - 2\vec{n}(\vec{i} \cdot \vec{n}) \quad (2.4)$$

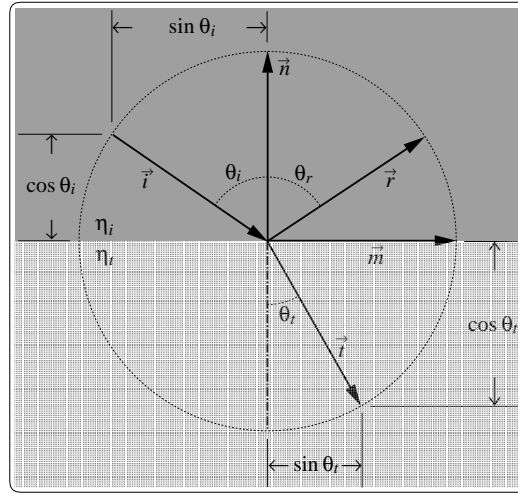


Figure 2.1: Geometry for light incident at an interface between different materials.

The transmission (refraction) direction, represented by the vector \vec{t} (Figure 2.1), is obtained using the law of refraction, also known as Snell's law [78]:

$$\eta_i \sin \theta_i = \eta_t \sin \theta_t \quad (2.5)$$

where:

- η_i = refractive index of the incidence material (medium),
- η_t = refractive index of the transmission material (medium).

More specifically, the transmission (refraction) direction \vec{t} is given by:

$$\vec{t} = -\vec{n} \cos \theta_t + \vec{m} \sin \theta_t \quad (2.6)$$

where:

\vec{m} = vector perpendicular to \vec{n} and in the same plane as \vec{i} and \vec{n} .

Equation 2.6 can be expanded to yield the expression presented by Heckbert [79]:

$$\vec{t} = \left[-\frac{\eta_i}{\eta_t} (\vec{i} \cdot \vec{n}) - \sqrt{1 - \left(\frac{\eta_i}{\eta_t}\right)^2 (1 - (\vec{i} \cdot \vec{n})^2)} \right] \vec{n} + \frac{\eta_i}{\eta_t} \vec{i} \quad (2.7)$$

The incident rays are not only reflected and/or transmitted (refracted) at an interface between dielectrics, but also attenuated. This attenuation is given by the Fresnel coefficients for reflection and transmission (refraction), which are computed through the Fresnel equations. For a complete derivation of these equations, the reader is referred to the texts by Hecht and Zajac [78] and Glassner [60]. The Fresnel equations for a smooth interface between two dielectrics ($\mu = 0$) can be simplified to the following expressions collected by Kajiyama [90]:

$$R_{\perp} = \frac{\eta_i \cos \theta_i - \eta_t \cos \theta_t}{\eta_i \cos \theta_i + \eta_t \cos \theta_t} \quad (2.8)$$

$$R_{\parallel} = \frac{\eta_t \cos \theta_i - \eta_i \cos \theta_t}{\eta_i \cos \theta_t + \eta_t \cos \theta_i} \quad (2.9)$$

$$T_{\perp} = \frac{2\eta_i \cos \theta_i}{\eta_i \cos \theta_i + \eta_t \cos \theta_t} \quad (2.10)$$

$$T_{\parallel} = \frac{2\eta_i \cos \theta_i}{\eta_t \cos \theta_i + \eta_i \cos \theta_t} \quad (2.11)$$

In the previous equations R_{\perp} and R_{\parallel} are the Fresnel coefficients for reflection of light polarized in directions perpendicular to (\perp) and parallel (\parallel) to the interface. Similarly, T_{\perp} and T_{\parallel} are the Fresnel coefficients for transmission (refraction) of light polarized in directions perpendicular to (\perp) and parallel (\parallel) to the interface.

The Fresnel coefficient for reflection, or reflectivity [114], R , for polarized light is the weighted sum of the polarized components, in which the weights must sum to unity [60]. In this tutorial we are interested in the Fresnel coefficients for unpolarized light. In this case, the Fresnel coefficient for reflection is simply the average of the two coefficients R_{\perp} and R_{\parallel} . Then, the equation used to compute this coefficient reduces to following expression used by Shirley *et al.* [136]:

$$R = \frac{(\eta_i^2 - \eta_t^2)^2 c_{it}^2 + (\cos \theta_i^2 - \cos \theta_t^2)^2 n_{it}^2}{(c_{it}(\eta_i^2 + \eta_t^2) + n_{it}(\cos \theta_i^2 + \cos \theta_t^2))^2} \quad (2.12)$$

where:

$$c_{it} = \cos \theta_i \cos \theta_t,$$

$$n_{it} = \eta_i \eta_t.$$

An important property of these equations is that they can be applied without regard to the direction of propagation [133], which becomes relevant when one applies ray tracing methods. To find the Fresnel coefficient for transmission (refraction), or transmissivity [114], T , we observe that there is no absorption at an interface between dielectrics. Thus, T can be easily obtained from R through a simpler relation: $T = 1 - R$, rather than resorting to an expression similar to Equation 2.12. Incidentally, absorption may occur once light is transmitted into a medium. Absorption of the transmitted light is discussed in Section 2.3.

2.2 Radiometric Terms and Properties

Radiometric terms describe measures of light integrated over all wavelengths. These measures may be also evaluated at a specific wavelength λ . When a radiometric term is written making this dependency on wavelength explicit, it is called a spectral radiometric term [60].

Radiant energy, denoted by Q (measured in joules, J), represents the energy of a packet of rays. In computer graphics we are interested in the amount of light hitting a surface or film plane during a set period of time. Radiant power or flux, denoted by Φ (measured in Watts, W , or $\frac{J}{s}$), is, therefore, often used as pointed out by Shirley [133]. Moreover, Shirley notes that radiant power is convenient to work with because it allows energy balance constraints to be applied, assuming that either the solution is steady state or the speed of light is infinite. The later assumption is usually appropriate, since the time it takes light to travel across a typical scene is very small compared to a camera shutter speed or the human temporal visual threshold [133]. The amount of radiant power traveling from a source in a certain direction, per unit of solid angle², is called the radiant intensity and denoted by I (measured in $\frac{W}{sr}$).

The underlying purpose of the rendering process is to determine the colors of the surfaces within an environment. The color of a given surface will depend on how much light is emitted, reflected, absorbed and transmitted by the surface. Since radiant intensity depends on the area of the light source, it is not convenient to approximate color, which is independent of surface area. As pointed out by Shirley [133], the radiometric quantity that more closely approximates the color of a surface, through an indication of its brightness³, is the radiance, denoted by L (measured in $\frac{W}{sr \cdot m^2}$), which is not dependent on the size of the object being viewed, or the distance to the viewer. The spectral radiance at a point x of a surface and in a direction ψ (usually represented by a pair of spherical coordinates) is denoted by $L(x, \psi, \lambda)$ and can be expressed as:

$$L(x, \psi, \lambda) = \frac{dI(x, \psi, \lambda)}{dA \cos\theta} = \frac{d^2\Phi(x, \psi, \lambda)}{d\vec{\omega} dA \cos\theta} = \frac{dM(x, \psi, \lambda)}{d\vec{\omega} \cos\theta} \quad (2.13)$$

where:

$dI(x, \psi, \lambda)$	=	spectral radiant intensity at x and in a direction ψ ,
$d\Phi(x, \psi, \lambda)$	=	spectral radiant power at x and in a direction ψ ,
$dM(x, \psi, \lambda)$	=	spectral radiant exitance at x and in a direction ψ ,
θ	=	angle between the surface normal and the direction ψ ,
dA	=	differential area surrounding x ,
$d\vec{\omega}$	=	differential solid angle at which $d\Phi$ arrives at or leaves from x .

The fraction of light at wavelength λ incident from a direction ψ_i at a point x that is neither absorbed into nor transmitted through a given surface is called the reflectance, $\rho(x, \psi_i, \lambda)$, of the surface. Similarly, the fraction of light transmitted through the surface is called the transmittance, $\tau(x, \psi_i, \lambda)$. The light that is neither reflected nor transmitted by the surface is absorbed. The parameter that describes the amount of absorbed light is absorptance [6]. The sum of the reflectance, transmittance and absorptance is one.

The reflectance and the transmittance do not describe the distribution of the reflected and transmitted light. The *bidirectional reflectance distribution function* (BRDF), f_r , and the *bidirectional transmittance function* (BTDF), f_t , are used to overcome this limitation. As suggested by Glassner [60], these functions can be combined into the *bidirectional surface-scattering distribution function* (BSSDF, or simply BDF [60]). The BDF, f , can be expressed in terms of the ratio between the spectral radiance propagated at a point x of a surface in the direction ψ and the spectral radiant energy (per unit of area and per unit of time) incident from a direction ψ_i at the point x of the surface:

² A solid angle is the three-dimensional analog to the two-dimensional concept of angle [60]. For example, the solid angle subtended by an area A on a sphere with radius \mathcal{R} is equal to $\frac{A}{\mathcal{R}^2}$. This quantity is the measure of the angle in steradians (radians squared), denoted by sr [39].

³ Brightness can be defined as the attribute by which an area of color of finite size is perceived to emit, transmit, or reflect a greater or lesser amount of light [6].

$$f(x, \psi_i, \psi, \lambda) = \frac{dL(x, \psi, \lambda)}{L_i(x, \psi_i, \lambda) d\vec{\omega}_i \cos\theta_i} \quad (2.14)$$

where:

- $f(x, \psi_i, \psi, \lambda)$ = BDF of the surface at x ,
- $dL(x, \psi, \lambda)$ = spectral radiance propagated at x and in a direction ψ ,
- $L_i(x, \psi_i, \lambda)$ = spectral incident radiance at x and in a direction ψ_i ,
- θ_i = angle between the surface normal at x_i and the direction ψ_i ,
- $d\vec{\omega}_i$ = differential solid angle at which L_i arrives at x .

An important property of the BDF is its symmetry or reciprocity condition, which is based on *Helmholtz Reciprocity Rule*⁴ [36]. This condition states that the BDF for a particular point and incoming and outgoing directions remains the same if these directions are exchanged (Figure 2.2). It allows, for instance, the “forward” simulation of light rays traveling from a viewer to a light source, which is used by global illumination methods such as path tracing [91, 133]. Quantitatively, this condition can be expressed as:

$$f(x, \psi_i, \psi, \lambda) = f(x, \psi, \psi_i, \lambda) \quad (2.15)$$

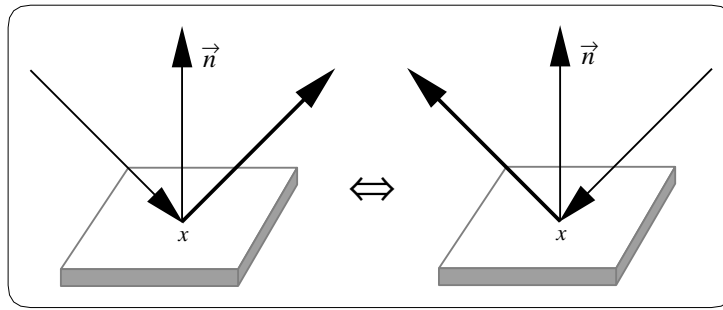


Figure 2.2: Reciprocity of the BDF.

Another important property of the BDFs is that they must be normalized, *i.e.*, conserve energy. This means that the total energy propagated in response to some irradiation must be no more than the energy received [60]. In other words, for any incoming direction the radiant power propagated over the hemisphere can never be more than the incident radiant power [95]. Any radiant power that is not propagated is absorbed. Formally, in the case of reflection of light, the so-called directional-hemispherical reflectance [6] should therefore be less than or at most equal to 1:

$$\rho(x, \psi_i, 2\pi, \lambda) = \int_{outgoing \psi} f_r(x, \psi_i, \psi, \lambda) \cos\theta d\vec{\omega} \leq 1, \quad \forall \psi_i \in \text{incoming directions} \quad (2.16)$$

where:

- $f_r(x, \psi_i, \psi, \lambda)$ = BRDF of the surface at x ,
- θ = angle between the surface normal and the outgoing direction ψ ,
- $d\vec{\omega}$ = differential solid angle at which the radiance is reflected.

A similar relation given in terms of the directional-hemispherical transmittance [6] and the BTDF is used for the transmission of light. Reflectance and transmittance models, or simply BDF models, that are energy-conserving and reciprocal are considered *physically plausible*⁵. This is a crucial requirement for physically-based rendering frameworks aimed at global illumination applications.

⁴The original statement of *Helmholtz Reciprocity Rule* does not include non-specular reflection of any sort [36, 146]. Recently Veah [146] derived a reciprocity condition for general BDFs using Kirchhoff’s laws regarding radiative transfer [138].

⁵Lewis [99, 100] uses the term “plausible” to describe BDF models whose existence does not violate the laws of physics.

Sometimes, when energy transport or energy balance is of concern as opposed to lighting at a point, it is more convenient to work with the radiant power (radiant flux) [6] than with the radiance [133]. Under these circumstances, it is more natural to describe the surface reflection and transmission properties in terms of the probability distribution of the reflected and transmitted light. This term is called the *scattering probability function* (SPF) [132, 133]. It describes the amount of energy scattered in each direction ψ , at a point x of a surface and at wavelength λ as:

$$s(x, \psi_i, \psi, \lambda) = \frac{dI(x, \psi, \lambda)}{\rho(x, \psi_i, \lambda)d\Phi(x, \psi_i, \lambda)} \quad (2.17)$$

where:

- $dI(x, \psi, \lambda)$ = spectral radiant intensity reflected at x and in a direction ψ ,
- $\rho(x, \psi_i, \lambda)$ = reflectance of the surface at x ,
- $d\Phi(x, \psi_i, \lambda)$ = spectral radiant power incident at x and in a direction ψ_i .

The term $\rho(x, \psi_i, \lambda)$ appears in the numerator when we are dealing with reflection of light. It scales the function to a valid *probability density function* (PDF) (Section 2.5) over the solid angle through which the reflected light leaves the surface [132, 133]. In the case of transmission of light, a similar expression is used, in which $\rho(x, \psi_i, \lambda)$ is replaced by $\tau(x, \psi_i, \lambda)$.

2.3 Absorption in a Homogeneous Medium

In this section we will focus on the losses affecting the transmittance in a homogeneous medium, *i.e.*, a material in which the physical properties that affect light propagation are assumed to be identical everywhere. The losses affecting the transmittance in an inhomogeneous medium can be simulated through successive application of the laws for homogeneous medium [2]. Another alternative is to think of an inhomogeneous material as a structure composed of two or more homogeneous layers [129]. The reader interested in the spectrophotometry regarding the transmittance in inhomogeneous materials is referred to the text by MacAdam [105].

The transmittance of a homogeneous material, after correction for surface losses, varies in accordance with Bouguer's law (Figure 2.3), also called Lambert's law of absorption [105]. This law states that the loss due to the process of absorption is proportional to the power of the light incident on the medium, to the thickness of the medium (or the distance traveled by the light in the medium) and to a constant of proportionality called absorptivity [114]. This constant, also known as absorption coefficient, is a characteristic of the medium and a function of wavelength. A complete derivation of this law is presented by Meyer-Arendt [114]. It is usually written as follows:

$$\tau(\lambda) = \frac{\Phi_t(\lambda)}{\Phi_i(\lambda)} = e^{-a(\lambda) h} \quad (2.18)$$

where:

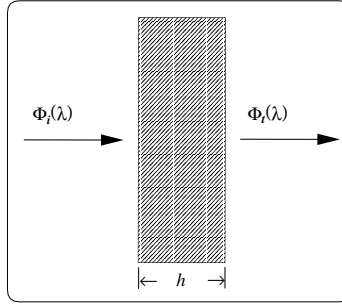
- $\Phi_t(\lambda)$ = spectral power after being transmitted through the medium,
- $\Phi_i(\lambda)$ = spectral power incident on the medium,
- $a(\lambda)$ = absorption coefficient of the medium at wavelength λ ,
- h = thickness of the medium.
- e = Euler's number (2.718281...).

Beer's law [102] states that for a dye solution, the absorption coefficient of the solution is directly proportional to its concentration. Combining Beer's law with Bouguer's law [105] for samples of thickness h and concentration c results in the following expression for the transmittance of a homogeneous material:

$$\tau(\lambda) = e^{-a(\lambda) c h} \quad (2.19)$$

where:

- $a(\lambda)$ = absorption coefficient of the medium at wavelength λ ,
- c = concentration of the solution,
- h = thickness of the medium,
- e = Euler's number (2.718281...).

Figure 2.3: Loss of light at wavelength λ in a medium of thickness h .

Sometimes it is more convenient to specify the absorption of a medium by means of the extinction coefficient [102], μ , which is given by:

$$\mu = \frac{a(\lambda)\lambda_m}{4\pi} \quad (2.20)$$

where:

- $a(\lambda)$ = absorption coefficient of the medium at wavelength λ ,
- λ_m = wavelength of light in the medium.

2.4 Rendering Equation

Three major global illumination approaches have been used in rendering to simulate the light transfer mechanisms: ray tracing, radiosity and hybrid methods. Kajiya [91] unified the discussion of global illumination methods with the rendering equation. This equation, also known as transport equation, can be expressed in terms of radiances (Equation 2.21) on the basis of the ray law (the radiance is constant along a line of sight between objects [133]), and the definition of the BDF. In a simplified form it is given by:

$$\underbrace{L(x, \psi, \lambda)}_{total} = \underbrace{L_e(x, \psi, \lambda)}_{emitted} + \underbrace{L_p(x, \psi, \lambda)}_{propagated} \quad (2.21)$$

Equation 2.21 states that the radiance of a point x on a surface, in a direction ψ and at wavelength λ is given by the sum of the emitted radiance component, L_e , and the propagated radiance component, L_p . Usually L_e is known from the input data, and the computation of L_p constitutes the major computational problem.

The term L_p can be written as an integral over all the surfaces within the environment (Figure 2.4), resulting in the formulation presented in the following equation:

$$L_p(x, \psi, \lambda) = \int_{all\ x_j} f(x, \psi, \psi_i, \lambda) L_i(x, \psi_i, \lambda) \cos \theta_i V(x, x_j) \frac{\cos \theta_j dA_j}{\|x_j - x\|^2} \quad (2.22)$$

where:

- $f(x, \psi, \psi_i, \lambda)$ = BDF of the surface at x ,
- $L_i(x, \psi_i, \lambda)$ = spectral incident radiance at x and in a direction ψ_i ,
- θ_i = angle between the surface normal at x and the direction ψ_i ,
- θ_j = angle between the surface normal at x_j and the direction ψ_i ,
- dA_j = differential area surrounding x_j ,
- $V(x, x_j)$ = visibility term.

The visibility term $V(x, x_j)$ used in the Equation 2.22 is one if a point x_j of a certain surface can “see” a point x of another surface, and zero otherwise. This equation is commonly used by deterministic rendering methods based on standard numerical

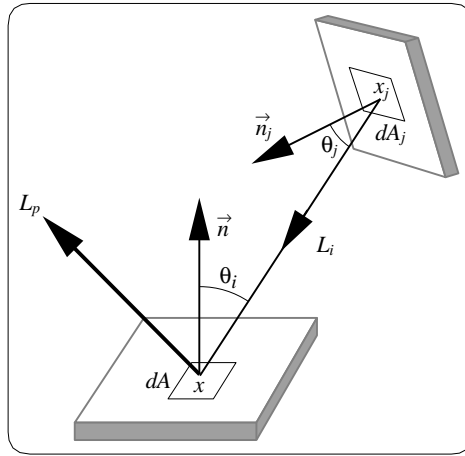


Figure 2.4: Geometry for computing L_p as an integral over all the surfaces within the environment.

techniques [95]. In the context of global illumination these techniques are used to solve the multiple integrals and linear systems of equations resulting from these when applying the radiosity method [39].

Alternatively, L_p can also be expressed in terms of all directions visible to x (Figure 2.5) [133]. This expression for L_p is more suitable to nondeterministic rendering methods based on Monte Carlo techniques [73], and it is given by:

$$L_p(x, \psi, \lambda) = \int_{\text{incoming } \psi_i} f(x, \psi, \psi_i, \lambda) L_i(x, \psi_i, \lambda) \cos \theta_i d\vec{\omega}_i \quad (2.23)$$

where:

- $f(x, \psi, \psi_i, \lambda)$ = BDF of the surface at x ,
- $L_i(x, \psi_i, \lambda)$ = spectral incident radiance at x and in a direction ψ_i ,
- θ_i = angle between the surface normal at x and the direction ψ_i ,
- $d\vec{\omega}_i$ = differential solid angle where L_i arrives.

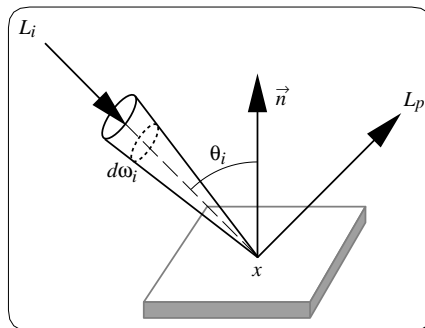


Figure 2.5: Geometry for computing L_p in terms of all directions visible to a point x .

2.5 Monte Carlo Techniques for Directional Sampling

In this section we outline some Monte Carlo definitions and techniques and present a concise derivation of warping functions used in physically-based rendering. The material presented in this section have been extensively examined by computer graphics researchers [60, 95, 96, 100, 133]. The material presented here differs by being oriented to scattering simulations and by

providing derivation details frequently omitted in computer graphics papers. For a more comprehensive treatment of Monte Carlo methods the reader is referred to classic Monte Carlo texts [73, 92].

2.5.1 Importance Sampling and Warping Transformations

The integral term of the rendering equation (Section 2.4) can be estimated using Monte Carlo techniques. Among these techniques one can highlight the *importance sampling* [73]. The idea behind this technique is simple. If the integrand is a product of two functions, and we know one of them, we can use this information to guide our sampling strategy. Usually areas that contribute more (large values) or vary more quickly will have more importance and will be sampled more densely. In this case we need to compensate for the non-uniform sampling to avoid the introduction of bias in the final result.

Suppose that we need to determine Θ given by the following integral involving a real-valued function g :

$$\Theta = \int g(x) dx = \int \frac{g(x)}{p(x)} p(x) dx \quad (2.24)$$

where $p(x)$ represents the importance (real-valued) function, also called the *probability density function* (PDF) [73], which satisfies the following conditions [92, 95]:

- $p(x) \geq 0$ for each $x \in [0, 1]$ for which $f(x) \neq 0$,
- $\int_0^1 p(x) dx = 1$,
- $\frac{g(x)}{p(x)} < \infty$ except perhaps on a (countable) set of points.

Thus, to solve Equation 2.24, we have two alternatives:

- draw samples from g , attach weights given by p and sum them, or
- draw samples ξ_i with the density given by p , evaluate $g(\xi_i)$ and sum them.

In this section we focus on the second alternative, and, in order to apply it, one often uses a technique called warping [60, 133]. This technique consists of generating uniform distributed samples in a canonical space, and, afterwards, deform that space to match the desired density given by p .

The key aspect of any importance sampling application is the selection of the PDF. For example, for the problem represented by Equation 2.24, an optimal PDF $p(x)$ would be given by $p(x) = Cg(x)$, with the constant C represented by $\frac{1}{\Theta}$! Clearly this is not an option, since, if already knew Θ , we would not need to use Monte Carlo techniques to estimate it. The practical solution is to choose a function $\tilde{p}(x)$ “close” to $p(x)$. We will examine this aspect in more detail in the next sections.

2.5.2 Probability Density Functions

For the sake of simplicity, since the transmission is usually handled very similarly to reflection, in the following presentation we will focus on the BRDF (f_r), implicitly including the BTDF by analogy.

In order to solve the rendering equation using importance sampling, one usually resorts to stochastic ray-tracing, in which new scattering directions have to be sampled recursively at each intersection point such that:

$$L_r(x, \psi) = L_e(x, \psi) + f_r(x, \psi, \psi_i) L_e(x', \psi') + f_r(x, \psi, \psi_i) f_r(x', \psi', \psi'_i) L_e(x'', \psi'') + \dots \quad (2.25)$$

where:

- L_r = reflected radiance,
- L_e = emitted radiance,
- x = point on the surface,
- f_r = BRDF,
- ψ_i = direction from which light comes in,
- ψ = direction in which light is reflected.

In a path tracing implementation of Equation 2.25, for example, the x^n is chosen by sending a ray from x^{n-1} in the direction $-\psi^{n-1}$, and ψ^{n-1} is chosen according to a PDF based on the BRDF of the surfaces of the environment. Ideally, to choose reflected ray directions for radiosity [134] or stochastic ray-tracing [91] calculations, one should be able to sample according to the following PDF:

$$PDF(\psi) = \frac{f_r(x, \psi_i, \psi) \cos\theta_i}{\int_{\Omega} f_r(x, \psi_i, \psi) \cos\theta_i d\omega_i} \quad (2.26)$$

where:

- Ω = hemisphere,
- $d\omega_i$ = differential solid angle around ψ_i ,
- $\cos\theta_i$ = cosine of the angle between ψ_i and the surface normal at x .

In practice one often has to use an approximating PDF. Before getting to the specifics of the PDFs presented in this section, it is relevant to examine more closely a BRDF which constitutes the basis for the derivation of a number of PDFs frequently used in rendering applications involving the simulation of non-Lambertian phenomena. The formulation of this BRDF is based on a modified version of the Phong model [96, 99].

The original Phong model [122] does not have a physical basis and cannot be used as a BRDF in physically-based rendering applications. Immel *et al.* [83] has suggested a Phong-like BRDF, however, which was later constrained by Lewis [100] to become physically plausible and used in rendering applications. This BRDF is given by:

$$f_r(x, \psi_i, \psi) = \frac{\rho_d}{S_d} + \frac{\rho_s}{S_s} \cos^n \alpha_b \quad (2.27)$$

where:

- α_b = angle between the halfway vector between the source and viewing directions and the normal,
- ρ_d = the diffuse reflectance,
- ρ_s = the specular reflectance,
- n = the specular exponent,
- S_d and S_s = constant factors included to conserve energy.

Recall that in order to conserve energy (Section 2.2) the following relation has to be satisfied:

$$\rho(x, \psi) = \int_{\Omega} f_r(x, \psi_i, \psi) \cos\alpha \, d\omega \leq 1 \quad \forall x, \psi_i \quad (2.28)$$

with the differential solid angle given by:

$$d\omega = \sin\alpha \, d\alpha \, d\beta \quad (2.29)$$

where:

- α = polar angle ($\alpha \in [0, \frac{\pi}{2}]$ for the upper hemisphere),
- β = azimuthal angle ($\beta \in [0, 2\pi]$).

Using Equation 2.28, the constant factor S_d is given by:

$$\begin{aligned} S_d = \int_{\Omega} \cos\alpha \, d\omega &= \int_{\beta=0}^{2\pi} \int_{\alpha=0}^{\frac{\pi}{2}} \cos\alpha \, \sin\alpha \, d\alpha \, d\beta \\ &= - \int_{\beta=0}^{2\pi} \int_{\alpha=0}^{\frac{\pi}{2}} \cos\alpha \, d\cos\alpha \, d\beta \\ &= -2\pi \left[\frac{\cos^2\alpha}{2} \right]_0^{\frac{\pi}{2}} = \pi \end{aligned} \quad (2.30)$$

and the constant factor S_s is given by:

$$\begin{aligned}
 S_s &= \int_{\Omega} \cos^{n+1} \alpha \, d\omega = \int_{\beta=0}^{2\pi} \int_{\alpha=0}^{\frac{\pi}{2}} \cos^{n+1} \alpha \sin \alpha \, d\alpha \, d\beta \\
 &= - \int_{\beta=0}^{2\pi} \left[\frac{\cos^{n+2} \alpha}{n+2} \right]_0^{\frac{\pi}{2}} d\beta \\
 &= \frac{1}{n+2} \int_{\beta=0}^{2\pi} d\beta \\
 &= \frac{2\pi}{n+2}
 \end{aligned} \tag{2.31}$$

Replacing S_d and S_s in Equation 2.27 [96] gives:

$$f_r(x, \psi_i, \psi) = \frac{\rho_d}{\pi} + \rho_s \frac{n+2}{2\pi} \cos^n \alpha_b \tag{2.32}$$

Usually specular directions are sampled according to the following PDF based on the specular component of Equation 2.32 [133]:

$$PDF(\alpha, \beta) = \frac{n+1}{2\pi} \cos^n \alpha \tag{2.33}$$

Diffuse directions, on the other hand, are commonly sampled using the following PDF [96, 133]:

$$PDF(\alpha, \beta) = \frac{1}{\pi} \cos \alpha \tag{2.34}$$

Another PDF based on the specular component of Equation 2.32 was proposed by Shirley and Wang [137], and it is given by:

$$PDF(\alpha_p, \beta_p) = \frac{n+2}{8\pi} \cos^n \left(\frac{\alpha_p}{2} \right) \tag{2.35}$$

where:

- α_p = angle between the perfect reflection direction and the outgoing direction,
- β_p = azimuthal angle around the reflection direction.

2.5.3 Warping Functions

As pointed out by Lafortune and Willems [96], the space of directions in 3D space is two-dimensional. Consequently, the PDFs presented in the previous section can be sampled by selecting two uniform stochastic variables, ξ_1 and ξ_2 , over the interval $[0,1]$, and transforming them using the warping technique mentioned in Section 2.5.1. In this section we present the derivation of the warping functions used in the research described in this tutorial (Chapters 7 and 8), which correspond to the PDFs described by Equations 2.33 and 2.34.

Before presenting the derivations, we shall briefly review some relevant concepts. If a random variable ξ ranges over some region \mathcal{U} , then the probability that ξ will take on a value in some subregion $\mathcal{U}_i \subset \mathcal{U}$ is given by:

$$\mathcal{P}(\xi \in \mathcal{U}_i) = \int_{\xi' \in \mathcal{U}_i} PDF(\xi') \, d\mu(\xi') \quad (PDF : \mathcal{U} \rightarrow \mathbb{R}^1) \tag{2.36}$$

where $\mathcal{P}(\text{event})$, also called cumulative distribution function [73], is the probability that the *event* is true [133]. In computer graphics applications \mathcal{U} is typically an area ($d\mu = dA = dx \, dy$) or a set of directions ($d\mu = d\omega = \sin \alpha \, d\alpha \, d\beta$).

Initially, consider the PDF given by Equation 2.33. The corresponding cumulative distribution function is given by:

$$\mathcal{P}(\alpha, \beta) = \int_0^\beta \int_0^\alpha \frac{n+1}{2\pi} \cos^n \alpha' \sin \alpha' d\alpha' d\beta' \quad (2.37)$$

Since the PDF presented in the integrand of Equation 2.37 is separable [133], derivation techniques can be applied on each dimension to find the warping function used to generate the corresponding scattered directions [133]. Solving Equation 2.37 in the dimension associated with α results in:

$$\int_0^\alpha \frac{n+1}{2\pi} \cos^n \alpha' \sin \alpha' d\alpha' = \left[-\frac{n+1}{n+1} \cos^{n+1} \alpha' \right]_0^\alpha = -\cos^{n+1} \alpha + 1 \quad (2.38)$$

then we have:

$$\xi_1 = -\cos^{n+1} \alpha + 1 \quad (2.39)$$

or:

$$\alpha = \arccos(1 - \xi_1)^{\frac{1}{n+1}} \quad (2.40)$$

Solving for the dimension associated with β gives:

$$\int_0^\beta \frac{1}{2\pi} d\beta' = \frac{\beta}{2\pi} \quad (2.41)$$

from which we get:

$$\xi_2 = \frac{\beta}{2\pi} \quad (2.42)$$

or:

$$\beta = 2\pi\xi_2 \quad (2.43)$$

Therefore, the corresponding warping function is represented by:

$$(\alpha, \beta) = (\arccos(1 - \xi_1)^{\frac{1}{n+1}}, 2\pi\xi_2) \quad (2.44)$$

Finally, consider the PDF given by Equation 2.34. Then the corresponding cumulative density function is given by:

$$\mathcal{P}(\alpha, \beta) = \int_0^\beta \int_0^\alpha \frac{\cos \alpha'}{\pi} \sin \alpha' d\alpha' d\beta' \quad (2.45)$$

Like in the previous case, the PDF presented in the integrand of Equation 2.45 is separable, and derivation techniques can be applied on each dimension to find the warping function used to generate the corresponding scattered directions. Thus, solving Equation 2.45 in the dimension associated with α results in:

$$\int_0^\alpha 2 \cos \alpha' \sin \alpha' d\alpha' = 2 \left[-\frac{\cos^2 \alpha'}{2} \right]_0^\alpha = 2 \left(-\frac{\cos^2 \alpha}{2} + \frac{1}{2} \right) = -\cos^2 \alpha + 1 \quad (2.46)$$

from which we get:

$$\xi_1 = -\cos^2 \alpha + 1 \quad (2.47)$$

or:

$$\alpha = \arccos(\sqrt{1 - \xi_1}) \quad (2.48)$$

Solving for the dimension associated with β gives:

$$\int_0^\beta \frac{1}{2\pi} d\beta' = \frac{\beta}{2\pi} \quad (2.49)$$

then we have:

$$\xi_2 = \frac{\beta}{2\pi} \quad (2.50)$$

or:

$$\beta = 2\pi\xi_2 \quad (2.51)$$

Therefore, the corresponding warping function is represented by:

$$(\alpha, \beta) = (\arccos(\sqrt{1 - \xi_1}), 2\pi\xi_2) \quad (2.52)$$

Chapter 3

Measurement Procedures

The group of measurements necessary to characterize both the color and surface finish of an object is called the *measurement of appearance* of an object [82]. This group of measurements involves the spectral energy distribution of propagated light, measured in terms of reflectance and transmittance, and the spatial energy distribution of that light, measured in terms of the bidirectional reflectance distribution function (BRDF) and the bidirectional transmittance distribution function (BTDF).

The variations in the spectral distribution of the propagated light affect appearance characteristics such as hue, lightness and saturation [82]. Hue is the attribute of color perception by means which an object is judged to be red, yellow, green, blue, purple and so forth. Lightness is the attribute by which white objects are distinguished from gray objects and light from dark colored objects. Finally saturation is the attribute that expresses the degree of departure from the gray of the same lightness.

The changes in the spatial distribution of the propagated light affect appearance characteristics such as gloss, reflection haze, transmission haze, luster and translucency. The reflection haze corresponds to the scattering of reflected light in directions near that of specular reflection by a specimen having a glossy surface [82]. The transmission haze corresponds to the scattering of light within or at the surface of a nearly clear specimen, responsible for cloudy appearance seen by transmission [82]. Finally, the luster, or contrast gloss, as described by Hunter and Harold [82], corresponds to the gloss associated with contrasts of bright and less bright adjacent areas of the surface of an object. Luster increases with increased ratio between light reflected in the specular direction and that reflected in diffuse direction which are adjacent to the specular direction.

Actual measurements of reflectance and transmittance are performed using spectrophotometers, and the actual measurements of BRDF and BTDF are performed using goniophotometers [82, 88]. These devices are important basic tools for fundamental research in colorimetry [105], solar engineering [50], remote sensing [42, 86] and plant biochemistry [24, 86]. In this section we discuss the computer simulations of such devices, henceforth called virtual measurement devices. The use of these virtual devices gives us control over the spectral data generation from computer models and allows us to perform experiments at different sampling resolutions, which are essential requirements for rendering applications as pointed out by Lalonde and Fournier [97].

Two applications of virtual measurements are especially relevant for biologically and physically-based rendering. The first application corresponds to virtual measurements aimed at the testing and evaluation of reflectance and BDF models through comparisons with actual measurements. Obviously, these models can be verified against measurements of real materials. However, in order to obtain the readings from the computer models in the first place one must perform a computer simulation of the inputs and outputs of the model, *i.e.*, use a virtual device. Moreover, the formulation of this virtual device has to reproduce actual measurement conditions as faithfully as possible to minimize the introduction of bias in the comparisons.

It may be argued that wildly different computer models can provide the same reflectance for a given illuminating, or incidence, geometry. However, for practical purposes the evaluation of a computer model will take into account how close, quantitatively and qualitatively, the overall curves provided by this model are from the actual curves for different measurement instances. For example, suppose that the spectral curves provided by a reflectance model A have an average discrepancy of 5% with respect to the actual curves and the curves provided by a model B have an average discrepancy of 30%. Which one should be incorporated into a rendering framework?

The second application corresponds to data generation from previously validated computer models. This may involve a large number of measurements of different wavelengths and illuminating geometries. Such data can sometimes be found in the literature where actual measurements from real materials are reported. However, more often it is not available and even when it is available it is only for a restricted number of measurement configurations. For example, the most comprehensive set of

experiments involving leaf optical properties performed to date [81] was limited to a small number of illuminating geometries.

In the computer graphics literature when virtual measurement devices are discussed, they are usually presented in connection with a scattering model. For example, Gondek *et al.* [64] have used a device for spectral and spatial measurements, a virtual goniospectrophotometer, presented as an optics model and a capture dome used in conjunction with a geometric model of surface microstructure. In this section the formulation of virtual measurement devices are considered regardless of the reflectance and transmittance model being used.

3.1 Virtual Spectrophotometry

There are many scattering models in the computer graphics literature classified as reflectance and transmittance models. This classification is in many cases not entirely accurate since they only model the BRDF and BTDF using reflectance and transmittance values, which correspond to input data, as scaling factors, or “weights”, for the spatial distribution of the scattered light. For example, the model described in Chapter 6 and the model described in Chapter 8 can be used to render a plant leaf under different lighting conditions, provided its reflectances and transmittances for different wavelengths and illuminating geometries are available as data for the model.

The question is: Where does the data for these models [75], for example, come from? This question highlights two important issues related to biologically and physically-based rendering. First, it shows the need for developing models to compute reflectances and transmittances, specially for organic materials. Second, it shows the need for developing accurate and efficient measurement procedures, as pointed out in the recent *Workshop on Metrology and Modeling of Color and Appearance*¹.

3.1.1 Characteristics of Actual Spectrophotometers

A spectrophotometer is defined to be any instrument for measuring the spectral distribution of reflected and transmitted radiant power, and spectrophotometry is defined as the quantitative measurement of reflection and transmission properties as a function of wavelength [48]. Spectrophotometers can also be used to determine the absorption characteristics of an object as a function of wavelength.

Actual measurements of reflectance and transmittance are performed using spectrophotometers equipped with an integrating sphere. An integrating sphere is usually used to measure the hemispherical reflectance factor, *i.e.*, a reflectance factor for a hemispherical reflected solid angle [117]. The numerical values of the reflectance and the reflectance factor are, however, identical under the conditions of hemispherical collection [60].

For absolute measurements, the sphere wall is the standard, and the integrating sphere theory [61] compensates for the absolute reflectance of the sphere wall by mathematically treating the wall reflectance as unity. Hence the hemispherical measurements made with such integrating spheres correspond to absolute values of reflectance (or transmittance), which are subject to small errors associated with factors such as aperture losses, small values of non-uniformity of sphere wall reflectance and stray reflectance from sample mounts [159].

The precision of a real spectrophotometer is estimated by the ability of the instrument to replicate a measurement for a given specimen under same spectral and geometrical conditions [88]. The best-designed, best-constructed, and best-calibrated spectrophotometers still yield results that differ from one measurement to the next. According to MacAdam [105], the differences among readings should be quite small and randomly different. These differences, or uncertainties, are net results of combinations of many small fluctuations due to mutually unrelated variations of different components of the instrument, different factors in the environment and how the specimen is handled. In theory, a spectrophotometer is considered to be of high precision if the spectral measurements have an uncertainty, μ , of approximately ± 0.001 [88, 105]. This means that at one time the device may read, for instance, a reflectance value equal to 0.375, but at other times it may read values as low as 0.374 or as high as 0.376. In practice, however, spectrophotometers usually have an absolute accuracy between 0.993 and 0.995, *i.e.*, an uncertainty between ± 0.007 and ± 0.005 measurement units [159]. The accuracy of a spectrophotometer is measured by the ability of the device to provide, for a given illuminating and viewing geometries, the true spectral reflectance and transmittances of a given specimen, apart from random uncertainties occurring in repeated measurements [88].

¹ <http://slp.nist.gov/>

3.1.2 Formulation of Virtual Spectrophotometers

Emitters and specimens used in actual measurements usually have circular areas [42, 61, 81, 159], which can be represented by disks with radii \mathcal{R}_1 and \mathcal{R}_2 separated by a distance D (Fig. 3.1). A spectrophotometer with integrating sphere is simulated by sending (or shooting) sample rays from the emitter towards the specimen. These rays arrive at the specimen through a solid angle, ω_i , in the direction of incidence ψ_i , which is given by a pair of spherical coordinates (ϕ_i, θ_i) (Fig. 3.1). We denote the total number of sample rays used in a virtual spectrophotometric measurement by N .

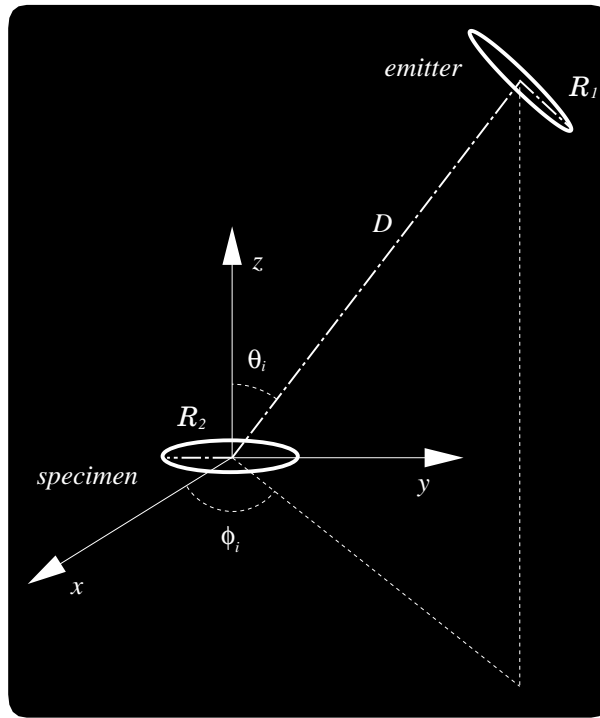


Figure 3.1: Sketch of a virtual spectrophotometer.

Consider N rays shot towards the specimen for a given wavelength λ . One can assume that each ray carries the same amount of radiant power, Φ . If the total radiant power to be shot is Φ_i , then the radiant power carried by each ray is given by [133]:

$$\Phi_{ray}(\lambda) = \frac{\Phi_i(\lambda)}{N} \quad (3.1)$$

Recall that reflectance describes the ratio of reflected power to incident radiant power and transmittance describes the ratio of transmitted radiant power to incident power [117]. Considering this ratio, if m rays are reflected towards the upper hemisphere Ω_r , the reflectance of the specimen with respect to a given wavelength λ of the incident light will be given by:

$$\rho(\lambda, \vec{\omega}_i, \Omega_r) = \frac{m}{N} \quad (3.2)$$

Therefore, since one can simply count the number of rays reflected to the upper hemisphere to determine a specimen's reflectance, a virtual spectrophotometer does not need to use an integrating sphere to collect the reflected rays. The specimen's transmittance is calculated in a similar manner, *i.e.*, by counting the number of rays transmitted to the lower hemisphere.

Model dependent issues, such as the use of weights associated with rays, will not be dealt with in this chapter. In the same way that an actual spectrophotometer is completely independent of how the specimen interacts with light, a virtual spectrophotometer shall also be independent of the reflectance model being tested. Moreover, these weights are usually based on reflectances and transmittance values. As mentioned before, if we knew these values *a priori* there would be no point in carrying out spectrophotometric measurements.

For applications involving data generation from a previously validated model, the sample rays are collimated since we are basically measuring directional-hemispherical reflectance [117]. In this case, the sample rays have the same origin and hit the specimen at the same point. For applications involving comparisons with actual measurements, as mentioned earlier, the actual measurement conditions must be reproduced as faithfully as possible. In these situations we are measuring conical-hemispherical reflectance [117], which requires the generation of sample rays distributed angularly according to the geometrical arrangement of the surfaces used to represent the emitter and the specimen. As mentioned by Crowther [42], the incident radiation from an emitter shows no preference for one angular region over the other. So, in order to simulate these measurement conditions, the origins and targets of the rays are random points (or sample points) chosen on the disks used to represent the emitter and the specimen respectively.

Several sampling strategies may be used to select the sample points on the disks [133]. In this tutorial we do not intend to determine the most accurate or the most efficient sampling strategy. The merits and drawbacks of different sampling strategies have been adequately covered elsewhere [60, 133]. One of the sampling strategies that can be used in virtual measurements is based on standard random sampling [133]. It consists of generating sample points inside a square with sides $2\mathcal{R}$ and throwing away points lying outside an inscribed disk of radius \mathcal{R} [42]. The sample points in the square are generated using uniformly distributed random numbers ξ_1 and ξ_2 on the interval $[0, 1]$ and the following transformation:

$$(x, y) = \mathcal{R}(2\xi_1 - 1, 2\xi_2 - 1) \quad (3.3)$$

where the pair (x, y) corresponds to the coordinates of a sample point.

Another strategy that can be used in virtual measurements is based on the classical Monte Carlo stratified sampling or jittered sampling [133]. It uses a warping transformation to guarantee that the sample points are reasonably equidistributed on a disk, and enables the computation of the pair (x, y) through the following warping function:

$$(x, y) = (2\pi\xi_1, \mathcal{R}\sqrt{\xi_2}) \quad (3.4)$$

After generating the x and y coordinates of a sample point, using either approach mentioned above, the z coordinate is added. For a sample point on the specimen, z is equal to zero, and, for a sample point on the emitter, z will correspond to the distance D between the disks (Fig. 3.1), which is given by the radius of the integrating sphere of a real spectrophotometer. Finally, to obtain the origin of a sample ray, the corresponding sample point (x, y, z) on the emitter shall be rotated according to a specified incidence geometry given by ϕ_i and θ_i (Fig. 3.1).

3.2 Virtual Goniophotometry

Virtual goniophotometric measurements allow the determination of the scattering profile of specimens. These measurements can also be used to verify the physical characteristics of the computer model used to simulate such scattering profile. Among these characteristics we can list reciprocity, energy conservation and anisotropy.

3.2.1 Characteristics of Actual Goniophotometers

A goniophotometer is defined as an instrument that measures flux (power) as a function of angles of illumination and observation [48]. Figure 3.2 presents a schematic diagram showing the principal components of a goniophotometer and their geometrical arrangement. The light flux incident on the specimen comes from the emitter through aperture I . The light flux viewed by the photometer is delimited by aperture V . Both the direction of illumination and viewing can be varied independently within the hemisphere above the specimen. The position of emitter and aperture I is given by its azimuth angle ϕ_i and its polar angle θ_i . The position of photometer and aperture V is given by its azimuth angle ϕ_r and its polar angle θ_r .

As mentioned by Judd and Wyszecki [88], to obtain a complete goniophotometric record for a simple specimen would be necessary to perform a formidable number of measurements. Both the emitter and the photometer would have to be moved independently of one another to every position on the hemisphere. In order to illustrate this aspect Judd and Wyszecki perform the following calculation. Suppose that one works with a fairly large solid angle of approximately 0.005 steradian for each aperture. To cover the entire hemisphere (2π steradian) as closely as possible with such an aperture without overlapping, we must use about 1000 different positions. With both the source and the photometer moved in each of the 1000 positions one ends up making 1 million measurements!

For many specimens the most informative goniophotometric data are taken in the plane containing the direction of the incident light and the normal of the specimen. Many actual goniophotometers are abridged to this extent. The emitter movement goes from $\theta_i = 0^\circ$ to $\theta_i = 90^\circ$ and the photometer movement ranges $\theta_i = 90^\circ$ to $\theta_r = -90^\circ$. Assuming the same aperture sizes as before, this abridged goniophotometric record would contain $18 \times 36 = 640$ data points. Like the accuracy of spectrophotometers (Section 3.1.1), the accuracy of a goniophotometer is also estimated by the ability of the instrument to replicate a measurement for a given specimen under same spectral and geometrical conditions [88].

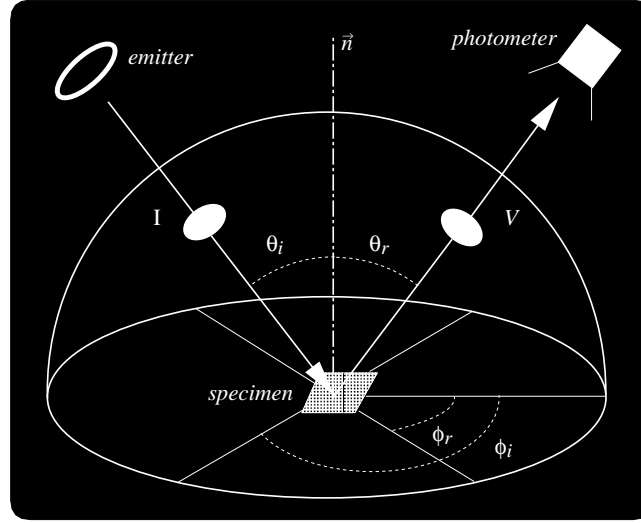


Figure 3.2: Sketch of a goniophotometer (redrawn from [88]).

3.2.2 Formulation of Virtual Goniophotometers

In order to simulate radiance measurements performed by placing the photometer at different viewing positions one can use radiance detectors, which are represented by the patches of a collector sphere placed around a specimen. Using this arrangement, the BRDF for a direction associated with a given radiance detector placed in the upper hemisphere is determined in terms of radiant power. More specifically, it is given by the ratio between the radiant power reaching the detector, Φ^r , after interacting with the specimen, and the incident radiant power, Φ^i [10, 65].

The corresponding expression used to compute the BRDF for light incident at wavelength λ , considering the solid angle in the direction of incidence, ω_i^r , and the solid angle in the direction associated with the radiance detector, ω_r^p , is given by:

$$f_r(\lambda, \omega_i^r, \omega_r^p) = \frac{\Phi^r(\lambda)}{\Phi^i(\lambda) \omega_r^p} \quad (3.5)$$

where:

ω_r^p = projected solid angle regarding the direction associated with the radiance detector.

In turn, the projected solid angle ω_r^p is given by:

$$\omega_r^p = \frac{A_r \cos \theta_r}{L^2} \quad (3.6)$$

where:

A_r = area of the radiance detector,

L = distance from the specimen to the radiance detector,

θ_r = angle between the direction associated with the radiance detector and the specimen normal.

Recall that the radiant power reaching the radiance detector can be written as:

$$\Phi^r(\lambda) = m_r \Phi_{ray}(\lambda) \quad (3.7)$$

Thus, replacing Equation 3.1 and Equation 3.7 in Equation 3.5, the expression to compute the BRDF reduces to:

$$f_r(\lambda, \vec{\omega}_i, \vec{\omega}_r) = \frac{m_r}{N \vec{\omega}_r^p} \quad (3.8)$$

Similarly, the BTDF is calculated considering radiance detectors placed in the lower hemisphere.

The origins of the rays are random points uniformly chosen from a disk used to represent the surface of the emitter. The coordinates of the points are given by pairs (Θ, l) , which are computed using the warping function given by Equation 3.4. The targets of the rays may also be random points uniformly chosen from a disk used to represent the specimen. Alternatively, we can use a pair of triangles used to represent it. In this case, to choose a random point q on a triangle defined by the vertices q_0 , q_1 and q_2 we can use the following expression:

$$q = q_0 + \varphi(q_1 - q_0) + \gamma(q_2 - q_0) \quad (3.9)$$

where φ and γ are obtained using another warping function suggested by Shirley [133]:

$$(\varphi, \gamma) = (1 - \sqrt{1 - \xi_3}, (1 - \varphi)\xi_4) \quad (3.10)$$

where:

ξ_3 and ξ_4 = uniformly distributed random numbers $\in [0, 1]$.

Chapter 4

Biological Issues

One of the major difficulties in biologically and physically-based rendering is the lack of available experimental data to be used as input or for testing parameters. Appropriately Ward [153] pointed out that good science requires both theory and data, and one is of little use without the other. Fortunately, in the case of plants, there is a reasonable amount of information that can be incorporated into rendering applications.

Most of this information consists of experimental data for plant leaves, which are the most important plant surface interacting with light [87]. Although other plant surfaces, such as stems and petals, present similar optical and structural characteristics [55, 93], the ways in which they absorb and propagate light and thus acquire their color have not been fully investigated. Recently Biolley and Jay [18] presented a work on the colorimetry of roses. However, there is still a noticeable lack of understanding of the relationships between petal structure and pigment distribution [93]. For these reasons, we are going to focus on light interaction with foliar tissues in this chapter.

4.1 Structural Description of a Plant Leaf

A leaf can be described as a diffusing and pigmented structure (mesophyll) having external plates of epidermal cells with a protective skin (cuticle) [156]. Figure 4.1 shows an idealized leaf cross-section.

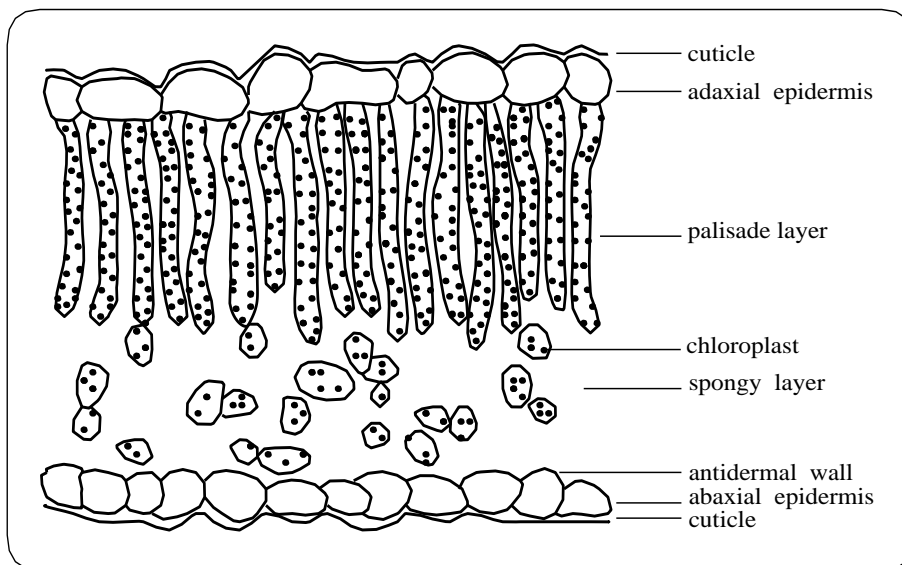


Figure 4.1: Typical cross-section of foliar tissues.

The cuticle is an extracellular, multilayered membrane of pectin, cellulose, cutin, and wax. The outermost portion of the

cuticles consists of epicuticular wax, which may be extremely thin, or so thick as to be visible to the naked eye [67, 104]. The epicuticular waxes may be amorphous, semicrystalline, or crystalline in form and exhibit a wide range of geometric configurations [68]. They may be orderly oriented vertical to the leaf surface or oriented at varying angles from the cuticle. The surface roughness characteristics and the refraction index of the epicuticular wax control the specularly reflected light from the adaxial (front) and abaxial (back) epidermis. No intercellular spaces are normally present in the epidermal tissues, and the cells usually fit one another like the pieces of a jigsaw puzzle (Figure 4.2).

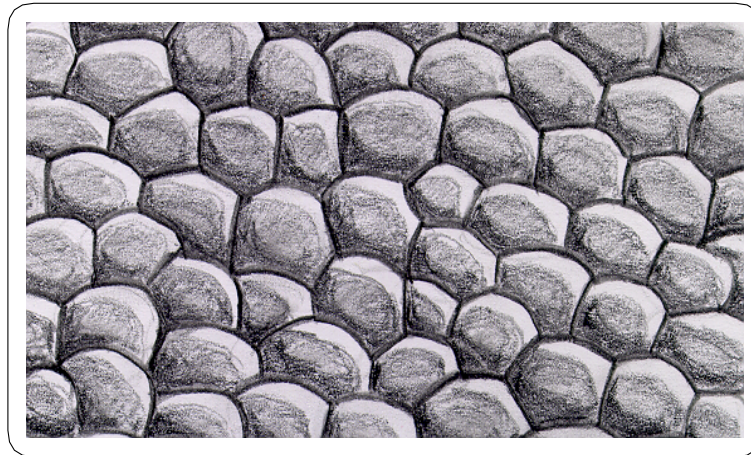


Figure 4.2: Artist's conception of a typical epidermis tissue. Redrawn from [10].

The mesophyll of bifacial leaves is usually composed of a densely packed layer of palisade cells, and a loosely packed layer of spongy cells. There are species of plants, however, that present unifacial leaves which either do not have palisade mesophyll [151] or have it attached to both the front and the back surfaces of a leaf [26]. The palisade cells have a cylindrical shape, and 5 to 20% of their volume is air space. These cells present a high concentration of chloroplast which contain pigments, namely chlorophylls (mainly *a* and *b* forms) and carotenoids. The concentration and distribution of these pigments control the absorption of the light in the visible region of the light spectrum within the leaf (see Section 4.2). The spongy tissue consists of smaller cells, roughly ovoid to round in shape, that present less densely packed chloroplasts, with 50 to 80% of their volume occupied by air space [156]. The spaces between the mesophyll cells are also filled with air.

4.2 Factors Affecting the Propagation of Light

In order to simulate the mechanisms of photon transport within the foliar tissues, it is necessary to account for the biological and structural characteristics of these tissues and their components. Factors like the presence of pigments and the internal distribution of the tissues have a significant impact on how leaves propagate and absorb light. In this section we outline the main factors that affect the reflection, transmission and absorption of light by plant leaves.

4.2.1 Internal Structure and Thickness

The intra-leaf scattering caused by refractive index differences between cellular organelles, walls, hydrated cells, and adjacent intercellular air spaces is compounded or amplified by the irregular shapes and organization of the cells within the leaf [144]. As pointed out by Grant [67], differences in the reflectance curves among species, as well as changes with maturation and senescence, have also been attributed to differences in the leaf internal structure. These differences directly affect the thickness of the leaves. Experiments by Wooley [156] showed that, although the reflectance of a leaf is not strongly dependent on the leaf thickness, the transmittance is strongly affected by this foliar characteristic. Allen *et al.* [5] assert that the differences in internal structure are substantial between sun and shade leaves of the same plant species. Clearly, even greater differences can be expected between leaves from different species.

4.2.2 Surface Features

A small amount of incident light is initially reflected from the upper cuticular surface for angles of incidence smaller than 45° [156]. Grant [67] states that the presence of hairs in some species affects qualitatively and quantitatively the reflectance, by presenting numerous light scattering interfaces which decreased the amount of light entering the leaf, thereby decreasing absorption. The reflectance curves of leaves are also affected by their venation system [156]. It is likely that their increased thickness and lower concentration of pigments affect the reflection and transmission of light [68]. However, biological data for these characteristics of the venation systems is scarce. As described by Esau [49], a leaf may have a single vein or two or more. Single-veined leaves are found among conifers¹, while multiveined leaves are common in higher ferns² and angiosperms³. Although the major venation system of these species can be divided in two main types of patterns, namely parallel (or striate) and reticulate (or net), the minor venation system exhibits a wide range of intergrading patterns (Figure 4.3).



Figure 4.3: Photographs of venation systems of different plant leaves. On the left the parallel venation system of a *hosta* leaf, and, on the right a reticulate venation system of a *magnolia* leaf. Redrawn from [26].

4.2.3 Pigments Composition, Concentration and Distribution

Experiments [144, 156] showed that the reflectance of leaves is relatively low in the visible portion of the light spectrum (400nm to 700nm), and that absorptance dominates. Most of the absorption in this region is caused by pigments presented in the leaf tissue. Pigments are materials that exhibit selective reflection and selective absorption [60]. The usual pigments found in leaves are the chlorophylls and the carotenoids. As pointed out by Devlin and Baker [44], the chlorophylls are by far the most important and abundant of these pigments, and they are usually concentrated in the palisade mesophyll. There are several forms of chlorophyll [149], and the dominant ones are chlorophylls *a* and *b*. Although the relative pigment concentrations vary within the species, most of the plants contain two to three times more chlorophyll *a* than *b* [128]. These two forms of chlorophyll present similar absorption spectra (curve showing the absorption coefficient of the material at various wavelengths), and some researchers combine them into a single curve due to the high correlation between them [85]. The carotenoids are a group of pigments which, in higher plants, are usually red, orange, yellow, or brown and are associated with chlorophyll in the chloroplasts [128]. Their yellow colors are evident in many autumn leaves from which the chlorophyll has disappeared. Senescent leaves present also brown pigments called tannis. However, to the best of our knowledge, there is not yet a method to determine the concentration of brown pigments [85].

¹ Conifers correspond to one of the major groups of gymnosperms (vascular and flowerless plants characterized by the presence of seeds). They typically bear cones and needle-like leaves, *e.g.* pine and redwood [17].

² Ferns form the most widely known group of pteridophytes (vascular and flowerless plants which do not produce seeds). They present feathery fronds formed by large leaves, usually deeply parted or divided, *e.g.* wood fern [17].

³ Angiosperms, or flowering plants, dominate large areas of the land surface and represent the climax of vascular plant evolution. They are very diversified in their form and range in size from few millimeters in diameter (aquatic *Lemma*) to over 90 meters in height (*Eucalyptus*) [26].

4.2.4 Water Content

The concentration and distribution of water affects the absorption of light in the infrared region, but have no significant effect on the absorption of light in the visible region [144]. However, as water is lost from a fully turgid leaf, the reflectance increases. Different patterns in this increase are seen in different types of leaves. Wooley [156] hypothesized that the reason might be the changes in intercellular air spaces.

4.3 Scattering Profile of Plant Leaves

For most of twentieth century the Willstatter-Stoll (W-S) theory [144] was the accepted explanation for the scattering profile of a plant leaf on the basis of the reflection of light at spongy mesophyll cells wall-air interfaces. According to this theory, the characteristics of the spongy cells causes the incident radiation to be diffused within the leaf. A portion of this scattered radiation escapes through the lower epidermis and is designated as transmitted energy. The other fraction diffuses upward and escapes through the upper epidermis. The development of this theory used an albino maple leaf and based its hypothesis upon internal geometrical optics of the leaf. This theory was based on an albino leaf to emphasize the interactions in the absence of pigment absorption. As mentioned in the previous section, a normal leaf, however, is characterized by the spectral absorption of incident radiation by pigments and water within its structure.

Since the W-S theory, several theories and models have been proposed to describe the mechanisms of light reflection, transmission and absorption by leaves resulting in a serious revision of Willstatter-Stoll's hypothesis. Grant *et al.* [67] describe leaves as having both specular and diffuse characteristics. The specular (non-Lambertian) character of the leaf reflectance arises at the surface of the leaf. For some viewing directions, the surface reflectance may be so large that the leaves appear to have the color of the light source instead of the color determined by the foliar pigments, which is usually green (Figure 4.4). This happens when the light reflected on the leaf's surface visually overwhelms the much smaller amounts of light scattered within the interior of the leaf. In other words, the leaf's surface reflectance is higher than its subsurface reflectance (Figure 4.5). The diffuse (Lambertian) character of leaf's reflectance emanates primarily from the mesophyll tissue through multiple scattering, with a small contribution of scattering from rough elements on the leaf surface. The multiple scattering within the foliar tissues also gives the leaf's transmittance a near-Lambertian distribution (Figure 4.4). Experiments performed by Wooley [156] also showed that the retroreflection⁴ associated with a plant leaf is negligible.

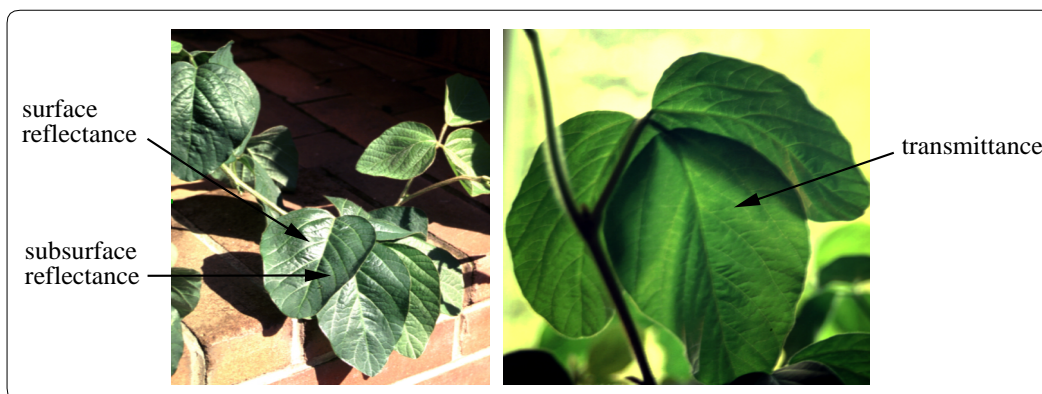


Figure 4.4: Photograph of soybean leaves showing the three components of the BDF of foliar tissues: surface reflectance, subsurface reflectance and transmittance.

Three types of scattering occur within the foliar tissues: Rayleigh, Mie and refractive-reflective scattering [144]. Rayleigh and Mie scatterings occur for particles of size equal to or less than the wavelength of the incident light respectively [60]. In the case of the foliar tissues these particles correspond to organelles and macromolecules. Although the extent and the exact

⁴ Usually a "surface" having a pronounced 3-D microstructure, such as that of a forest viewed from an airplane, is likely to show retroreflection, *i.e.* the peak of reflectance along the angle of incidence, instead of near that of mirror reflection [88].

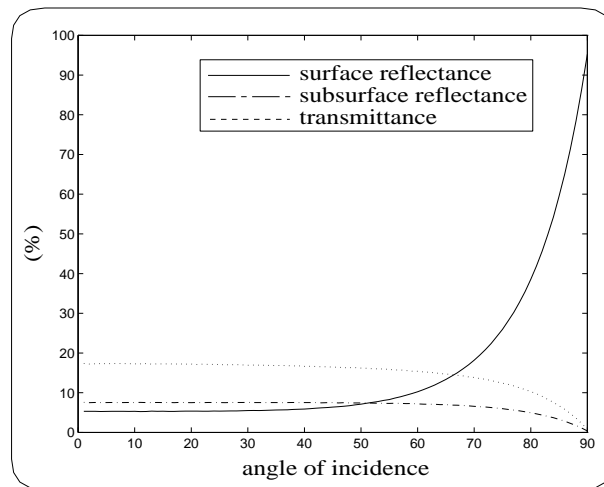


Figure 4.5: Curves of reflectance and transmittance of a soybean leaf obtained using the ABM (Chapter 7) at a wavelength of 550nm and considering the front (adaxial epidermis) of the leaf towards the light source.

causes of these forms of scattering in foliar tissues have not yet been completely resolved, their contribution to the total internal scattering is considered to be very low compared with the reflective-refractive scattering [144]. This type of scattering accounts for most of the diffusion or internal scattering, and it is mainly caused by the arrangement of tissues, and the refractive index differences, which, for the most part, are associated with air-cell wall interfaces regarding cells whose dimensions are quite large compared with the wavelength of light such as the palisade and spongy cells.

In species having bifacial leaves the adaxial epidermis is attached to the mesophyll over most of its inner surface (Figure 4.1), so that once light has passed the outer epidermal surface, it can easily pass into the center of the leaf. The light entering or leaving the abaxial surface of a leaf must, however, pass through two semiplanar interfaces, namely the air-abaxial epidermis and the air-antidermal wall interfaces (Figure 4.1). Thus light from a source on the back side of a leaf can penetrate the back epidermis and be reflected back by the inside surface of the epidermis without encountering the mesophyll. It is largely because of this aspect that the back of the leaves is often pale (Figure 4.6). Moreover, these structural differences make the abaxial surface of a leaf a greater barrier to the escape of the oblique light than the adaxial surface. These factors explain why leaves that differ markedly in the structure of their two sides show corresponding differences in their reflectance and transmittance curves [156].

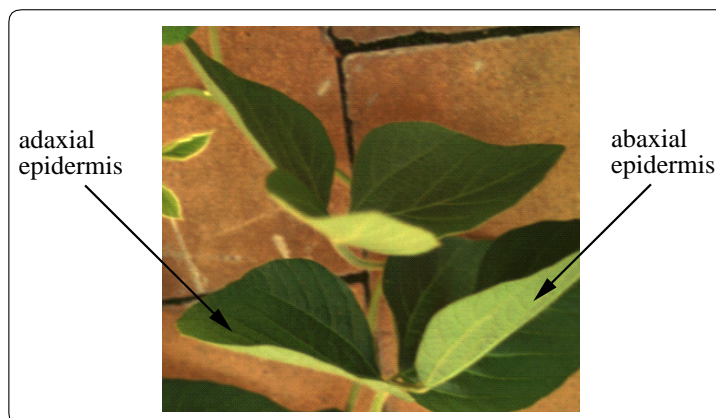


Figure 4.6: Photograph of soybean leaves showing the reflectance differences between the adaxial and abaxial surfaces.

Chapter 5

Review of Models for Botany and Remote Sensing Applications

Many researchers from areas like botany and remote sensing have proposed reflectance and transmittance models for leaves where the goal is to understand the physiological processes that relate foliar optical properties to biophysical characteristics [87]. Although we have different goals in realistic image synthesis, some concepts used in those models, such as the intuitive concept of plates or layers, can be useful in computer graphics applications as well.

In this chapter we examine relevant reflectance and transmittance models for leaves, designed mainly for botany and remote sensing applications, and group them according to their similarities. For a comprehensive literature review on this topic the reader is referred to the texts by Grant [67], Bjorn [19], Vogelmann [150] and Jacquemoud and Ustin [86].

5.1 Plate Models

Allen *et al.* [2] developed the “plate model” where the complex structure of a plant leaf can be simulated by a transparent plate with rough plane-parallel surfaces. The parallel surfaces are assumed to be Lambertian. After its penetration inside the leaf, the light flux is assumed to be diffuse (Figure 5.1). This model has two optical parameters: an effective¹ index of refraction and an effective coefficient of absorption. This model was successful in reproducing the reflectance signature of a compact corn leaf which is characterized by a relative small number of air-cell wall interfaces. Unfortunately, it cannot be applied to leaves which cannot be described as a unique compact layer such as dicotyledons² and senescent leaves.

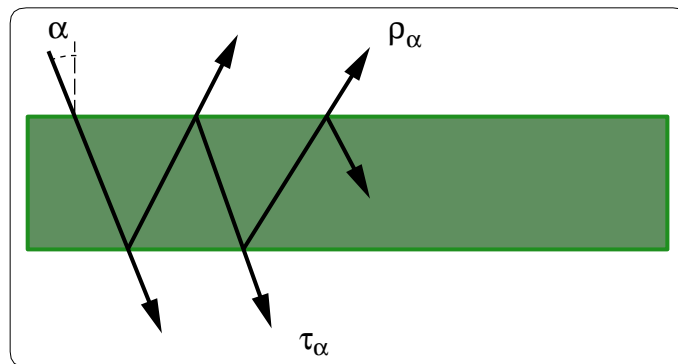


Figure 5.1: Sketch of the geometry used by the “plate model”.

Allen *et al.* [1] extended the model to non compact leaves. These leaves are regarded as piles of N plates separated by $N - 1$ air spaces (Figure 5.2). This additional parameter N plays is used to describe the leaf’s internal structure and plays a

¹ In this context the term *effective* is used to indicate that the parameters refer to the whole leaf instead of any of its constituent materials such as epicuticular wax, chlorophyll and water.

² The dicotyledons form the larger group of angiosperms bearing two cotyledons (first leaves formed in the embryo), including, for example, the broad-leaved trees, roses and sunflowers. The other group of angiosperms is formed by the monocotyledons bearing one cotyledon, including, for example, grasses, lilies, orchids, irises, palms and cannas [17].

role similar to that of the scattering coefficient used in the Kubelka-Munk theory (Section 5.2). This model is known as the “generalized plate model”.

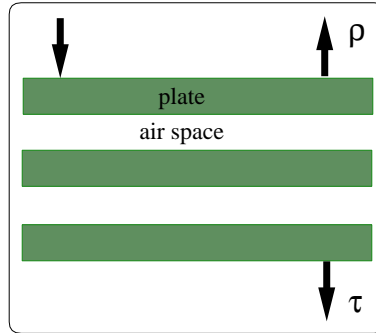


Figure 5.2: Sketch of the geometry used by the “generalized plate model”.

Jacquemoud and Baret [85] presented another generalized version of the “plate model” to be used in inversion procedures in remote sensing applications [52]. An inversion procedure is a way to derive leaf biochemical properties from *in situ* and nondestructive optical experiments. Their generalization of the “plate model” resulted in a reflectance and transmittance model for a plant leaf called *Prospect*. This model has three main parameters: pigment concentration, water content and a structure parameter N . A leaf is then assumed to be composed of a pile of N homogeneous plates or layers separated by $N - 1$ air spaces. The authors assumed a uniform distribution of water and pigments inside the leaf. The *Prospect* model was recently improved [87] using experimental data [81] to provide specific absorption coefficients for biochemical constituents (protein, lignin and cellulose).

5.2 K-M Theory Based Models

In the beginning of the century, Kubelka and Munk developed a simple relationship between the scattering and absorption coefficients of paint and its overall reflectance. This relationship is known as the K-M theory [60]. It applies the transport theory to describe the radiation transfer in diffuse scattering media with two parameters: the scattering and the absorption coefficients. Paint is physically composed of many small colored pigment particles suspended in some sort of colorless base such as oil or water [60, 145]. Similarly, a leaf or a petal may be described as a diffuse scattering medium containing pigments.

The original K-M theory is, however, valid only for “macrohomogeneous” layers, *i.e.*, layers characterized by invariant scattering and absorption coefficients, with laterally infinite extensions. As pointed out by Bjorn [19], a leaf or a plant canopy cannot be described as a single macrohomogeneous layer. Moreover, the original K-M theory is strictly valid only if the light is completely diffuse. Duntley [47] has extended it to incorporate, among other factors, specular (directional) light. The extensions proposed by Duntley have been applied to plant canopies by Allen and Richardson [4], Allen *et al.* [3] and Suits [141].

The K-M theory as originally stated is considered to be a two-flux theory, since only two types of radiant flux are involved, namely a diffuse downward flux and a diffuse upward flux. The relations between the fluxes are expressed by two simultaneous linear differential equations [147]. Allen and Richardson [4] proposed a reflectance and transmittance model for leaves based on the K-M-Duntley theory, which later resulted in the *AGR* model [3] (named after its developers). In this model, used to simulate stacked leaves, a direct solar flux is included, making it a three-flux theory with three differential equations and five coefficients.

Suits [141] added another flux type associated with the radiance in the direction of observation, making it a four-flux theory (Figure 5.3), with four differential equations and nine coefficients. Verhoef [147, 148] improved the angular responses of the model proposed by Suits through a detailed analysis of extinction and scattering of radiant flux by leaf layers. The results of the improvements proposed by Verhoef resulted in the *SAIL* model (Scattering by Arbitrarily Inclined Leaves). The original *AGR* model was later simplified by Baret *et al.* [14] and applied to wheat leaves.

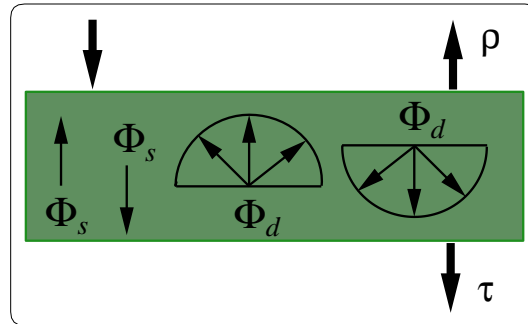


Figure 5.3: Four flux approach used by the *SAIL* model.

Yamada and Fujimura [158] proposed a K-M model of reflectance and transmittance for individual leaves aiming at inversion applications to determine chlorophyll content. They considered four macrohomogeneous layers (two cuticles, a palisade layer and a spongy layer), each described by the K-M theory, and assumed that the scattering and absorption coefficients of the K-M theory can be expressed as a linear function of the pigment content of a plant leaf. In the formulation of their model Yamada and Fujimura use several constants which are not biologically meaningful. These constants are determined using a least square method [29]. Their model was tested on different leaves and the direct relationship between the reflectance and transmittance of a plant leaf and its chlorophyll content was confirmed through experiments and direct measurements.

5.3 Ray Tracing Based Models

Ray tracing based approaches were used to simulate the propagation of light within foliar tissues in remote sensing and biological sciences even before being extensively used in computer graphics. Allen *et al.* [5] and Kumar and Silva [94] developed models where they simply traced the passage of a light ray through a drawing of a leaf cross section. Unfortunately, their experiments were not in the visible region of light spectrum and the techniques used were computationally expensive. In spite of that their conclusions form the basis of the current understanding of diffuse reflectance in leaves as pointed out by Grant [67],

Allen *et al.* [5] investigated the W-S theory of leaf reflectance (Section 4.3) by tracing rays through a two-dimensional (2-D) model of a leaf consisting of a single medium and air, in which the internal cellular structures were approximated by arcs. The optical properties of the medium were specified by a complex index of refraction. For a given incident ray, new reflected and transmitted rays were generated at each interface using Snell's law, Fresnel equations (Section 2.1) and Lambert's law of absorption (Section 2.3). Although their results were not in good agreement with the theory (the predicted reflectance was too high and the predicted transmittance was too low), their experiments suggested that a ray tracing approach might yield more accurate results if it was generalized to a more realistic model of a plant leaf.

In the model proposed by Kumar and Silva the leaf was assumed to consist of homogeneous and isotropic media³ This assumption was made for mathematical simplicity so that the Fresnel equations could be applied to each interface. The Rayleigh and Mie scattering, as in the previous models, were not considered. Kumar and Silva proposed two different levels of detail to trace the rays within the leaf. In the first level only the two most important interfaces are considered: air to cell wall and cell wall to air. In the second level the four leaf main constituents, namely cell wall, chloroplasts, cell sap and air, give raise to the following eight optical interfaces in the leaf, all of which were considered in the ray tracing:

- air to cell,
- cell sap to cell wall,
- chloroplasts to cell wall,

³In an isotropic medium only the angle between the incident and scattered directions matters, not their absolute location [60]. In other words, as described by Glassner [60], the direction of the incident and scattered directions don't matter.

- cell sap to chloroplasts,
- chloroplasts to cell sap,
- cell wall to chloroplasts,
- cell wall to cell sap and
- cell wall to air.

Their experiments showed that considering only cell wall to air and air to cell wall interfaces is likely to give less diffuse reflectance and transmittance than that given by considering all the eight interfaces. Kumar and Silva also claimed that their model can be used to simulate the optical phenomena in the visible region of the light spectrum through the use of appropriate indexes of refraction of the leaf constituents in the visible region.

Recently Govaerts *et al.* [66] proposed a Monte Carlo ray tracing based model, *Raytran*, to simulate the propagation of light in a typical dicotyledon leaf. In their simulation approach the three-dimensional (3-D) internal cellular structure of various leaf tissues is explicitly geometrically modeled (Figure 5.4). A typical foliar cell is defined by Govaerts *et al.* as a set of concentric objects filled with three different media, namely cell wall material, water and chlorophyll, and the different shapes of these cells are approximated by primitive objects such as spheres, ellipsoids and cylinders. Although the modeling of individual cells may improve the accuracy of the simulations, the complexity of the resulting (3-D) geometrical model is likely to place a substantial demand on computational resources to trace the ray paths.

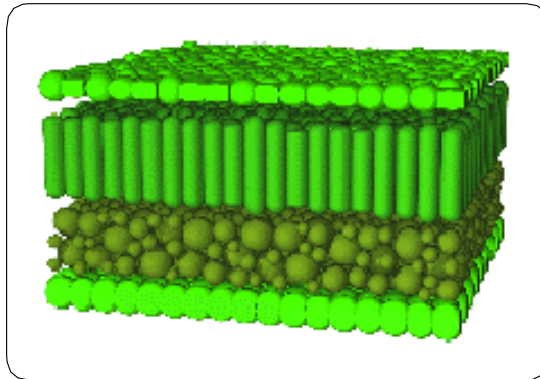


Figure 5.4: Three-dimensional model of the internal cellular structure of various leaf tissues used by *Raytran*. Redrawn from [86].

In the *Raytran* each cell constituent is characterized by an index of refraction and an absorption coefficient. The interaction of light with various cell constituents is also simulated using the Fresnel Equations (Section 2.1). The absorption testing assumes a homogeneous distribution of pigments, and it is performed probabilistically, using an expression based on Beer's law (Section 2.3), and considering the incident rays perpendicular to the interfaces. Although the results presented by the model proposed by Govaerts *et al.* seemed to qualitatively approximate the spectral curves of a plant leaf, direct comparisons with curves obtained experimentally would be needed to determine the quantitative accuracy of their results.

5.4 Radiative Transfer Theory Based Models

Tucker and Garret [144] proposed a stochastic leaf radiation model, *LFMODI*, based upon leaf structure, pigment composition and concentration of water content. The radiative interactions within a leaf are considered as a random walk process [73], using the *Markov chain*⁴ approach. Their stochastic model compartmentalizes a leaf to represent the radiation states, cell

⁴A sequence of random variables, x_0, x_1, x_2, \dots , generated such that at each time $t \geq 0$, the next state x_{t+1} is sampled from a distribution $P(x_{t+1} | x_t)$, which depends only on the current state of the chain, x_t , is called a *Markov chain* [59].

parts, and internal scattering. The radiation states, namely solar, reflected, absorbed, and transmitted, are represented by six compartments:

- solar input;
- reflection from cuticle;
- absorption in the palisade cells;
- diffuse reflected radiation;
- absorption in the spongy cells;
- diffuse transmitted radiation.

Although the model predictions for leaf spectral absorption, reflection, and transmission closely agree with measured values for the non-visible region of the light spectrum, the simulation results did not account for the high degree of absorption which occurs in the visible region. Nevertheless, this model provides a technically sound approach for simulating light interactions with plant leaves. Tucker and Garret claim that the success in their modeling approach depends upon the calculation and justification of accurate probabilities to represent the flows between and within states. This approach was extended by Lüdeker and Günther [103] with the introduction of another radiation state and a revision of the transition probabilities provided by Tucker and Garrat. These improvements resulted in the *SLOP* (Stochastic model for Leaf Optical Properties) model, which was further improved by Maier *et al.* [106].

Ma *et al.* [104] also used the radiative transfer theory combined with wave optics to develop a model in which a leaf is modeled as a slab of water with a irregular surface and containing randomly distributed scatterers (Figure 5.5). They assume that the surface roughness is of relatively great size compared with the incident light wavelength and it undulates on a large scale. This assumption allowed them to apply the Kirchhoff rough surface scattering theory [15] to describe the leaf surface reflectance. Ma *et al.* assumed that the scatterers inside the leaf are spherical to enable them to apply a scattering function derived from the Mie scattering theory. The optical scattering within a leaf was simulated by combining the multiple scattering with the Kirchhoff rough surface theory.

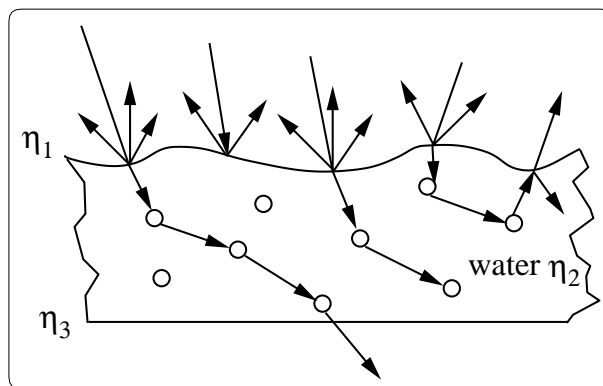


Figure 5.5: Sketch of the geometry used by the model proposed by Ma *et al.* [104].

Ma *et al.* solved the radiative transfer equations with Stokes vectors and boundary conditions [32] numerically using Fourier expansion, a discrete-ordinate technique and an eigenvalue-eigenvector method [84, 115]. Instead of providing spectral curves of reflectance and transmittance, the model proposed by Ma *et al.* determines optical parameters for different plant leaves, such as optical thickness⁵, surface roughness and refractive indexes. These parameters can, in turn, be incorporated into standard reflectance and transmittance models. Ma *et al.* also considered the depolarization of the polarized incident beam used in their

⁵The optical thickness, as presented by Ma *et al.*, is given by the product of the distance along z axis (thickness) by the particle number density and the total scattering cross section per particle.

experiments. Although Ma *et al.* claimed that they have modeled a leaf as a slab of water because the high water content of fresh leaves, as mentioned earlier, the role of the absorption pigments in the optical phenomena occurring within a leaf cannot be overlooked.

Recently Ganapol *et al.* [53, 54] used a similar approach in the design of the *LEAFMOD* (Leaf Experimental Absorptivity Feasibility MODEL). In this model the one-dimensional radiative transfer equation is solved considering a slab of leaf material with homogeneous optical properties. In the forward mode *LEAFMOD* generates an estimate of leaf reflectance and transmittance given the leaf thickness and optical characteristics of the leaf material such as the absorption and scattering coefficients. In the inverse mode *LEAFMOD* computes the total within-leaf absorption and scattering coefficient profiles from measured reflectance and transmittance, and leaf thickness. The estimates of leaf optical properties provided by this model show good agreement with measured data.

All previous models are not adapted to needle-shaped leaves. The size of individual conifer needles makes the measurement of their optical properties difficult. In practice, only the infinite reflectance of stacked samples can be performed. Recently Dawson *et al.* [43] designed the *LIBERTY* (Leaf Incorporating Biochemistry Exhibiting Reflectance and Transmittance Yields) model, which has the capacity of predicting the spectral response of both dried and fresh stacked pine needles. This model is an adaptation of radiative transfer theory for determining the spectral properties of powders proposed by Melaned [113]. *LIBERTY* provides a simulation leaf spectral properties for stacked and single samples. The determination of a single leaf optical properties was achieved through the modification of the Melaned's model in order to determine the radiation components as a function of leaf thickness. This was accomplished through an adaptation of a radiative transfer procedure proposed by Benford [16]. The results provided by this model with respect to stacked and single needles also show good agreement with measured data.

Chapter 6

The H-K Multiple-Layer Scattering Model

Hanrahan and Krueger [75] proposed a model to simulate subsurface reflection and transmission from layered surfaces, known as the *H-K* multiple-layer scattering model [60]. This intuitive idea of a layered surface model has appeared several times in physics [129], remote sensing (see Chapter 5) and computer graphics [129, 133]. The algorithm to compute the BDF is based on the linear transport theory and uses a Monte Carlo sampling scheme. The *H-K* model explicitly evaluates the reflection and transmission of light at media boundaries, like in the ocean model proposed by Nishita *et al.* [118]. It can be used to simulate the scattering profile of layered materials appearing in nature, such as biological tissues (*e.g.* skin, leaves etc.) or inorganic materials (*e.g.* snow, sand etc.). In the context of this tutorial we will focus on the application of this model to the rendering plant leaves.

6.1 Overview

The algorithm used in the scattering simulation is based on a 1D transport model which is solved with a Monte Carlo sampling scheme [60]. Transport theory is a heuristic theory based on abstracting microscopic parameters into statistical averages. It also forms the computational framework for solving the rendering equation [75]. Hanrahan and Krueger assume planar surfaces and use the Fresnel coefficients to find how much light will pass through the outermost surface of the coating. The model then evaluates the scattering and absorption within each layer, including the reflection and transmission effects at each internal boundary. The BRDF and BTDF are then described by a combination of the reflection function on the outer surface and the internal subsurface scattering handled by the Monte Carlo evaluation.

Hanrahan and Krueger assumed that if a material is a mixture of several materials, then the mixture is a uniform and homogeneous combination whose coefficients are given by a sum of the components weighted by percentage. The materials descriptors include the index of refraction, the absorption cross section, the scattering cross section, the depth (or thickness), and the phase function. The index of refraction considered is on the order of the index of refraction of water (1.33). The scattering and the absorption cross sections affect the the intensity of the backscattered and transmitted light. In this context cross section may be interpreted as the probability per unit length of an interaction of a particular type [75]. The total scattering cross section is given by the sum of the absorption cross section and the scattering cross section. The phase function represents the directional scattering of the light incident onto a particle. Hanrahan and Krueger use the one term Henyey-Greenstein phase function [80].

6.2 Scattering Simulation

The *H-K* multiple-layer model assumes that the reflected radiance from a surface has two components (Figure 8.1). One arises due to surface reflectance (L_{rs}) and the other due to subsurface volume scattering (L_{rv}). It also assumes that the transmitted radiance has two components (Figure 8.1). One, called *reduced intensity*, represents the amount of light transmitted through the layer without scattering inside the layers, but accounting for absorption (L_{ri}), and the other is due to scattering in the volume (L_{iv}). Similarly, the BRDF and BTDF have also two components, and the relative contributions of the surface and subsurface terms are modulated by Fresnel coefficients. Clearly the variations on the polar angle of incidence, given by θ_i , will affect

the value of these coefficients, which in turn will affect the magnitude of BRDF and BTDF components. The *H-K* model incorporates directional scattering within the layer through the use of the phase function, so the resulting subsurface reflection is not isotropic. However, this model does not provide the means to capture the anisotropy of plant leaves associated with different reflection behavior for different values of the azimuthal angle of incidence.

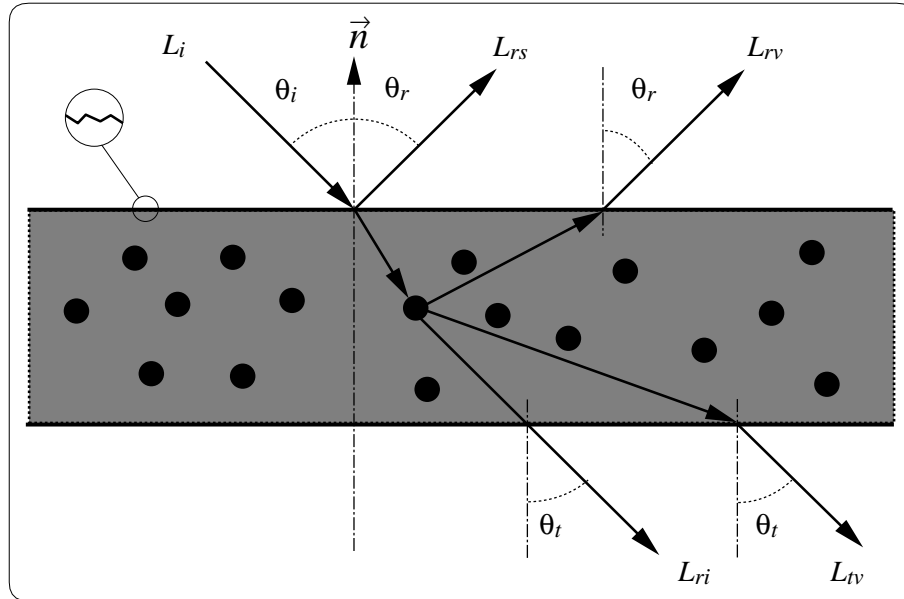


Figure 6.1: Sketch of the scattering geometry used in the *H-K* multiple-layer model.

6.3 Evaluation and Implementation Issues

The physical plausibility of the *H-K* model was not demonstrated either analytically or experimentally in spite of its physical basis. In order to test the application of their model to the rendering of plant leaves, Hanrahan and Krueger constructed a leaf model using the technique described by Bloomenthal [21]. The color of a leaf was obtained from an image acquired from a digital scanner. An albedo image was texture mapped onto a series of simply-shaped, bent polygons to create the leaf. Where the texture map is transparent the polygon is considered transparent and the leaf is not visible. In the context of the multiple-layer model the albedo represents the ratio between the scattering cross section and the total scattering cross. If the albedo is close to zero, absorption is more likely to occur than scattering. The thickness of the leaf was modeled using a thickness map drawn on top of the original leaf image. The texture maps used in this process are shown in Figure 6.2. The waxy cuticle was modeled using a rough specular surface with a specular exponent of 10. The interior of the leaf was modeled as a single homogeneous layer with an optical depth of 5 and a mean scattering cosine of 0.3 [104].

Images of plant leaves were generated by modifying a conventional ray tracer to account for subsurface reflection and transmission. When a ray encounters a leaf, the BRDF and BTDF are evaluated for direct illumination from light sources. This is done by biasing the Monte Carlo procedure to estimate the energy transported to the light. A simple method to do this is to send a ray to the light at each scattering event. This ray must be weighted by the phase function and the attenuation caused by the traversal through turbid media on the way to the light. The advantage of computing the BDF on the fly using an algorithmic process like this is that if material parameters are varying across the surface, the correct answer is still estimated with a reasonable degree of accuracy.

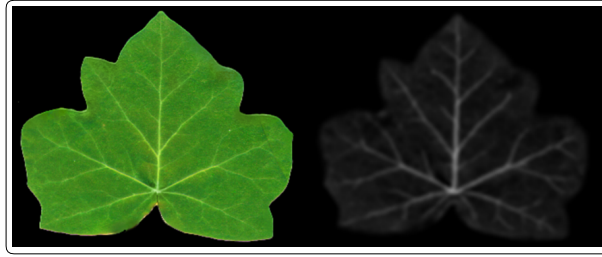


Figure 6.2: Leaf model used by Hanrahan and Krueger. On the left is the albedo image, and on the right is a thickness image in which white indicates increased thickness. Redrawn from [75].

6.4 Strengths and Limitations

The H - K multiple-layer model has the merit of addressing issues related to both inorganic and organic materials. However, its generality causes it to overlook important specific characteristics and properties of organic materials, such as the absorption of light by pigments present in foliar tissues. Moreover, the reflectance and transmittance are not computed directly, but implicitly introduced into the model as the albedo. In other words, the H - K multiple-layer model has to be considered as a scattering model, instead of a reflectance model, since reflectance and transmittance are input parameters. As mentioned in the previous section, in the testing of the model on a plant leaf, Hanrahan and Krueger obtained the albedo values of a leaf from an image acquired from a digital scanner. Recall that, although spectral curves of reflectance and transmittance available in the literature could be used instead, for a large group of natural materials, specially plant leaves, these spectral curves are only available for a few illuminating and viewing angles.

As mentioned in the previous section, the evaluation of the H - K multiple-layer model was based solely on visual inspection. Figure 6.3 shows a picture of a cluster of leaves with the sun in different positions. We can notice that when the light source is on the same side of the leaf as the viewer, the leaf is quite dark. The transmission term, however, can be quite large, and, therefore, the leaves may actually be brighter when they are illuminated from behind. These two aspects are qualitatively consistent with the scattering profile of many species of plant leaves. Note also that the increased thickness of the veins cause dark shadows to be cast on other leaves. According to Hanrahan and Krueger, the veins also appear dark when the leaf is back lit because they absorb more light, and bright when the leaf is front lit because their increased thickness causes more light to be reflected. This assessment is not entirely correct since for many species the veins' scattering profile is the net result of the combination of two factors, namely their thickness and the specific absorption coefficient of their pigments (Section 7.3). In many species the absorption coefficient of the veins' pigments is one order of magnitude smaller than the absorption coefficient for the tissues between the veins [111]. Therefore, for many species, even though the veins present an increased thickness, they appear bright instead of dark since less light is absorbed by their pigments.

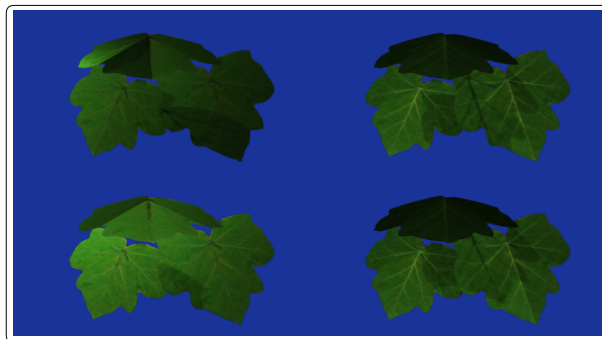


Figure 6.3: Images of a cluster of leaves under different lighting conditions which were generated using the H - K multiple-layer model. Back lit images on the left, and front lit images on the right. Redrawn from [75].

Chapter 7

The Algorithmic Reflectance and Scattering Model

Many BDF models used in computer graphics rely on values of reflectance and transmittance either set by the user or obtained from the literature. Spectral reflectance and transmittance curves are available for leaves [56, 68, 69], but restricted to a narrow range of illuminating and viewing angles. Thus, it becomes necessary to design a reflectance and scattering model for plant tissue in which the reflectances and transmittances are calculated by the model itself.

An exact geometrical model of a plant tissue would model individual cells and their interior details explicitly. The geometrical model used by Govaerts et al. [66] (Section 5.3) is an example of such an approach. The drawbacks of using such a detailed geometrical model in the simulation of light interaction with foliar tissues are the large number of parameters involved, which makes control difficult, and its significant implementation overhead. Another strategy is to use a higher level of abstraction, which allows a reflectance and scattering model to be controlled by a small number of biologically meaningful parameters and enables its easy incorporation into global illumination frameworks. In this chapter we examine the design of such a model, the algorithmic BDF model (*ABM*) [8, 10].

The implementation of the *ABM* is based on an algorithmic process using Monte Carlo methods [73, 107]. Thus, the BDF of a foliar tissue can be calculated and used on the fly during the rendering process, or computed off-line and stored to be reconstructed during rendering [8, 11]. The comparison of the results obtained using the *ABM* with available experimental data is also shown in this chapter.

7.1 Overview

In the *ABM* light propagation is described in terms of ray optics. The foliar tissues are assumed to be isotropic due to the lack of experimental data on factors affecting the anisotropy of plant leaves (Chapter 9). Moreover, the refractive-reflective scattering is assumed to be the dominant form of scattering within the foliar tissues, which is consistent with the literature regarding this topic (Chapter 9).

Instead of geometrically modeling many cells individually, the propagation of light within these tissues is simulated as a stochastic process whose states are associated with the air-cell wall interfaces represented in Figure 7.1. Once a ray hits a leaf at interface 1 or interface 4 (state 1 or state 4), it can be reflected back to the environment or refracted to the interior of the leaf. Then, it can be reflected or refracted multiple times until it is absorbed at state 2 or leaves the leaf at the states 1 or 4.

The light interactions in the *ABM* may therefore be seen as a *random walk*¹ process in which the transition probabilities are associated with the Fresnel coefficients computed at each interface (using the Fresnel equations presented in Section 2.1), and the termination probabilities are associated with the free path length computed when a ray travels in the mesophyll layer towards or from interface 2. The free path length concept is examined more closely in Section 7.3.

Although the Fresnel equations are valid only for infinite plane surfaces, in practice, as pointed out by Govaerts [65], these equations may still be used since a cell is large with respect to the wavelength of the incident light, and the portion of the cell wall interacting with a ray can be considered locally flat. Each time a ray hits an interface we compute the corresponding coefficient

¹ A *random walk* is a *Markov chain*, whose successive states (connected by the transition and termination probabilities) comprise all possible positions of the particle within the boundary, together with a special “absorbing” state, that the system enters as soon as the particle hits the boundary and remains in for ever after [73].

(R). Only the real parts of the refractive indexes are considered, since for the spectral region covered in this work (400nm to 700nm), and for the materials considered, the complex parts are so small that they can be neglected [65, 66, 121, 157].

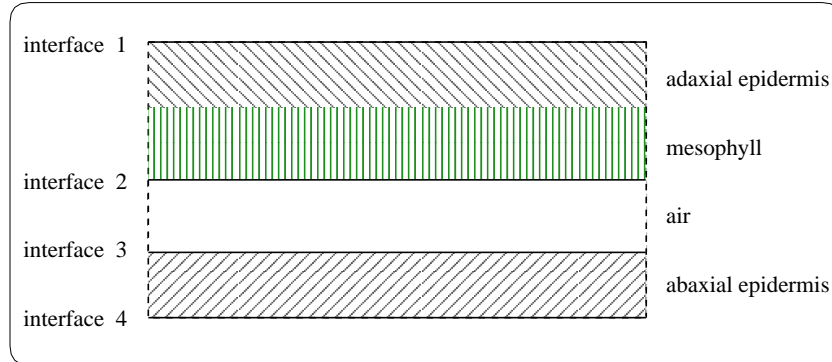


Figure 7.1: Interfaces and tissues considered by the *ABM*.

Using these simplifying assumptions the equation used to compute the Fresnel coefficients at each interface, assuming unpolarized light, reduces to Equation 2.12 [133]. After computing the Fresnel coefficient at an interface, we generate a uniform random number $\xi \in [0, 1]$. If the random number ξ is smaller than or equal to the Fresnel coefficient R , a reflected ray \vec{r} is generated, otherwise a refracted ray \vec{t} is generated. The reflected ray is obtained using the law of reflection (Equation 2.4). The refracted ray is obtained using Snell's law (Equation 2.7).

The *ABM* takes into account the three components of the BDF of plant tissues: surface reflectance, subsurface reflectance and transmittance (Figure 4.4). They are affected by the surface roughness, the internal scattering and the light absorption in the mesophyll tissue. In the next sections we describe how these aspects are simulated by the *ABM*.

7.2 Scattering Simulation

Brakke *et al.* [27] have noted that the scattering profile of a plant leaf can be approximated by an exponentiated cosine function. We have used a similar approach to simulate the distribution of the rays reflected or refracted at the foliar tissues. A rough surface, like a leaf epidermis, can contain more than one distinct scale of roughness. The contour of the epidermal walls represents large surface features with respect to the wavelength of the incident light. The microdetails of the epicuticular waxes represent the small surface features relative to the wavelength of the incident light.

For the plant epidermis the large-scale roughness will dominate scattering in the specular direction, as pointed out by Grant [67], and the small-scale roughness will control scattering away from the specular direction. The epicuticular waxes exhibit a wide range of geometric configurations, and their contribution to the overall reflectance is not as significant as the overall shape of the epidermal cells. For these reasons we decided to concentrate our simulation efforts on the large scale features.

Govaerts *et al.* [66] have shown that the epidermal cells can be approximated by oblate ellipsoids. An oblate ellipsoid has semi-axes a_1, a_2 and a_3 , with $a_1 = a_2$ and $a_1 > a_3$ [140]. For the plant cells we consider a_1 and a_2 as the axes in the plane of the foliar tissues, with values corresponding to average radius of the cell, a_r . Unlike the oblateness definition used by Govaerts *et al.* we define the oblateness of the cell as $\frac{a_r}{a_3}$. The dimensions of the epidermal cells of several species of plants can be found in the literature [23, 65, 108].

To simulate the effects of the shape of the epidermal cells on the reflected rays at the air→epidermal cells interface, the rays are perturbed using a warping function (Equation 7.1). This function corresponds to a PDF based on an exponentiated cosine distribution (Section 2.5), and the exponent is given by the oblateness of the epidermal cells. The perturbation is performed through angular displacements, α_e and β_e . The angle α_e corresponds to the polar angle with respect to the ideal reflection or ideal transmission direction. The angle β_e corresponds to the azimuthal angle around the ideal reflection or ideal transmission direction. These angles are given by:

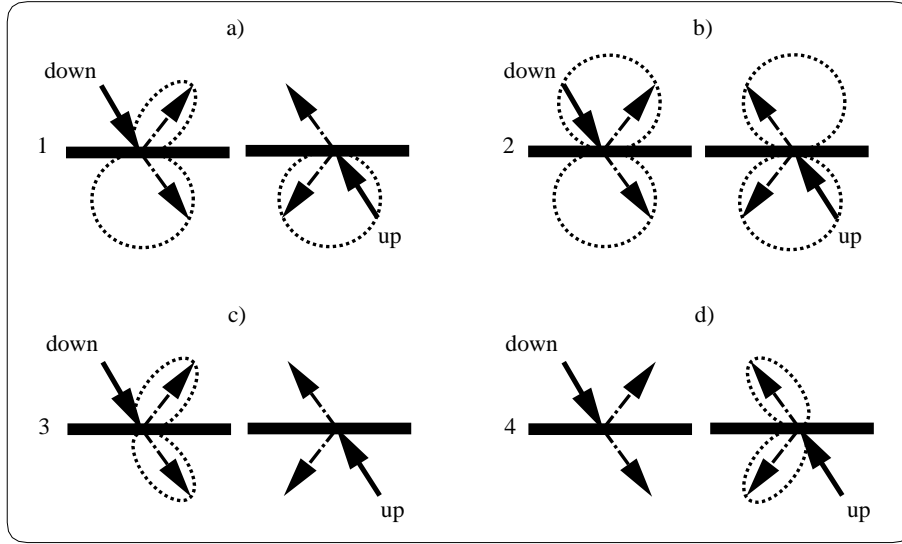


Figure 7.2: Perturbations performed by the *ABM* on the rays distributions at the four interfaces in the upwards and downwards directions of propagation considering the adaxial surface on the top and the abaxial surface on the bottom. a) Interface 1. b) Interface 2. c) Interface 3. d) Interface 4.

$$(\alpha_e, \beta_e) = (\arccos((1 - \xi_1)^{\frac{1}{ob+1}}), 2\pi\xi_2) \quad (7.1)$$

where:

- ξ_1 and ξ_2 = uniformly distributed random numbers $\in [0, 1]$,
- ob = oblateness of the epidermal cells.

Therefore, leaves with large epidermal cells' oblateness will have a surface reflectance closer to a specular distribution than leaves with small epidermal cells' oblateness. As pointed out by Shirley [137], the energy conservation properties of a PDF based on an exponentiated cosine function become less physical as the exponent gets smaller, and the resulting behavior becomes that of a mirror when the exponent becomes larger. By associating this exponent with a biological meaningful parameter, boundaries for the values assumed by this exponent are set and, consequently, the chances of violating the energy conservation properties of this PDF are reduced. Based on the dimensions of the epidermal cells for several species of plants found in the literature, an appropriate range for the oblateness would be [1,4,5].

When light passes to the mesophyll its direction of travel is randomized and it becomes diffuse. The distribution of the rays in this tissue is simulated using another warping function (Equation 7.2). In this case the PDF corresponds to a diffuse or cosine distribution (Section 2.5). The perturbation is also performed through angular displacements, α_m and β_m . The angle α_m corresponds to the polar angle with respect to the reflection or transmission direction of the propagated ray. The angle β_m corresponds to the azimuthal angle around the propagation direction. These angles are given by:

$$(\alpha_m, \beta_m) = (\arccos(\sqrt{(1 - \xi_3)}), 2\pi\xi_4) \quad (7.2)$$

where:

- ξ_3 and ξ_4 = uniformly distributed random numbers $\in [0, 1]$.

Figure 7.2 presents a sketch showing the perturbations performed in each interface in both directions, upwards and downwards. In order to be consistent with available biological information and avoid undue complexity, a conservative strategy was adopted. In other words, the rays are not perturbed when the impact of the perturbation is not significant to the overall BDF.

7.3 Absorption Simulation

A ray may encounter the mesophyll tissue after interacting with interface 1 or interface 2. Once it enters the mesophyll tissue it proceeds through the *mesophyll loop* (Figure 7.3), where it may be propagated diffusively or absorbed. As mentioned in Chapter 4, the diffuse propagation is due to multiple interactions with the many reflective-refractive discontinuities of the air-cell walls interfaces, and the absorption is associated with the presence and concentration of pigments.

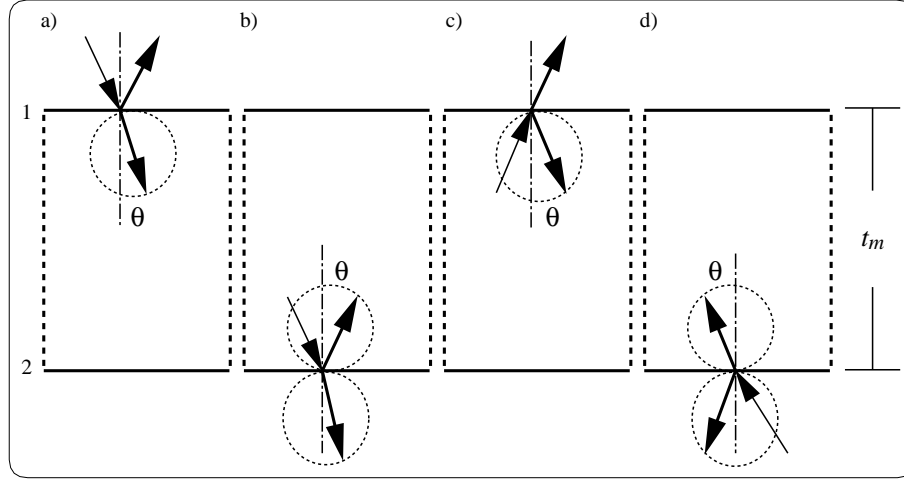


Figure 7.3: *Mesophyll loop*. a) Ray coming from outside interacts with interface 1. b) Refracted ray from interface 1 interacts with interface 2. c) Reflected ray from interface 2 interacts with interface 1. d) Ray coming from interface 3 interacts with interface 2.

When a perturbed refracted ray comes from interface 1 (Figure 7.3a), it is tested for absorption. If it is not absorbed, the ray is tested for reflection or refraction at interface 2 (Figure 7.3b). If the outcome of this test is the refraction of the ray, it is perturbed and transmitted to interface 3, otherwise the reflected ray is perturbed and tested for absorption. If it is not absorbed, it may be reflected back to the mesophyll at interface 1 (Figure 7.3c), restarting the *mesophyll loop*, or refracted to the environment.

When a ray comes from interface 3 (Figure 7.3d), it is also tested for reflection or refraction at interface 2. If the outcome of the test is a reflected ray, it is perturbed and sent back to interface 3 without accounting for absorption. Otherwise, the refracted ray is perturbed and tested for absorption. If the ray is not absorbed, it proceeds in the *mesophyll loop*.

The absorption of light in dye solutions varies with the thickness of the sample and the concentration of pigments in accordance with a combination of Beer's law and Bouguer's law (Section 2.3). This combination, however, assumes that the incident ray is perpendicular to the interface between the incident medium and the transmission medium. Allen *et al.* [2] have included an additional term to this combination to account for different angles of incidence. The resulting expression states that the transmissivity of a plate along a slant ray is given by:

$$T = e^{-a(\lambda) c h \sec \theta} \quad (7.3)$$

where:

- $a(\lambda)$ = absorption coefficient,
- c = concentration of pigment,
- h = thickness of plate,
- θ = angle of slant ray with respect to normal direction.

The absorption testing performed by the *ABM* is based on Equation 7.3, and assuming a homogeneous distribution of pigments. It is performed probabilistically every time a ray starts a run in the mesophyll tissue. It consists of the estimation of

the ray geometrical path length², p , through the following expression:

$$p = -\frac{1}{a_e(\lambda)} \ln(\xi) \cos \theta \quad (7.4)$$

where:

- ξ = uniformly distributed random number $\in [0, 1]$,
- $a_e(\lambda)$ = effective absorption coefficient of pigments,
- θ = angle between the ray direction and the normal direction.

The effective absorption coefficient, as described by Jacquemoud and Baret [85], is given by:

$$a_e(\lambda) = \sum_{i=1}^n a_i(\lambda) c_i \quad (7.5)$$

where:

- $a_i(\lambda)$ = specific absorption coefficient of a given pigment i ($\frac{cm^2}{\mu g}$),
- c_i = concentration of a given pigment i ($\frac{\mu g}{cm^2}$).

If p is greater than the thickness of the pigmented medium, t_m (both expressed in cm), then the ray is propagated, otherwise it is absorbed. The thickness value used in this comparison corresponds to a fraction of the total thickness of the leaf. Since the palisade tissue presents a higher concentration of pigments than the spongy tissue, and it is largely responsible for the internal scattering, we suggest to use its thickness (around 45% of the total thickness) for most cases. For species that present an undifferentiated mesophyll tissue, *e.g.* characterized by the presence of spongy cells only [56, 151], it is more appropriate to use the entire thickness of the mesophyll tissue (around 75% of the thickness).

A comprehensive set of leaf optical experiments, called *LOPEX*³ [81], provides the pigment concentrations and thickness values for 120 leaf samples representative of more than fifty species. The absorption spectra of chlorophyll and carotenoids pigments can be found in the literature [24, 31, 37, 44, 85, 128, 130, 149, 160, 161]. Additional information on optical parameters of foliar tissues is available in a survey by Gausman and Allen [56].

7.4 Implementation Issues and Summary of Parameters

The *ABM* is implemented using the *C++* language and the *ggLibrary* [136], a set of *C++* utilities designed to be used in computer graphics applications. In the *ggLibrary*, materials are classified as families such as metals and dielectrics, and grouped by parameters that affect their behavior, following the ray tracing framework for global illumination proposed by Shirley *et al.* [135]. A set of routines specific for each family computes the BDF for that family.

In the case of the *ABM*, the new family corresponds to the plant tissues, and each of its four states is implemented through a different routine. These routines are called recursively by a controlling routine until the ray is either absorbed or abandons the foliar tissues. The parameters used in the *ABM* are the following:

- η_e - refractive index of the external cutinized wall of the epidermis: used in the Fresnel computations in states 1 and 4;
- ob - oblateness of epidermal cells: used in the perturbation of the rays in state 1 (Figure 7.2a), in state 3 (Figure 7.2c), and in state 4 (Figure 7.2d);
- η_m - refractive index of the mesophyll cell wall: used in the Fresnel computations in state 2;
- t_m - thickness of mesophyll tissue: used in the absorption testing performed in state 2 (measured in cm);
- c - concentration of pigments: also used in the absorption testing performed in state 2 (measured in $\frac{\mu g}{cm^2}$);

² In this context the ray geometrical path length represents the spatial distance covered by a slant ray transmitted through a medium until it is absorbed or leaves the medium.

³ The *LOPEX* data set was also used in the evaluation of some models presented in Chapter 5 such as *Raytran*, *SLOP* and *LEAFMOD*.

- η_a - refractive index of the antidermal wall: used in the Fresnel computations in state 3.

The refractive indexes come from experiments described in the literature [57, 85, 157]. The remaining parameters are also available in the literature, as mentioned earlier. The user may also adjust the optical parameters, *e.g.* t_m , depending on the conditions at hand. For example, for some species, a leaf in the sunlit and a leaf in the shady portions of a tree, may present differences of thickness of around 25% [5]. Notice that one can use the same parameters for the adaxial and abaxial epidermis. This approach is accurate for most cases, but for some species it may be more appropriate to use a set of parameters with slightly different values.

The absorption spectra of chlorophyll *a* and *b* provided by Jacquemoud and Baret [85] can be used in the absorption computations. Although these curves refer to pigments commonly present in the foliar tissues of most species, they may be adjusted according to the lengthening of the optical path of a given plant leaf, also called ratio of intensification [31] or factor of intensification [127]. This factor represents a combination of light that passes through plant tissues without encountering an absorber (sieve effect) and the light that is scattered and has an increased path length (detour effect). As mentioned by Vogelmann [150], these two phenomena have opposite outcomes: the sieve effect lowers absorption (specially at or near wavelengths for which the absorption has a maximum value), whereas the detour effect increases absorption (specially at or near wavelengths for which the absorption has a minimum value). Nonetheless, in dispersive samples, such as plant leaves, the absorption is enhanced by the combination of these two effects [127].

The factor of intensification of a plant leaf depends on the chlorophyll content. The greater the chlorophyll content, the shorter the length of the optical path. For example, McClendon and Fukshansky [111] made estimates of factors of intensification for plant leaves of nine different species with a chlorophyll content between 40 and $70 \frac{\mu g}{cm^2}$, and the resulting value, *i.e.*, the mean and the standard deviation, was 2.30 ± 0.25 .

7.5 Evaluation Issues

One possible approach for validating a reflectance and scattering model is visual inspection by comparing images generated using the model with images generated using previous models. This approach is not suitable in our case, since the graphics literature lacks realistic models for plants. Recall that, although the *H-K* multiple-layer scattering model can be applied to plants (Chapter 6), it does not compute the reflectances and transmittances by itself. Therefore, comparing such a model with the *ABM*, which actually computes the reflectances and transmittances by itself, would not be appropriate.

Another alternative would be to compare images generated using the *ABM* with photographs of real plants. In this case, since the computer generation of images is highly dependent on rendering parameters, the validation of the *ABM* could be biased by errors generated by other stages of the rendering pipeline, such as geometrical modeling, spectral modeling and directional sampling. As appropriately stated by DeYoung and Fournier [45], the shape of an object, the lighting, and the viewing position can all greatly affect how much BDF properties affect an image, and attempting to measure how much effect these properties will have on generated images would necessitate a separate investigation.

Another valid alternative is to test a computer model as a separate unit of the rendering pipeline and compare the results with the best available experimental data. In order to perform a comprehensive validation of a BDF model it would be necessary to consider all possible illuminating and viewing geometries. The very large number of measurements needed as well as the lack of experimental data for all possible geometries precludes the use of this approach. Moreover, as mentioned in Section 3.2.1, in many goniophotometric measurements the most interesting and informative data for practical samples are taken in the plane given by the direction of the incident light and the normal of the specimen. Therefore, due to the practical reasons mentioned above and the isotropic characteristic of the *ABM*, this plane was used in its testing.

The set of leaf optical experiments cited in Section 7.3, *LOPEX* [81], includes measured spectral curves of reflectance and transmittance. In order to compare the results provided by the *ABM* with these measured curves, the actual measurement conditions used in the *LOPEX* were reproduced as faithfully as possible. The same area for the specimen, $40mm^2$, and the same angle of incidence, 8° , with respect to the normal of the specimen were used. The emitter used in these measurements has a radius of $8mm$, and it is positioned at a distance of $30mm$ from the center of the specimen. These values correspond respectively to the area of the apertures and radius of the integrating sphere of the spectrophotometer used by *LOPEX*.

A leaf from the soya species (*Glycine max*, *Soja hispida*), commonly known as a soybean leaf, was selected to be used in the experiments because of its standard foliar characteristics and the large variety of experimental data available for comparison [28, 68, 69, 81, 110, 152, 156] besides *LOPEX*. The parameters used in the testing of the *ABM* experiments are presented

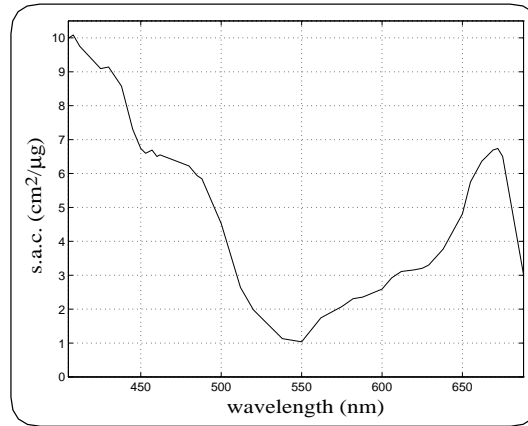


Figure 7.4: Absorption spectra of chlorophylls $a + b$ used in the testing of the *ABM*.

in Table 7.1. The refractive indexes were obtained from the work by Wooley [157], and the oblateness corresponds to the average dimensions of the epidermal cells of plant leaves belonging to the dicotyledons group ($a_r = 12.5$, $a_3 = 2.5$), which are available in the texts by Govaerts *et al.* [66] and Norman [119].

η_c	ob	η_m	c	t_m	η_a
1.6	5.0	1.41	43.62	0.0072	1.42

Table 7.1: Parameters used in the testing of the *ABM*.

The concentration of chlorophyll was obtained directly from *LOPEX*, and the thickness was computed using 45% of the total soybean leaf thickness, also provided by *LOPEX*, as proposed in Section 7.3. The combined absorption spectra of chlorophylls $a + b$ used in the testing of the *ABM* (Figure 7.4) is based on the curve provided by Jacquemoud and Baret [85], but adjusted according to a factor of intensification of 2.13 [111, 127] and values of free path length (Section 7.3) given in *cm*.

7.6 Strengths and Limitations

The spectrophotometric curves obtained using the *ABM* are qualitatively in agreement with the actual measured values (Figure 7.5). The quantitative discrepancies may be due in part to the fact that we did not consider the carotenoids (which account for 20% of the total amount of pigments) and that we did not separate different chlorophyll pigments. Moreover, the underestimation of surface microdetails, and shadowing and masking effects [51] may also contribute.

Nevertheless, it shall be noted that the curves presented in Figure 7.5 represent good qualitative comparisons between modeled and measured values, since some parameters used in the simulation, such as the refractive indexes and the oblateness, correspond to average values published in the literature. Besides, as stated by Salisbury and Ross [128], the exact positions of the absorption peaks depend on the solvents in which the pigments are dissolved, and one can expect small shifts considering *in vivo* values. For these reasons one must account for possible variations between the average values used by the *ABM* and the exact values regarding the leaf specimen used in the actual measurements performed by *LOPEX*.

As pointed out by Vogelmann [150], the asymmetry in a bifacial leaf anatomy gives different reflectance and transmittance readings for its adaxial (front) and abaxial (back) surfaces. Spectrophotometric curves obtained experimentally by Wooley [156] showed greater reflectance for the back than for the front of soybean leaves in the visible region of the spectrum (Figure 4.6). Figure 7.6a shows that the *ABM* can capture this aspect of foliar tissues optics, which is responsible for the fact that the backs of bifacial leaves appear pale to the eye. The experiments by Wooley also showed greater transmittance when the leaf's back is toward the light, although in the visible region the differences of magnitude of the transmittances are not so high as the differences of magnitude of the reflectances. Figure 7.6b shows that the *ABM* can capture these characteristics of the transmittance curves as well.

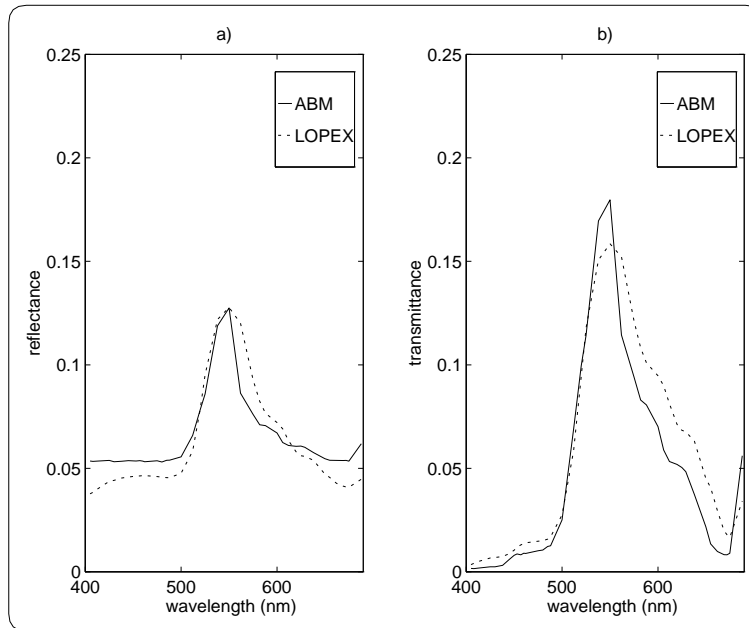


Figure 7.5: Comparison of spectral curves of a soybean leaf computed with the *ABM* with measured spectral curves provided by *LOPEX*, for an angle of incidence of 8° and 10^6 rays. a) Absolute spectral reflectance. b) Absolute spectral transmittance.

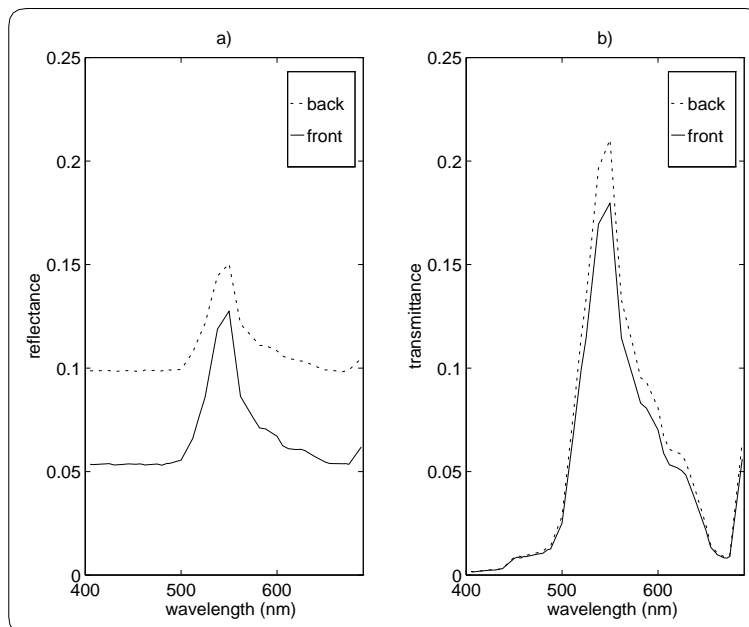


Figure 7.6: Spectrophotometric curves of a soybean leaf obtained using the *ABM* and from its front surface (adaxial surface) towards the light and its back surface (abaxial surface) towards the light, for an angle of incidence of 8° and 10^6 rays. a) Absolute spectral reflectance. b) Absolute spectral transmittance.

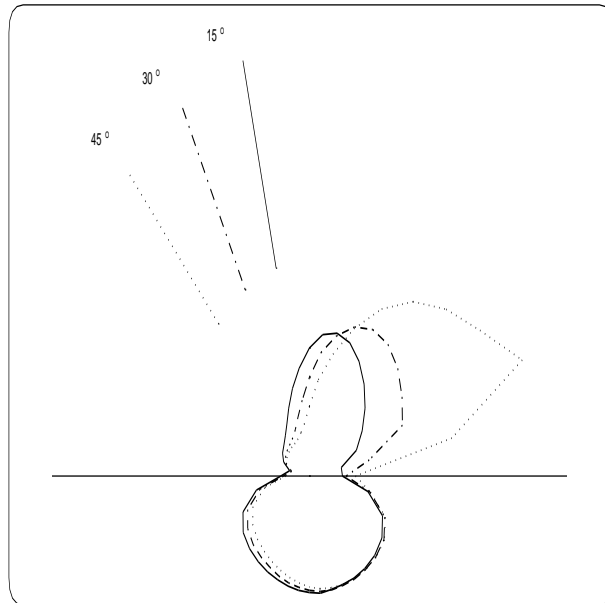


Figure 7.7: BDF of a soybean leaf at a wavelength of 550nm (which corresponds approximately to the reflectance and transmittance peaks), for angles of incidence of 15° , 30° and 45° , in the plane given by the incidence direction and the normal of the specimen, 10^7 rays, and the collector sphere divided into 20 patches along its latitude and 40 patches along its longitude.

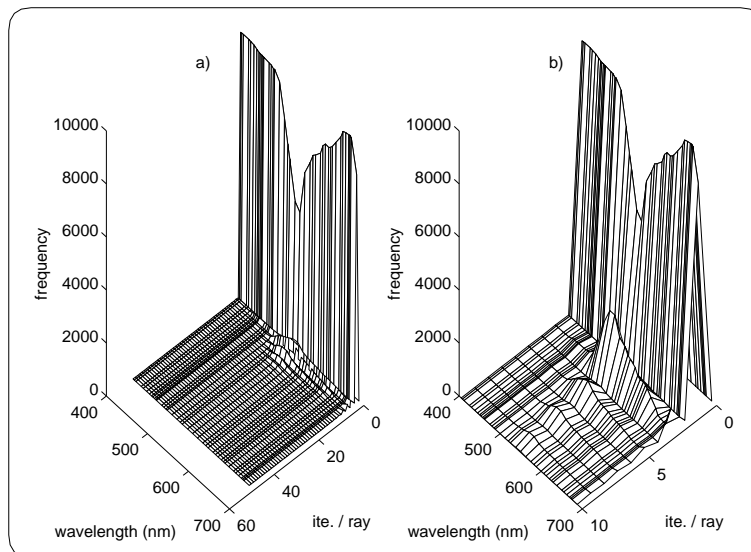


Figure 7.8: Number of interactions per ray and per wavelength for 10^4 rays. a) Graph for zero to fifty interactions per ray, b) Zoom in of the region with high frequency of interactions per ray.

Figure 7.7 (upper part) shows that the simulated BRDF exhibits an angular dependency on the incident angle intermediate to that expected of diffuse and specular reflectors, which corresponds to the characteristics of the real BRDF of leaves [67]. It also shows (lower part) that the simulated BTDF has a near-Lambertian distribution, which is also a characteristic of the real BTDF of leaves [67]. Moreover, the curves in Figure 7.7 agree with the experimental BDF curves of soybean leaves published by Breece and Holmes [28] and Wooley [156].

Even though a performance analysis should in general not be based only on counting the number of interactions, since it does not account for differing amounts and types of work performed on each interaction, we believe that it may be illustrative of the behavior of the *ABM*. Figure 7.8 shows that, despite the stochastic nature of the *ABM* and the number of interfaces involved, the number of interactions (state transitions) is usually low. This aspect suggests that in applications where the accuracy requirements for individual elements, such as a leaf or a petal, are not very high, *e.g.* the rendering of a tree with hundreds of leaves, the model may be reduced to its most important states, namely states 1 and 2. Nevertheless the computational costs of the *ABM* may be rather high for applications involving a large number of primitives. In the next chapters we examine alternatives to reduce the computational costs involved in the simulation of light interaction with foliar tissues.

Besides the comparison of the predictions of the *ABM* with experiments, images were generated (using modified version of Kajiya's path tracing [91, 133]) to illustrate its applicability to the rendering of plant leaves (Figure 7.9). Lilley *et al.* [101] mention that to provide the correct color in high quality computer graphics, the CIE XYZ values should be converted to the RGB color space of a monitor using the SMPTE⁴ monitor chromaticity coordinates. In fact, many monitors used in the current workstations use these coordinates. Thus, the absorption spectra of chlorophyll (Figure 7.4) was sampled in the dominant wavelengths corresponding to these coordinates (Table 7.2) in order to generate the curves and the images presented in Figure 7.9. Note that the dominant wavelength regarding the green channel corresponds approximately to the wavelength for which the absorption of light by chlorophyll is minimum (Figure 7.4). The spectral curves of reflectance and transmittance used to represent veins' chromatic attributes were obtained scaling the absorption spectra of chlorophyll (Figure 7.4) by a factor of 0.1 according to biological data provided by McClendon and Fukshansky [111].

	x	y	wavelength
Red	0.630	0.340	608nm
Green	0.310	0.595	551nm
Blue	0.155	0.070	465nm
white (D65)	0.313	0.329	

Table 7.2: Chromaticity coordinates and wavelength values.

In order to obtain the geometrical descriptions of soybean leaves used in the images presented in Figure 7.9, a soybean plant was grown. After the plant was fully matured, a few leaves were removed and a digital scanner was used to obtain black and white texture maps of their contour (contour map) and venation system (venation map). This positional information was mapped to polygons to create the leaves, using a technique similar to the one applied by Bloomenthal [21] and Hanrahan and Krueger [75]. For areas of the contour map outside the leaf contour the polygon is considered transparent and the leaf is not visible. Similarly, the veins are not visible for transparent areas of the venation map.

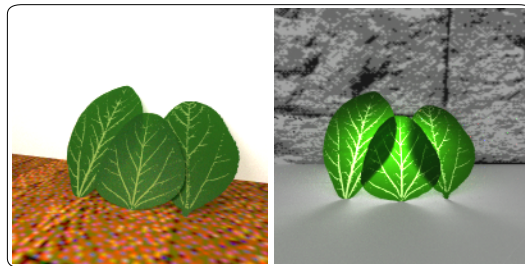


Figure 7.9: Image generated using the *ABM*. On the left back lit, on the right, front lit.

⁴ Society of Motion Picture and Television Engineers.

Chapter 8

The Foliar Scattering Model

The accuracy of simulations of light interaction with plants depends on the reflectance and transmittance models for foliar tissues. The use of physically-based models is important for ensuring that rendering methods used in these simulations do not violate the laws of physics [99]. Moreover, these models have to be biologically-based in order to appropriately account for the natural processes involved in these simulations. Simplicity is also an important requirement for a reflectance model, since a model may otherwise become computationally impractical, as pointed out by Ward [153]. Thus, it is necessary to design practical reflectance and transmittance models that allow us to render these materials fast without undermining the image quality.

In this chapter we present a foliar scattering model [8, 12], henceforth called *FSM*, which aims to provide a balance between two seemingly conflicting goals, namely accuracy and efficiency. This model accounts for the three components of plant tissues' BDF (surface reflectance, subsurface reflectance and transmittance), and uses pre-computed reflectances and transmittances as scale factors in a stochastic simulation of the scattering profile of these tissues. The use of these scale factors replaces the time consuming random walk process used by the *ABM* to simulate the randomization and the absorption of light within the foliar tissues. Moreover, this approach reduces the number of rays needed to achieve a desired accuracy level in the results.

These scale factors are computed off-line using the *ABM*, since the spectral curves provided by this model have already been compared with experimental data of real foliar specimens, showing good agreement (Section 7.6). Although the *FSM* is oriented to leaves, like the *ABM* it can easily be extended to other plant surfaces like petals and stems. In this chapter we also compare the results obtained using the *FSM* with results obtained applying the *ABM* in-line.

8.1 Overview

In the *FSM* light propagation is also described in terms of ray optics, and the interaction of light with the foliar tissues is described in terms of their SPF (Section 2.2). As pointed out by Glassner [60], the BDF (or, in this case, the SPF) is a difficult function to work with due to its multivariate nature. Fortunately, one can make some simplifying assumptions about the foliar tissues that provide a more computationally convenient expression to manipulate.

First, it is assumed that the physical properties describing the light propagation are identical everywhere within the foliar tissues, *i.e.* they can be considered as homogeneous interacting media [66]. This assumption allows one to leave out the positional argument. Second, since the anisotropy of plant leaves is considered to be associated with their venation system (Section 4.2), and considering that the biological data regarding these systems is scarce to support the design of a biologically-based anisotropic reflectance model for these materials, it is also assumed they are isotropic. This assumption allows one to work with only one parameter for the incidence direction ψ_i , which is given by the angle of incidence, θ_i , of an incident ray with respect to the normal of a leaf.

8.2 Scattering Simulation

The *FSM* takes into account the three components of the SPF of a plant tissue, namely surface reflectance, subsurface reflectance and transmittance. The contribution from each of these components is scaled using the respective values of absolute

spectral surface reflectance ($\rho_s(\theta_i, \lambda)$), absolute spectral subsurface reflectance ($\rho_d(\theta_i, \lambda)$) and absolute spectral transmittance ($\tau(\theta_i, \lambda)$), as sketched in Figure 8.1. These spectral values are computed off-line using the *ABM*¹ and stored in a table.

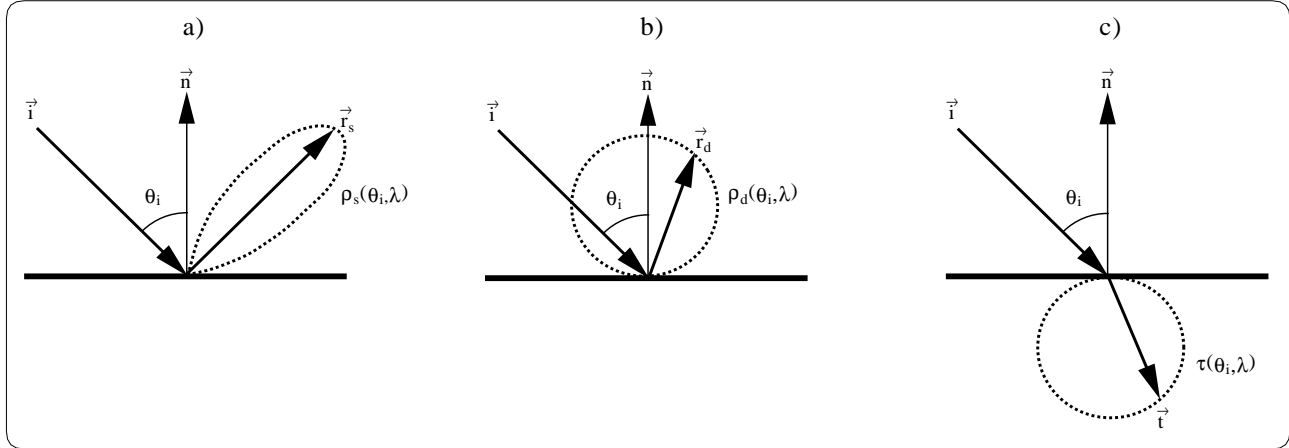


Figure 8.1: Scattering distribution performed by the *FSM* to represent the three components of a foliar specimen's SPF: a) surface reflectance b) subsurface reflectance and c) transmittance.

The parameter space of a foliar specimen's SPF is represented by the input directional parameter space and the output directional parameter space. The first, considering the assumption regarding isotropy made earlier, is given by the angle of incidence θ_i ($[0, \pi]$), and the second is given by the azimuthal angle α ($[0, 2\pi]$) and the polar angle β ($[0, \pi]$). The domain chosen for θ_i accounts for differences in the reflectance and transmittance curves of foliar specimens that differ markedly in the structure of their two sides. For specimens that do not present this characteristic (Section 4.1), or for applications that assume identical optical properties for both sides [109], the domain of θ_i can be narrowed to $[0, \frac{\pi}{2}]$.

Initially, to account for the surface component of a foliar specimen's SPF for a given incident ray, the corresponding reflected ray using the law of reflection (Section 2.1) is obtained. Then, to simulate the effects of the epidermal cells' shape on the reflected rays at the air→epidermal cells interface, the reflected rays are perturbed using a warping function (Equation 7.1) based on an exponentiated cosine distribution (Section 2.5) employed by the *ABM*.

As mentioned earlier, when light passes to the internal foliar tissues its direction of travel is randomized and it becomes diffuse. This randomization of the incident rays results in a near-Lambertian distribution for the subsurface reflectance of a foliar specimen, and a near-Lambertian distribution for its transmittance. In order to simulate the distribution of rays for these two components, the normal of the foliar specimen is perturbed instead of the incident ray. The orientation of the normal used in the perturbation depends on the incidence geometry. If the incident ray hits the foliar specimen's front (adaxial epidermis) the normal is used for the subsurface reflectance component and its opposite vector for the transmittance component. Otherwise, we use the normal and its opposite vector the other way around. For these perturbations we use a warping function (Equation 7.2) based on a cosine distribution (Section 2.5), also employed by the *ABM*.

8.3 Implementation Issues and Summary of Parameters

The *FSM* was also implemented using *C++* in order to take advantage of the object oriented features of this programming language. This model, like the *ABM*, can be incorporated as a self-contained class in a graphics library, such as the *ggLibrary* [136], and be used by different global rendering methods.

Since the values for spectral reflectance and transmittance are pre-computed, the set of model parameters is reduced to the oblateness of the epidermal cells, ob , used in the perturbations of the reflected rays, and the angle of incidence, θ_i , used to access the table of absolute spectral reflectances and transmittances. The angle of incidence is computed using Equation 2.3.

¹ The outgoing rays generated by the *ABM* have tags which allow the computation of separated values for the surface reflectance, subsurface reflectance and transmittance (Figures 8.2 and 8.3).

The images presented in Figure 8.5 were generated using a modified version of Kajiya's path tracing [91, 133]. For the computation of the direct light contribution we selected the scale factors $\rho_d(\theta_i, \lambda)$ and $\tau(\theta_i, \lambda)$ according to the position of the light source with respect to the foliar specimen. This selection was made using the angle of the shadow ray with respect to the specimen's normal, θ_s , and applying the following criteria:

$$\begin{aligned}
 & - \text{for light coming from above } 0^\circ < \theta_s \leq 90^\circ \left\{ \begin{array}{l} \frac{\rho_d(\theta_i, \lambda)}{\pi} \quad \text{if } 0^\circ < \theta_i \leq 90^\circ \\ \frac{\tau(\theta_i, \lambda)}{\pi} \quad \text{if } 90^\circ < \theta_i < 180^\circ \end{array} \right. \\
 & - \text{for light coming from below } 90^\circ < \theta_s < 180^\circ \left\{ \begin{array}{l} \frac{\tau(\theta_i, \lambda)}{\pi} \quad \text{if } 0^\circ < \theta_i \leq 90^\circ \\ \frac{\rho_d(\theta_i, \lambda)}{\pi} \quad \text{if } 90^\circ < \theta_i < 180^\circ \end{array} \right.
 \end{aligned}$$

While the *ABM* uses an explicit mechanism to simulate the absorption of light, the *FSM* relies on the absorption probabilities implicitly associated with the scaling factors. In order to perform fair comparisons between these two models (Section 8.5), an adaptive tree-depth control [71] based on cumulative ray attenuation (attenuation, for short) was used in the implementation of the modified path tracing algorithm. In this context the attenuation of a given ray is obtained through the product of reflectances and/or transmittances of the surfaces which are hit in the ray's path [133].

During rendering this attenuation is compared with a cutoff attenuation threshold, ζ_c , to control the depth of the tree during the ray tracing. If the attenuation is smaller than ζ_c , the ray's path is terminated. For a given scene we select a value for ζ_c to limit the maximum depth of both trees (one associated with the process using the *FSM* and the other with the process using the *ABM*) to the same percentage of rays to be propagated (0.01%). We examine this issue in more detail in the next section. Since the attenuation has three values corresponding to the three RGB channels, we convert it to luminance in order to compare it with a selected ζ_c . This conversion is made using the following SMPTE formula [101]:

$$Y = 0.21222 R + 0.7013 G + 0.0865 B \quad (8.1)$$

8.4 Evaluation Issues

Foliar data regarding a soybean leaf (Section 7.6) was also selected for the evaluation experiments of the *FSM*. The spectral measurements needed to compute the table of absolute spectral reflectances and transmittances were made using a virtual spectrophotometer (Section 3.1.2) and 10^6 rays in regular intervals of 1° for the angle of incidence θ_i ($[0, \pi]$). The comparisons for the foliar specimen's BDF presented in the next section were performed using a virtual goniophotometer (Section 3.2.2) with a collector sphere divided into 20 patches along its latitude and 40 patches along its longitude, and using 10^8 rays to generate each BDF curve associated with a given wavelength.

For reasons presented in the previous chapter, the absorption spectra of chlorophyll (Figure 7.4) were sampled in the dominant wavelengths corresponding to SMPTE monitor chromaticity coordinates (Table 7.2). Then, the table of absolute spectral reflectances and transmittances used to generate the curves and images presented in the next section were computed using the *ABM*. Figure 8.2 presents the graphs correspondings to the entries of this table.

A table of absolute spectral reflectances and transmittances for the veins, as described in the previous chapter, was also obtained using the *ABM* and the SMPTE monitor chromaticity coordinates, but with the absorption spectra of chlorophyll (Figure 7.4) scaled by a factor of 0.1 according to biological data provided by McClendon and Fukshansky [111]. Figure 8.3 presents the graphs corresponding to the entries of this table.

The geometrical descriptions of soybean leaves presented in Section 7.6 were used to generate the images presented in the next section. For a given graphics setting the measurements regarding both models were performed on the same machine. Moreover, the models were implemented using the same software guidelines to avoid differences that could affect the timing. The root-mean-square (RMS) errors [60] of the difference images, presented in the next section, were computed from normalized pixel values (scaled to $[0, 1]$), and using Equation 8.2.

The convergence graphs presented in the next section were obtained using the following approach. After choosing a value for the attenuation ζ_c we run both processes. During the execution time it was used identical "probes" inserted in the respective

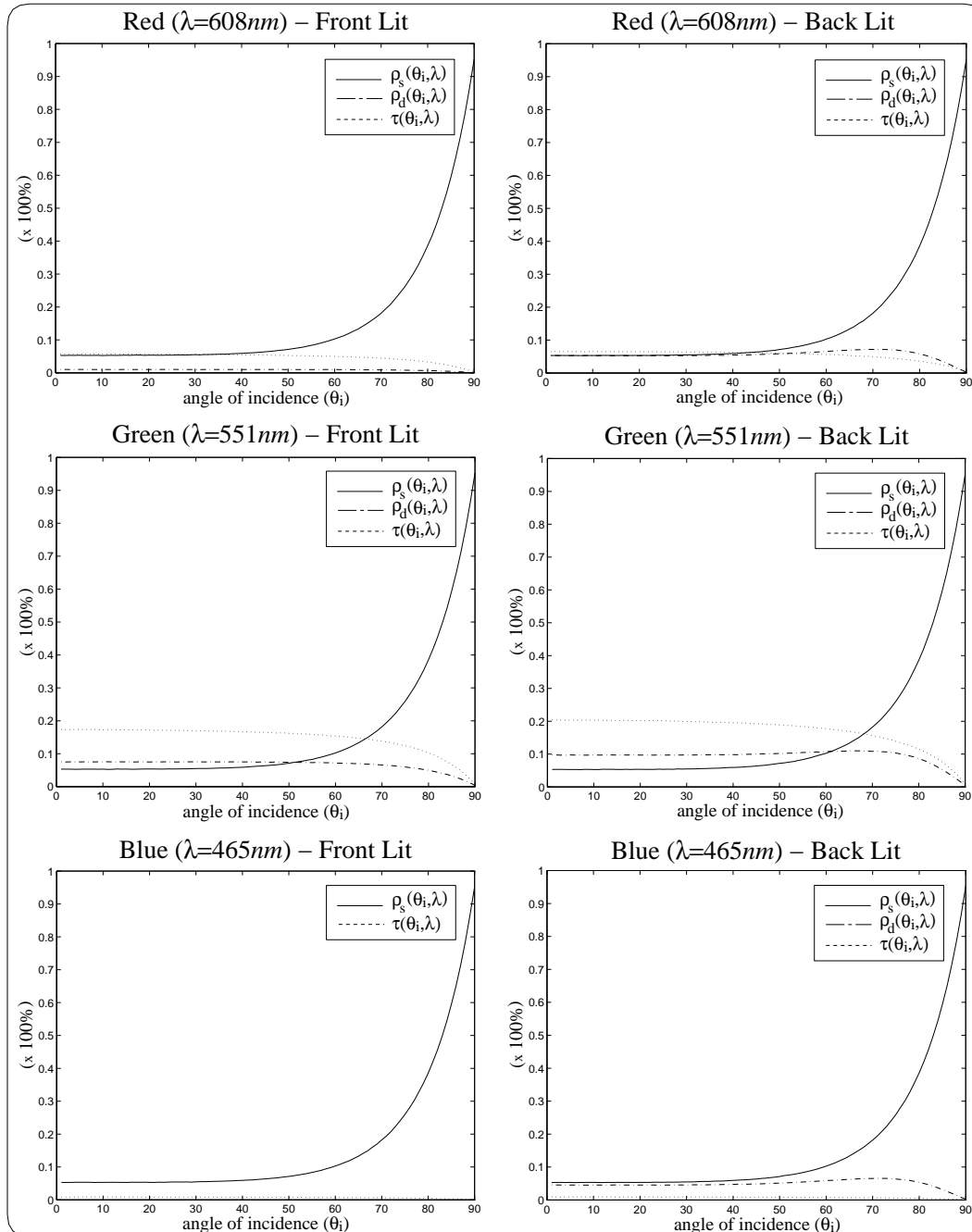


Figure 8.2: Graphs corresponding to the entries of the table of absolute spectral reflectances and transmittances for a soybean leaf.

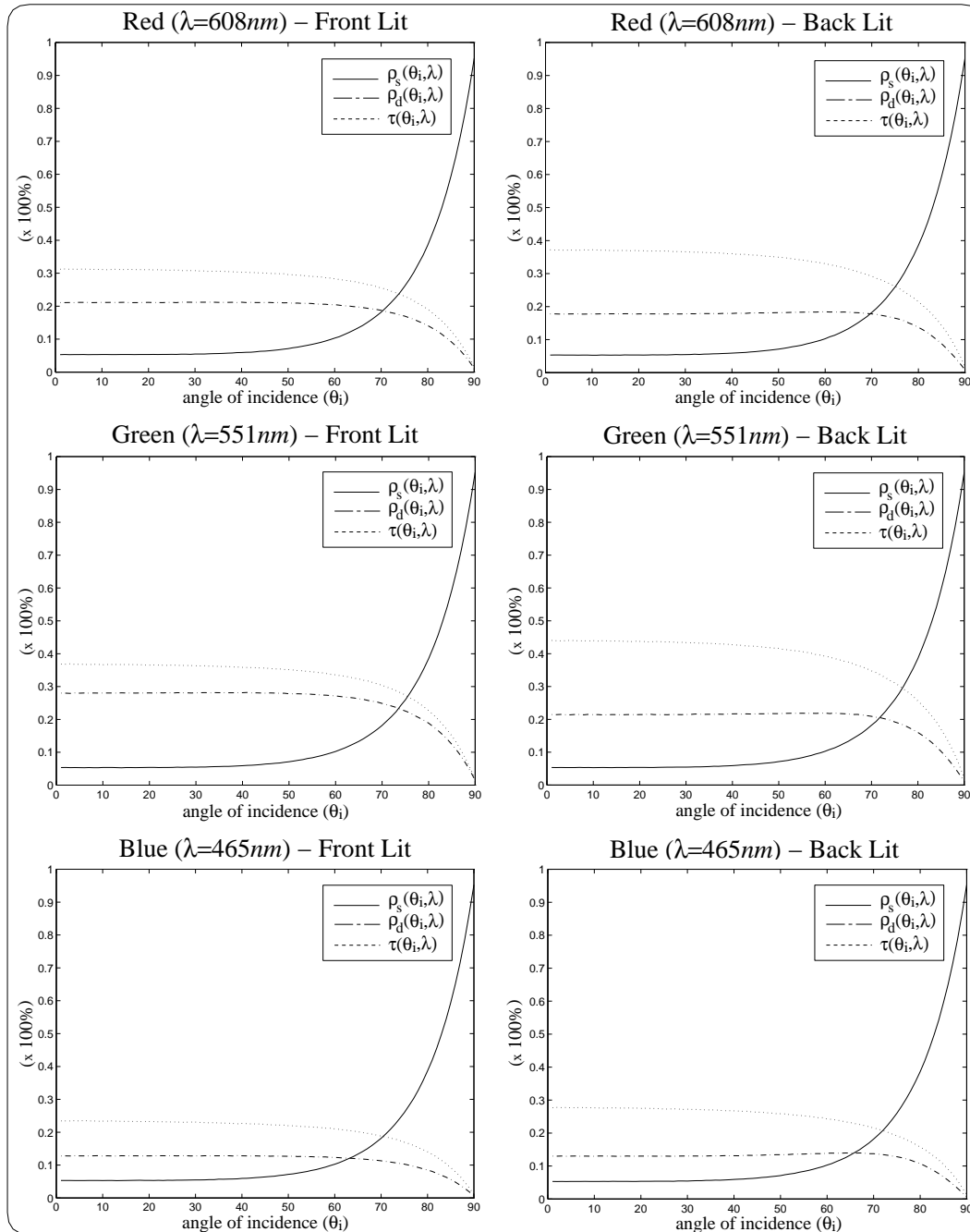


Figure 8.3: Graphs corresponding to the entries of the table of absolute spectral reflectances and transmittances for the veins of a soybean leaf.

codes to collect the number of rays shot at each depth of the respective ray tracing trees. The data collected by the “probes” was used to statically fine-tune our initial selection of ζ_c . Once the stopping criterion was satisfied by both processes the data collected by the “probes” was used to plot the convergence graphs (Figure 8.6).

These convergence graphs (Figure 8.6) show the percentage of rays that still need to be propagated after each depth of propagation. At depth zero 100% of the rays still need to be propagated. For a certain depth k , where $0 < k \leq n$ (n being the total number of depths considered), this percentage is computed using the following ratio:

$$\frac{\sum_{i=0}^n (rpd_i) - \sum_{i=0}^k (rpd_i)}{\sum_{i=0}^n (rpd_i)} \times 100\% \quad (8.2)$$

where rpd_i represents the number of rays propagated at depth i (Figure 8.7).

8.5 Strengths and Limitations

As mentioned in Section 7.5, in order to perform a comprehensive evaluation of spectral curves provided by a BDF model it would be necessary to consider all possible testing geometries. However, due to the large number of measurements needed, the examination of the *FSM* was limited to selected representative cases. Figure 8.4 shows the BDF curves generated using the *ABM* and the *FSM*, for angles of incidence of 30° and 45° , and in the plane given by the direction of incidence and the specimen’s normal².

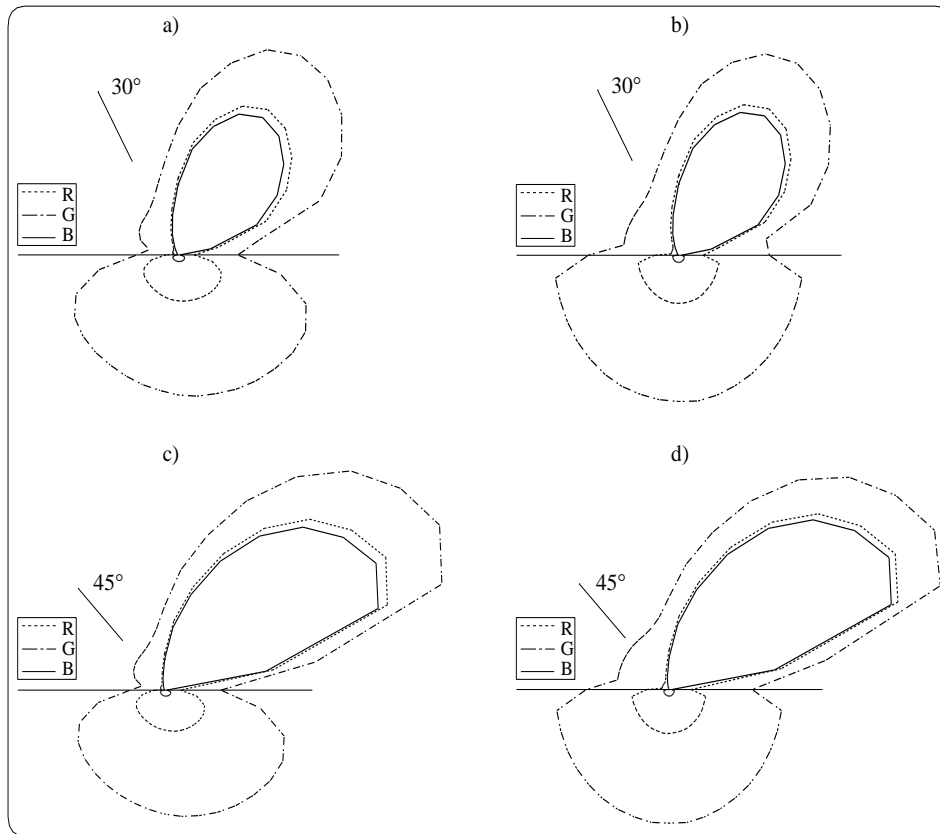


Figure 8.4: BDF curves for a front lit leaf obtained at the wavelengths associated with the RGB channels (Table 6.1). a) and c) Using the *ABM*. b) and d) Using the *FSM*.

² The choice of this plane is consistent with the isotropic characteristic of the *FSM*.

Notice that the curves provided by the *FSM* capture the main characteristics of the foliar specimen's BDF, namely an angular dependency on the incident angle for the BRDF intermediate to that expected of diffuse and specular reflectors and a near-Lambertian distribution for the BTDF. They also present a good qualitative agreement with the curves provided by the *ABM*, which agree with the experimental curves published by Breece and Holmes [28] and Wooley [156]. The small discrepancies are mainly related to the simplified nature of the *FSM*, and do not significantly affect the image quality as we can see in Figure 8.5.

Figures 8.5a and 8.5b show the first set of images with front lit leaves. The curves presented in Figure 8.6a show that for this graphics setting the rendering process using the *FSM* converges faster, in terms of the ray tracing tree-depth, than the rendering process using the *ABM*. Figures 8.5c and 8.5d show the second set of images with back lit leaves. Similarly, Figure 8.6b shows that for this graphics setting we can also observe a faster convergence for the rendering process using the *FSM*.

Figures 8.5e and 8.5f show the third set of images where only ambient light is used, *i.e.* direct lighting calculations are involved in the rendering processes. Figure 8.6c shows that, as in the previous settings, the rendering process using the *FSM* converges faster. However, for this graphics setting the curves for the *FSM* and the *ABM* are closer.

The spikes in the *FSM* curves presented in Figures 8.7a and 8.7b are caused by the fact that at each ray/interface interaction the *ABM* propagates at most one ray, while the *FSM* always propagates three rays. The presence of non-diffuse (glossy) surfaces other than the foliar tissues in the third graphics setting has a similar effect on the process using the *ABM* (Figures 8.7c), *i.e.* more than one ray is propagated after an interaction with a glossy surface. This aspect, in turn, makes the curves for the *FSM* and the *ABM* (Figure 8.6c) closer.

Although the convergence graphs for the three sets of images (Figure 8.6) are illustrative of the behavior of both models, they do not account for different types and amounts of work performed at each depth of the ray tracing trees. In order to extend our performance evaluation, we have measured the speed-up gains of the *FSM* over the *ABM* for the three graphics settings. These speed-up gains depend on a number of factors: the illuminating and viewing angles, the ratio of the number of pixels associated with the specimen(s) to the total number of pixels (in our case, called foliar ratio), the scene geometry, and the loss of quality threshold (in our case, given by the RMS errors).

As mentioned earlier, the large number of measurements required for an in depth comparison precludes the consideration of all the factors and their combinations in this evaluation procedure. However, the figures presented in Table 8.1 indicate that the use of the *FSM* model can provide noticeable performance gains without a significant loss of image quality. This aspect, in turn, suggests that the *FSM* is more suitable than the *ABM* for applications involving several foliar primitives. The figures presented in Table 8.1 are also consistent with the curves presented in Figure 8.7. These curves show that, to have a relatively small RMS error in the difference images, the *FSM* involves a considerably smaller number of propagated rays than the *ABM*.

Image set	foliar ratio	RMS error			speed-up
		Red	Green	Blue	
1 st	24.97%	0.009	0.009	0.012	5.14
2 nd	19.42%	0.011	0.014	0.010	4.47
3 rd	37.61%	0.020	0.016	0.012	9.77

Table 8.1: Comparison of accuracy vs. performance gain.

In order to reduce noise in the images due to Monte Carlo path tracing integration, a large number of sample points per pixel was used, which increased the absolute time measurements. For instance, the image presented in Figure 8.5f was generated using 400 sample points per pixel and it took 95 minutes (elapsed CPU time) on a SGI R10000. The incorporation of the model into more efficient global illumination frameworks may considerably reduce the overall rendering time.

The overhead of pre-computing the table of reflectances and transmittances is reduced by the fact that, for a given foliar specimen, this operation must be performed only once. Then, the resulting table can be used several times not only in the rendering of individual leaves, but also in global illumination calculations involving vegetation canopies [109]. Furthermore, the table look-ups are performed through direct indexing, and its storage requirements are within reasonable limits. For instance, the table used in our testing experiments requires only 14.5 Kb of storage space. Even if finer sampling resolutions are used in the measurement of reflectances and transmittances, the use of such a table provides a reasonable trade-off between accuracy and computational costs, specially considering the sizes of the memories available nowadays and their decreasing costs.

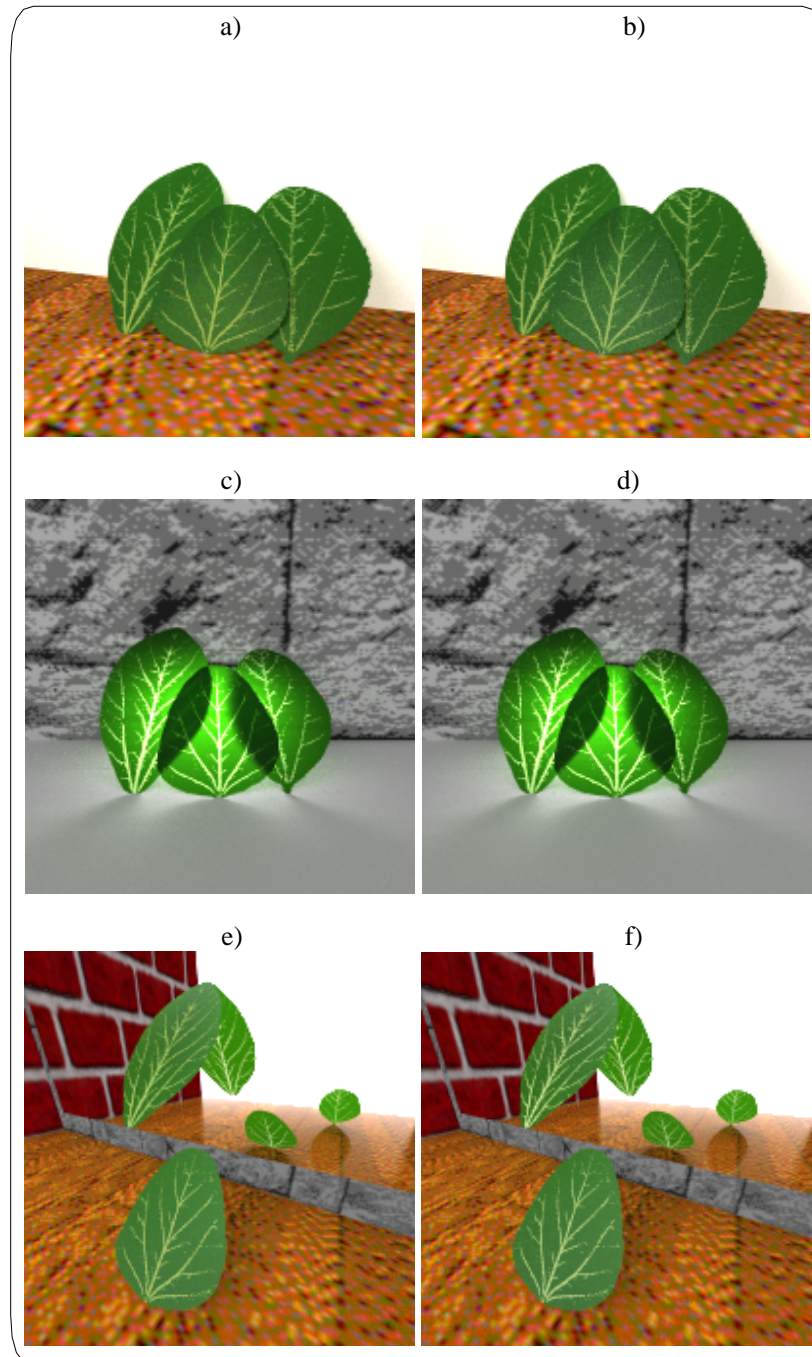


Figure 8.5: Top row: front lit leaves (1^{st} set) using the *ABM* (a) and the *FSM* (b). Middle row: back lit leaves (2^{nd} set) using the *ABM* (c) and the *FSM* (d). Bottom row: Images with ambient light only (3^{rd} set) and using the *ABM* (e) and the *FSM* (f). For all three scenes we used $\varsigma_c = 0.01$.

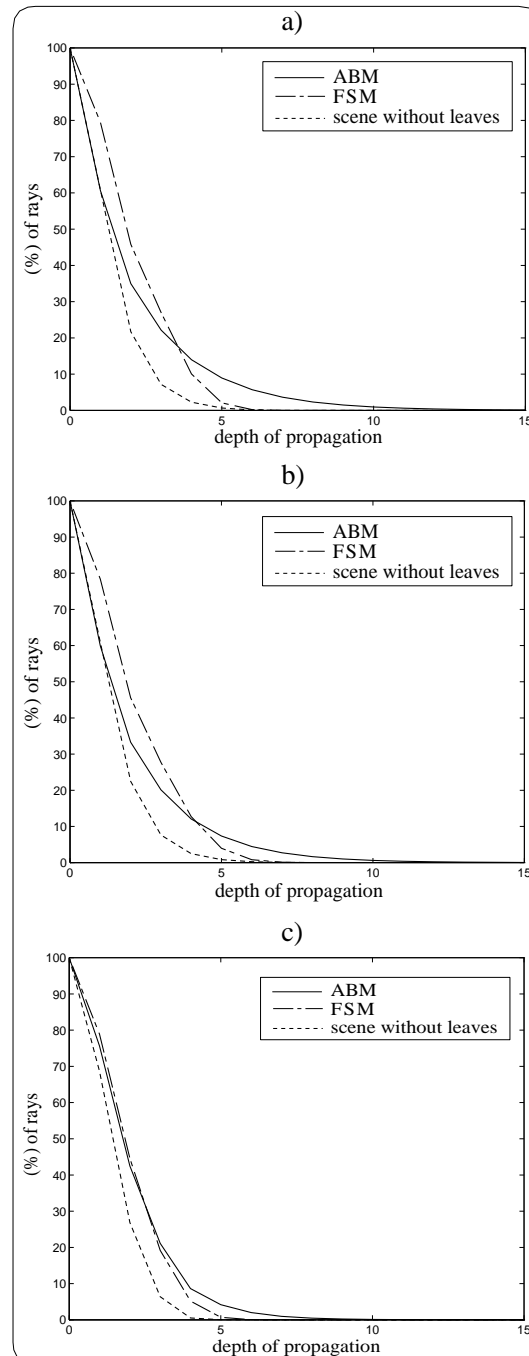


Figure 8.6: Convergence graphs for: a) 1st set, b) 2nd set and c) 3rd set, showing the percentage of rays that still need to be propagated after each depth of propagation.

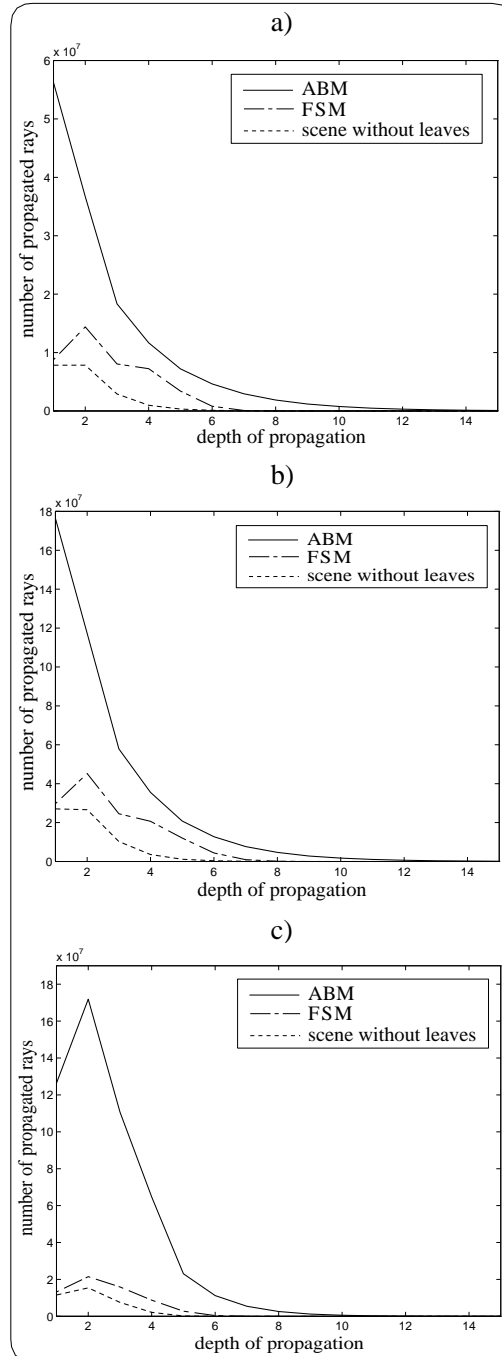


Figure 8.7: Number of rays propagated at each depth of propagation for: a) 1^{st} set, b) 2^{nd} set and c) 3^{rd} set.

Chapter 9

What Next?

In this course we have taken a broad view of the problems related to the design of reflectance and scattering models for light interaction with plant tissues. Many questions remain to be answered, however. Fortunately so, since, as appropriately stated by Hammel [72], “the avenues of open research that a piece of work creates are just as important as the accomplishments it produced”. In this chapter we examine a number of ways that the models and algorithms discussed in this tutorial can be extended to add new features. We also look at more general open problems, their implications and recent developments.

9.1 Accuracy Issues

9.1.1 Surface Reflectance

Several factors need to be taken into account to improve the accuracy of the surface reflectance readings provided by the current models. Among these factors are the presence of hairs and the simulation of shadowing¹ and masking² effects (Figure 9.1) associated with different venation systems and wax configurations.

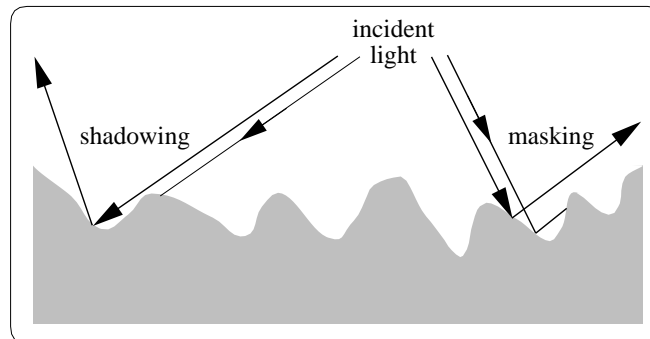


Figure 9.1: Shadowing and masking.

9.1.2 Anisotropy

The models discussed in this tutorial are isotropic. Experiments performed by Wooley on maize leaves [156] showed that these leaves reflect light more diffusively in a plane perpendicular to the veins than in a plane parallel to the veins. This aspect suggests that the anisotropy of plant leaves is associated with the venation systems. Due to the complexity of these systems (Section 4.2.2, further experiments are required to determine the full extent of their relationship with the anisotropy of plant leaves. Unfortunately, as of today, very few publications have presented experiments and data regarding this topic. The modular

¹ Shadowing corresponds to the fraction of incoming light which is shadowed on the way in.

² Masking corresponds to the fraction of reflected light which is obscured in the way out.

and algorithmic nature of the models discussed in this tutorial, however, might allow the incorporation of features to account for anisotropy as more information becomes available in the literature.

9.1.3 Geometrical Representation of Veins

The quality of images of organic materials is affected by several factors beyond the scope of this tutorial. Certainly, the use of more realistic geometric models would improve the realism of these images. However, it is important to notice that despite the sophisticated geometrical models of foliar tissues available in the graphics literature [22, 46, 72, 74, 124], to the best of our knowledge, there is still a lack of geometrical models that accurately account for their venation systems. In fact, this is considered to be an open problem in computer graphics. Currently researchers are investigating the use of cellular texture basis functions [30] and genetically-based algorithms to reproduce the structural characteristics of the veinlets (Figure 9.2) that compose the complex intergrading patterns of the venation systems (Section 4.2.2).

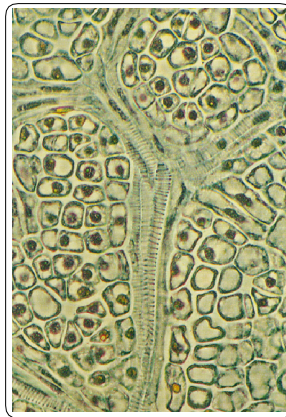


Figure 9.2: Photograph showing the veinlets of a *privet* leaf. Redrawn from [26].

Bump mapping [20] can be used to reduce this problem, by perturbing the normal of the surface to simulate a wrinkle or a vein. However, as pointed out by Glassner [60], it precludes the simulation of phenomena such as the self-blocking and self-shadowing of incident light by the veins, since it does not alter the geometry of the surface. Displacement mapping [40], a technique that actually alters the geometry of the surface, allows the simulation of these phenomena, but, as pointed out by Watt and Watt [154], it presents the drawback of being difficult to incorporate in a standard polygonal mesh renderer.

9.1.4 Environmental Factors

Environmental factors such as deposition of snow, water, dust and chemical substances should also be considered in the design of reflectance and scattering models. For example, these factors could be incorporated to the design of the *ABM* by adding new states to its stochastic simulation of light propagation. Another alternative to account for these factors would involve the application of the K-M theory (Section 5.2).

9.1.5 Spectral Dependency

The use of accurate luminaire data, including its geometrical description, positional information, and spatial and spectral intensity information [71], can also improve the quality of the images of organic materials significantly. Moreover, since the rendering of organic materials like plants have a strong wavelength dependency, the use of more efficient methods for guiding the wavelength selection as well as an investigation to determine the group of wavelengths that fits best the perceptual requirements of these applications could also improve the overall quality of the images of these materials.

9.1.6 Wave Optics Phenomena

Accounting for wave optics phenomena, such as interference³, diffraction⁴ and polarization⁵, however, would require more substantial changes, since the current models are based on geometrical optics. In the context of plant leaves polarization would be the most relevant wave optics phenomenon to be taken into account [68, 104]. Since the perpendicular component of reflectance drops to zero at a particular angle of incidence, θ_f , known as Brewster's angle, the effects of polarization on the overall reflectance become extremely pronounced for certain viewing and illuminating geometries. This angle is given by Brewster's law [60]: $\tan\theta_f = \frac{n_t}{n_i}$. From a remote sensing point of view, since polarization is altered by surface effects, the measurement of this phenomenon allows the decoupling between surface and subsurface components of reflectance. Moreover, the sky receives its color by reflecting light and blue sky light in clear sky is naturally polarized [120]. Therefore, polarization can be important in simulations of natural scenes, particularly those involving the reflection of sky light.

9.2 Efficiency Issues

The efficiency of the current models could also be improved through a detailed analysis of the ray density required to obtain readings with a certain accuracy. This analysis would allow the use of the minimal possible number of rays in data collection and measurement procedures [13]. In addition, their performance could be further maximized through the use of specialized parallel software [33, 143] or hardware [123].

9.3 Extensions

9.3.1 Simulation of Senescence

As mentioned in Chapter 4, besides the carotenoids senescent leaves present also brown pigments called tannis. However, to the best of our knowledge, there is not yet a method to determine the concentration of these pigments [85]. As this data become available, it would be possible to accurately render natural scenes incorporating seasonal variations.

9.3.2 Scattering Profile of Petals and Stems

As also mentioned in Chapter 4, petals and stems have structural and optical characteristics that are similar to plant leaves. However, the accurate simulation of the scattering profile of these biological surfaces would also require specific biological data, which, to the best of our knowledge, either does not exist or is still not readily available.

9.3.3 Near-Infrared and Infrared Applications

In this tutorial we have focussed on aspects associated with the visible region of the light spectrum. In remote sensing applications involving reflectance signatures, however, the near-infrared and the infrared regions are also important. The *ABM* could be adapted to be used in the applications involving these regions.

For example, in the infrared region (beyond $1300nm$ to $2500nm$) the absorption is controlled by the water content. Then, for this region, one would have to consider the absorption coefficients of water [121], instead of the absorption coefficients of pigments, in the absorption testing performed in state 2.

The near-infrared region ($700nm$ to $1300nm$), however, is characterized by a lack of absorption and high values for reflectance and transmittance [144]. For this region weights (initially unit) may be associated with the rays at each interaction according to the Fresnel coefficient. In this case, instead of tracking just one ray after each interaction, we would have to track two. This would represent an additional implementation overhead, but it would reduce considerably the number of rays needed to satisfy the accuracy criteria. Moreover, it would also allow the use of a fractional method, such as the *Russian roulette*, to stop the rays probabilistically.

³ The term interference refers to the phenomenon that waves, under certain conditions, intensify or weaken each other [114].

⁴ Diffraction is the slight bending of light that occurs when light passes very close to an edge [120].

⁵ Polarization of light refers to having the electrical portion of the light waves moving in a single direction rather than in random directions [120].

The *Russian roulette*, a fractional method named by Kahn [89] after the lethal game, has been used in rendering applications with this purpose [60]. In order to cut down the number of particles (rays), we select one whose weight is below some threshold due to multiple bounces during the *random walk*. Then we use some probability \mathcal{P} [41] to discard it (*i.e.* we say the particle is absorbed) or to allow it to continue. In the later case its weight is multiplied by $(1 - \mathcal{P})^{-1}$. This procedure can be repeated (with the same or different values for \mathcal{P}) until the number of particles is reduced to a manageable size [73].

9.4 Radiative Transfer in Regions of Vegetation

In the previous sections we addressed issues mainly related to the interaction of light with individual leaves. In this section we focus on the application of global illumination methods to simulate radiative transfer of energy in regions of vegetation such as forest canopies or crops. Radiation transport in plant canopies has been extensively studied for interpreting remote sensing data [116], such as satellite images used to survey land use and resources, and for predicting vegetation productivity, litter decomposition processes and nutrient cycles within an ecosystem [52].

From the point of view of a satellite regions of vegetation are “surfaces” with a characteristic BDF that determines their appearance under various observation conditions [39]. In order to determine the BDF of a region of vegetation, such as a forest canopy, a model of this vegetation canopy can be constructed and evaluated through computer simulations [62]. Simplified models used in these applications usually treat a canopy as a system of homogeneous volume elements with a certain density. A model of radiative transfer is then used to compute the radiation transport between these volumes [39, 62].

For heterogeneous environments the radiative transfer processes are simulated using Monte Carlo methods [125, 126], which were introduced to plant canopy radiative transfer studies by Tanaka [142]. The application of these methods is done through the simulation of solar radiation transfer processes as an aperiodic *Markov chain* of collisions between photons and foliar tissues. Ross and Marshak [126] provide a detailed review of works in this area and their contributions to the development of a plant canopy radiative transfer theory.

As mentioned by Ross and Marshak, besides its suitability to the simulation of radiative transfer in 3-D inhomogeneous canopies, the use of Monte Carlo methods involves additional advantages. It allows the consideration of the detailed architecture of individual plants, the shape and the area of the leaves, the penumbral effects by penetration of direct solar radiation. Moreover, it also permits the calculation of the statistical characteristics of fluxes and intensities. However, to obtain results of acceptable accuracy a great number of trials is needed, which may increase the computational costs considerably.

Recently, remote sensing researchers and plant biologists started to resort to global illumination approaches developed or improved by the computer graphics community as alternative solutions to simulate radiation transport in plant canopies. Among these approaches is the radiosity method [39]. Gerst and Borel [58] and Borel *et al.* [25] have applied this method to simulate radiative transfer in canopies with several thousand of leaves, and Goel *et al.* [63] have applied it to simulations of radiative transfer in cornfields.

As mentioned by Borel *et al.* [25], the strength of the radiosity method for these applications is the capability of describing quantitatively and physically correctly the interactions of radiation with many surfaces that may be arranged in a complex structure such as a plant canopy. Among the drawbacks of this method one can highlight the difficulties to handle non-Lambertian phenomena. Moreover, this method may demand large computational resources for certain applications, *e.g.* scenes with millions of primitives. Fortunately, one can take advantage of techniques used in computer graphics, such as the clustering of objects hierarchically into volumes [139] and the application of hierarchical radiosity methods [38, 76, 77, 131], to minimize the computational costs.

Methods combining different global illumination techniques have also been used to perform radiative transfer simulations in plant canopies. Govaerts [65] used a Monte Carlo ray tracing algorithm, and Chelle [34] proposed an hybrid approach in which the radiosity method is used for elements of a region of vegetation close to a point of interest and the *SAIL* model (Section 5.2) is used for elements distant from this point of interest. This approach was called nested radiosity for plant canopies [35]. Recently, Mech [112] used a radiosity via ray tracing algorithm [134], also based on Monte Carlo methods, to compute the amount of light reaching plant organs in a given environment.

The Monte Carlo ray tracing based algorithms can be applied to complex environments and are easy to implement. A large number of rays, however, is usually required in order to converge to an accurate solution. Moreover, if there are lighting and reflectance changes in the environment the entire process of “shooting” rays to determine the energy balance in the environment must be repeated. For this case, the application of the classical radiosity method, which consists in solving a system of linear

equations representing the balance of energy of a given environment, may be more appropriate.

Recently Max *et al.* [109] proposed a plane-parallel radiance transport approach for global illumination in vegetation. In this approach the radiance transport problem is reduced to one dimension (1-D) by assuming that the radiance depends angularly on light flow directly on the unit sphere, but positionally only on z , the height above the ground. The resulting partial differential equations are solved by the Runge-Kutta method [29]. Max *et al.* claim that it is a good approximation for dense vegetation, although it is not suitable for isolated trees.

One of the problems of applying global illumination methods in the simulation of radiative transfer in regions of vegetation, such as forest canopies and crops, is the scarce amount of analytical or experimental results to evaluate these methods under these circumstances. Usually the results regarding a proposed approach are compared with the results provided by a different approach based on similar assumptions. If they present a good agreement, the accuracy of the proposed approach is considered satisfactory, although they may be both far from the real solution.

The local and global levels of light interaction with plants, namely the reflectance and scattering models for individual leaves and the radiative transfer processes for canopies, are directly connected. New developments or improvements on either level, or in both, will have a direct influence on the accuracy and efficiency of the rendering methods for natural scenes. For instance, since most of the approaches used to compute radiative transfer in regions of vegetation consider the volume elements or leaves as presenting only Lambertian characteristics, the incorporation of physically and biologically-based models including non-Lambertian effects and absorption for these elements is likely to increase the overall accuracy of these approaches. Furthermore, since the computation of radiance at all positions necessary to account for all sources of radiation in a vegetation canopy usually involves the iterative solution of a large linear system, the investigation of faster solutions for such systems would also improve the efficiency of the radiative transfer approaches for plant canopies.

It was demonstrated that for environments with high average reflectance and high level of occlusion the Chebyshev method [8, 9] can outperform methods usually used to solve such systems (such as Gauss Seidel, progressive refinement, overrelaxation etc.). Recall that a vegetation canopy is characterized by a high level of occlusion between the elements. Moreover, in the near-infrared region the scattering of light by a plant leaf is more than 85%, *i.e.*, vegetation canopies are environments with reasonably high average reflectance. Therefore, as pointed out by Chelle *et al.* [35], the Chebyshev method is the appropriate tool to be used in simulation of radiative transfer in regions of vegetation in the near-infrared. Recently Leblond *et al.* [98] have extended the research on this area with the application of hybridization techniques to speedup the solution of radiative transfer systems.

Chapter 10

Conclusion

Physically-based rendering techniques allow us to generate very realistic images of inorganic objects such as chairs, cars, buildings and so on. However, when it comes to organic or biological materials, such as human skin or foliar tissues, one realizes that there is still a long way to go in order to achieve a similar degree of realism. This gap is mostly due to our lack of understanding on how light interacts with these materials, what are the physical processes involved and what are the biological factors affecting them.

In order to bridge this gap we should not dismiss the existing physically-based rendering techniques available, but proceed further by incorporating biologically-based techniques as well. The computer graphics community is always looking for new challenges. It only takes a quick look through our office window to realize that some of the most interesting open problems in our field lay on the simulation of natural phenomena, specially in outdoor scenes. Plants are everywhere, and any simulation of a natural scene has to address the way that they reflect, transmit and absorb light. After all, leaves are the most important biological surface interacting with light. In this tutorial we examined biological issues involved in these processes, presented the current state of art in terms of the simulation of light interaction with plants and pointed out aspects that shall be addressed to improve the rendering of natural scenes.

The contents of this tutorial may be viewed as a starting point for future research in areas that still represent open frontiers for computer graphics, such as the visual simulation of natural environments, and visual simulation of biological processes. One of the important ways in which a plant interacts with environment is through the radiative transfer of luminous energy, which, in turn, depends on the accurate modeling of the processes of light interaction with foliar tissues. As discussed in the previous chapter, there are still many aspects of these processes that are not considered in the current models. In addition, more comprehensive and accurate models would be useful not only in the realistic rendering of natural scenes, but also in areas outside the scope of computer graphics such as remote sensing (to obtain data for regions of vegetation through the use of inversion procedures) and biology (to evaluate theories and data).

In closing, despite recent advances in rendering, there are many questions that need to be solved in order to achieve a true realism of natural environments using reasonable computational resources. In these course notes many problems and issues that are worth looking into are listed. However, several aspects of the rendering pipeline that affect the realism of computer generated images of life forms are beyond the scope of this tutorial, such as geometrical modeling, spectral sampling, use of accurate luminaire data, participating media and so on. Viewed in this context, the main topic of this tutorial this tutorial, namely the biologically-based simulation of light interaction with plants, might be seen as a growing branch in a growing tree. The other branches of the tree would represent other areas of research related to the different stages of the rendering pipeline. They are equally important and we hope that, eventually, they will form a well balanced canopy whose final size, shape and reflectance signature remain to be seen.

References

- [1] ALLEN, W., GAUSMAN, H., AND RICHARDSON, A. Mean effective optical constants of cotton leaves. *Applied Optics* 9, 11 (1970), 2573–2577.
- [2] ALLEN, W., GAUSMAN, H., RICHARDSON, A., AND THOMAS, J. Interaction of isotropic light with a compact plant leaf. *Journal of the Optical Society of America* 59, 10 (1969), 1376–1379.
- [3] ALLEN, W., GAYLE, T., AND RICHARDSON, A. Plant canopy irradiance specified by the Duntley equations. *Journal of the Optical Society of America* 60, 3 (1970), 372–376.
- [4] ALLEN, W., AND RICHARDSON, A. Interaction of light with a plant leaf canopy. *Journal of the Optical Society of America* 58, 18 (1968), 1023–1028.
- [5] ALLEN, W., AND RICHARDSON, A. Willstater-stoll theory of leaf reflectance evaluated by ray tracing. *Applied Optics* 12, 10 (1973), 2448–2453.
- [6] ANSI. Nomenclature and definitions for illuminating engineering. In *ANSI/IES RP-6-1986*. Illuminating Engineering Society of North America, New York, 1986.
- [7] ARVO, J. *Analytic Methods for Simulated Light Transport*. PhD thesis, Yale University, 1995.
- [8] BARANOSKI, G. *Biologically and Physically-Based Rendering of Natural Scenes*. PhD thesis, Department of Computer Science, University of Calgary, November 1998.
- [9] BARANOSKI, G., BRAMLEY, R., AND SHIRLEY, P. Fast radiosity solutions for environments with high average reflectance. In *Rendering Techniques'95 (Proceedings of the Sixth Eurographics Rendering Workshop)* (Dublin, June 1995), P. M. Hanrahan and W. Purgathofer, Eds., Springer-Verlag, pp. 345–356.
- [10] BARANOSKI, G., AND ROKNE, J. An algorithmic reflectance and transmittance model for plant tissue. *Computer Graphics Forum (EUROGRAPHICS Proceedings)* 16, 3 (September 1997), 141–150.
- [11] BARANOSKI, G., AND ROKNE, J. A nondeterministic reconstruction approach for isotropic reflectances and transmittances. *The Journal of Visualization and Computer Animation* 10, 4 (1999), 225–231. Special issue, selected papers of the Sixth Pacific Conference on Computer Graphics and Applications - Pacific Graphics'98, Singapore, October, 1998.
- [12] BARANOSKI, G., AND ROKNE, J. Efficiently simulating scattering of light by leaves. *The Visual Computer* (2001). To appear.
- [13] BARANOSKI, G., ROKNE, J., AND XU, G. Virtual spectrophotometric measurements for biologically and physically-based rendering. *The Visual Computer* (2001). To appear.
- [14] BARET, F., ANDRIEU, B., AND GUYOT, G. A simple model for leaf optical properties in visible and near infrared: application to the analysis of spectral shifts determinism. In *Applications of Chlorophyll Fluorescence* (1988), Kluwer Academic, pp. 345–351.
- [15] BECKMANN, P., AND SPIZZICHINO, A. *The Scattering of Electromagnetic Waves from Rough Surfaces*. MacMillan, New York, 1963.

- [16] BENFORD, F. Radiation in a diffusing medium. *Journal of the Optical Society of America* 36 (1946), 524–537.
- [17] BENSON, L. *Plant Classification*. D.C. Heath and Company, Boston, 1957.
- [18] BIOLLEY, J., AND JAY, M. Anthocyanins in modern roses: Chemical and colorimetric features in relation to colour range. *Journal of Experimental Botany* 44, 268 (1993), 1725–1734.
- [19] BJORN, L. Interception of light by plant leaves. In *Crop Photosynthesis: Spatial and Temporal Determinants* (Amsterdam, 1992), N. R. Baker and H. Thomas, Eds., Elsevier, pp. 253–276.
- [20] BLINN, J. Simulation of wrinkled surfaces. *Computer Graphics (SIGGRAPH Proceedings)* 12, 3 (1977), 286–292.
- [21] BLOOMENTHAL, J. Modeling the mighty maple. *Computer Graphics (SIGGRAPH Proceedings)* 19, 3 (July 1985), 305–311.
- [22] BLOOMENTHAL, J. *Skeletal Design of Natural Forms*. PhD thesis, Department of Computer Science, University of Calgary, January 1995.
- [23] BONE, R., LEE, D., AND NORMAN, J. Epidermal cells functioning as lenses in leaves of tropical rain-forest shade plants. *Applied Optics* 24, 10 (May 1985), 1408–1412.
- [24] BONNER, J., AND VARNER, J. *Plant Biochemistry*. Academic Press, New York, 1965.
- [25] BOREL, C., GERSTL, S., AND POWERS, B. The radiosity method in optical remote sensing of structured 3-d surfaces. *Remote Sensing of Environment* 19 (1991), 13–44.
- [26] BOWES, B. *A Colour Atlas of Plant Structure*. Manson Publishing, 1997.
- [27] BRAKKE, T., SMITH, J., AND HARNDEN, J. Bidirectional scattering of light from tree leaves. *Remote Sensing of Environment* 29 (1989), 175–183.
- [28] BREECE, H., AND HOLMES, R. Bidirectional scattering characteristics of healthy green soybean and corn leaves in vivo. *Applied Optics* 10, 1 (January 1971), 119–127.
- [29] BURDEN, R., AND FAIRES, J. *Numerical Analysis*, fifth ed. PWS-KENT Publishing Company, Boston, 1993.
- [30] BURGE, T. A branching cellular texture basis function. In *SIGGRAPH 2000 Conference Abstracts and Applications* (New York, 2000), T. Appolloni, Ed., ACM SIGGRAPH, p. 181.
- [31] BUTLER, W. Absorption spectroscopy in vivo: Theory and applications. *Annual Review of Plant Physiology* 15 (1964), 451–470.
- [32] CHANDRASEKAR, S. *Radiative Transfer*. Dover Publications, New York, 1960.
- [33] CHANDY, K., AND KESSELMAN, C. CC++: A declarative concurrent object-oriented programming notation. In *Research Directions in Concurrent Object-Oriented Programming* (Cambridge, Massachusetts, 1993), G. Agha, P. Wegner, and A. Yonezawa, Eds., The MIT Press, pp. 282–313. Chapter 11.
- [34] CHELLE, M. *Développement d'un modèle de radiosité mixte pour simuler la distribution du rayonnement dans les couverts végétaux*. PhD thesis, L'Université de Rennes I, France, March 1997.
- [35] CHELLE, M., ANDRIEU, B., AND BOUATOUCH, K. Nested radiosity for plant canopies. *The Visual Computer* 14, 3 (1998), 109–125.
- [36] CLARKE, F., AND PARRY, D. Helmholtz reciprocity: Its validity and application to reflectometry. *Lighting Research and Technology* 17, 1 (1985), 1–11.
- [37] CLAYTON, R. *Molecular Physics in Photosynthesis*. Blaisdell Publishing Company, Cambridge, England, 1965.

- [38] COHEN, M., GREENBERG, D., IMMEL, D., AND BROCK, P. An efficient radiosity approach for realistic image synthesis. *IEEE Computer Graphics and Applications* 6, 3 (March 1986), 26–35.
- [39] COHEN, M., AND WALLACE, J. *Radiosity and Realistic Image Synthesis*. Academic Press Professional, Cambridge, 1993.
- [40] COOK, R. Shade trees. *Computer Graphics (SIGGRAPH Proceedings)* 18, 4 (July 1984), 223–231.
- [41] COVEYOU, R., CAIN, V., AND YOST, K. Adjoint and importance in Monte Carlo application. *Nuclear Science and Engineering* 27 (1967), 219–234.
- [42] CROWTHER, B. Computer modeling of integrating spheres. *Applied Optics* 35, 30 (1996), 5880–5886.
- [43] DAWSON, T., CURRAN, P., AND PLUMMER, S. LIBERTY-modeling the effects of leaf biochemical concentration on reflectance spectra. *Remote Sensing of Environment* 65 (1998), 50–60.
- [44] DEVLIN, R., AND BARKER, A. *Photosynthesis*. Van Nostrand Reinhold Company, New York, 1971.
- [45] DEYOUNG, J., AND FOURNIER, A. Properties of tabulated bidirectional reflectance distribution functions. In *Proceedings of Graphics Interface* (1997), pp. 47–55.
- [46] DIMIAN, D. Physically-based model of folded surfaces. Master’s thesis, Department of Computer Science, The University of Calgary, November 1997.
- [47] DUNTLEY, S. The optical properties of diffusing materials. *Journal of the Optical Society of America* 32, 2 (February 1942), 61–70.
- [48] E284-91C, A. S. Standard terminology of appearance. In *Physics-Based Vision Principles and Practice: Radiometry* (Boston, 1992), L. Wolff, S. Shafer, and G. Healey, Eds., Jones and Bartlett Publishers, pp. 146–161.
- [49] ESAU, K. *Plant Anatomy*. John Wiley & Sons, Inc., New York, 1953.
- [50] FENDLEY, J. An analysis of the measuring procedure for the integrating sphere spectrophotometer. *Solar Energy* 35, 3 (1985), 281–282.
- [51] FOURNIER, A. From local to global illumination and back. In *Rendering Techniques’95 (Proceedings of the Sixth Eurographics Rendering Workshop)* (Dublin, June 1995), P. M. Hanrahan and W. Purgathofer, Eds., Springer-Verlag, pp. 127–136.
- [52] FOURTY, T., BARET, F., JACQUEMOUD, S., SCHMUCK, G., AND VERDEBOUT, J. Leaf optical properties with explicit description of its biochemical composition: Direct and inverse problems. *Remote Sensing of Environment* 56 (1996), 104–117.
- [53] GANAPOL, B., JOHNSON, L., HAMMER, P., HLAVKA, C., AND PETERSON, D. A new within-leaf radiative transfer model: preliminary results. In *IGARSS’95: 15th International Geoscience and Remote Sensing Symposium* (Florence, Italy, 1995), pp. 1457–1459.
- [54] GANAPOL, B., JOHNSON, L., HAMMER, P., HLAVKA, C., AND PETERSON, D. LEAFMOD: A new within-leaf radiative transfer model. *Remote Sensing of Environment* 63 (1998), 182–193.
- [55] GATES, D., KEEGAN, H., SCHELTER, J., AND WEIDNER, V. Spectral properties of plants. *Applied Optics* 4, 1 (January 1965), 11–20.
- [56] GAUSMAN, H., AND ALLEN, W. Optical parameters of leaves of 30 plant species. *Plant Physiology* 52 (1973), 57–62.
- [57] GAUSMAN, H., ALLEN, W., AND ESCOBAR, D. Refractive index of plant cell walls. *Applied Optics* 13, 1 (1973), 109–111.

- [58] GERSTL, S., AND BOREL, C. Principles of the radiosity method for canopy reflectance modeling. In *International Geoscience and Remote Sensing Symposium - IGARSS'90* (Washington, May 1990), pp. 1735–1737.
- [59] GILKS, W., RICHARDSON, S., AND SPIEGELHALTER, D. *Markov Chain Monte Carlo in Practice*. Chapman & Hall, London, 1996.
- [60] GLASSNER, A. *Principles of Digital Image Synthesis*. Morgan Kaufmann, San Francisco, 1995.
- [61] GOEBEL, D. Generalized integrating-sphere theory. *Applied Optics* 6, 1 (January 1967), 125–128.
- [62] GOEL, N. Models of vegetation canopy reflectance and their use in the estimation of biophysical parameters from reflectance data. *Remote Sensing Review* 4, 1 (1988), 221.
- [63] GOEL, N., ROZEHNAL, I., AND THOMPSON, R. A computer graphics based model for scattering from objects of arbitrary shapes in the optical region. *Remote Sensing of Environment* 36 (1991), 73–104.
- [64] GOERTLER, S., COHEN, M., AND SLUSALLEK, P. Radiosity and relaxation methods. *IEEE Computer Graphics and Applications* 14, 6 (November 1994), 48–58.
- [65] GOVAERTS, Y. *A model of light scattering in three-dimensional plant canopies: a Monte Carlo ray tracing approach*. PhD thesis, Département of Physique, Faculté des Sciences, Université Catholique de Louvain-la-Neuve, 1995.
- [66] GOVAERTS, Y., AND M. VERSTRAETE, S. J., AND USTIN, S. Three-dimensional radiation transfer modeling in a dycotyledon leaf. *Applied Optics* 35, 33 (November 1996), 6585–6598.
- [67] GRANT, L. Diffuse and specular characteristics of leaf reflectance. *Remote Sensing of Environment* 22 (1987), 309–322.
- [68] GRANT, L., DAUGHTRY, C., AND VANDERBILT, V. Polarized and specular reflectance variance with leaf surface features. *Physiologia Plantarum* 88, 1 (1993), 1–9.
- [69] GUPTA, R., AND WOOLEY, J. T. Spectral properties of soybean leaves. *Agronomy Journal* 63 (1971), 123–126.
- [70] HALL, R. A characterization of illumination models and shading techniques. *Visual Computer* 2, 5 (November 1986), 268–277.
- [71] HALL, R., AND GREENBERG, D. A testbed for realistic image synthesis. *IEEE Computer Graphics and Applications* 3, 8 (November 1983), 10–20.
- [72] HAMMEL, M. *Differential L-systems and their application to the simulation and visualisation of plant development*. PhD thesis, Department of Computer Science, University of Calgary, June 1996.
- [73] HAMMERLEY, J., AND HANDSCOMB, D. *Monte Carlo Methods*. Wiley, New York, 1964.
- [74] HANAN, J. *Parametric L-Systems*. PhD thesis, University of Regina, June 1992.
- [75] HANRAHAN, P., AND KRUEGER, W. Reflection from layered surfaces due to subsurface scattering. *Computer Graphics (SIGGRAPH Proceedings)* (August 1993), 165–174.
- [76] HANRAHAN, P., AND SALZMAN, D. A rapid hierarchical algorithm for unoccluded environments. In *Eurographics Workshop on Photosimulation, Realism and Physics in Computer Graphics* (Amsterdam, June 1990), K. Bouatouch and C. Bouville, Eds., Elsevier, pp. 151–171.
- [77] HANRAHAN, P., SALZMAN, D., AND AUPPERLE, L. A rapid hierarchical radiosity algorithm. *Computer Graphics (SIGGRAPH Proceedings)* 25, 4 (July 1991), 197–206.
- [78] HECHT, E., AND ZAJAC, A. *Optics*. Addison-Wesley, Reading, Massachusetts, 1974.
- [79] HECKBERT, P. Writing a ray tracer. In *An Introduction to Ray Tracing* (San Diego, CA, 1989), A. Glassner, Ed., Academic Press.

- [80] HENLEY, L., AND GREENSTEIN, J. Diffuse radiation in galaxy. *Astrophysics Journal* 93 (1941), 70–83.
- [81] HOSGOOD, B., JACQUEMOUD, S., ANDREOLI, G., VERDEBOUT, J., PEDRINI, G., AND SCHMUCK, G. Leaf optical properties experiment 93. Tech. Rep. Report EUR 16095 EN, Joint Research Center, European Commission, Institute for Remote Sensing Applications, 1995.
- [82] HUNTER, R., AND HAROLD, R. *The Measurement of Appearance*, second ed. John Wiley & Sons, New York, 1987.
- [83] IMMEL, D., COHEN, M., AND GREENBERG, D. A radiosity method for non-diffuse environments. *Computer Graphics (SIGGRAPH Proceedings)* 20, 4 (1986), 133–142.
- [84] ISHIMURA, A. *Wave Propagation and Scattering in Random Media*. Academic Press, New York, 1978.
- [85] JACQUEMOUD, S., AND BARET, F. Prospect: A model of leaf optical properties spectra. *Remote Sensing of Environment* 34, 2 (1990), 75–92.
- [86] JACQUEMOUD, S., AND USTIN, S. Leaf optical properties: A state of the art. In *8th International Symposium of Physical Measurements & Signatures in Remote Sensing* (Aussois, France, 2001), CNES, pp. 223–332.
- [87] JACQUEMOUD, S., USTIN, S., VERDEBOUT, J., SCHMUCK, G., ANDREOLI, G., AND HOSGOOD, B. Estimating leaf biochemistry using prospect leaf optical properties model. *Remote Sensing of Environment* 56 (1996), 194–202.
- [88] JUDD, D., AND WYSZECKI, G. *Color in Business, Science and Industry*, third ed. John Wiley & Sons, New York, 1975.
- [89] KAHN, H. Use of different Monte Carlo sampling techniques. In *Symposium on Monte Carlo Methods* (New York, 1956), H. Meyer, Ed., John Wiley & Sons, pp. 146–190.
- [90] KAJIYA, J. Anisotropic reflection models. *Computer Graphics (SIGGRAPH Proceedings)* 19, 3 (July 1985), 15–22.
- [91] KAJIYA, J. The rendering equation. *Computer Graphics (SIGGRAPH Proceedings)* 20, 4 (August 1986), 143–150.
- [92] KALOS, M., AND WHITLOCK, P. *Monte Carlo Methods*, vol. Volume I: Basics. John Wiley & Sons, New York, 1986.
- [93] KAY, Q., DAOUD, H., AND STIRTON, C. Pigment distribution, light reflection and cell structure in petals. *Botanic Journal of the Linnean Society* 83 (1981), 57–84.
- [94] KUMAR, R., AND SILVA, L. Light ray tracing through the leaf cross section. *Applied Optics* 12, 12 (1973), 2950–2954.
- [95] LAFORTUNE, E. *Mathematical Models and Monte Carlo Algorithms for Physically Based Rendering*. PhD thesis, Department of Computer Science, Faculty of Engineering, Katholieke Universiteit Leuven, 1996.
- [96] LAFORTUNE, E., AND WILLEMS, Y. D. Using the modified phong reflectance model for physically based rendering. Tech. rep., Department of Computer Science, K.U. Leuven, November 1994.
- [97] LALONDE, P., AND FOURNIER, A. A wavelet representation of reflectance functions. *IEEE Transaction on Visualization and Computer Graphics* 3, 4 (October 1997), 329–336.
- [98] LEBLOND, M., ROUSSELLE, F., AND RENAUD, C. Hybridization techniques for fast radiosity solvers. In *Proceedings of the Computer Graphics International 2000* (Geneva, Switzerland, June 2000), pp. 269–278.
- [99] LEWIS, R. Making shaders more physically plausible. In *Proceedings of the Fourth Eurographics Rendering Workshop* (Paris, June 1993), M. Cohen and C. Puech, Eds., pp. 47–62.
- [100] LEWIS, R. Making shaders more physically plausible. *Computer Graphics Forum* 13 (June 1994), 109–120.
- [101] LILLEY, C., LIN, F., HEWITT, W., AND HOWARD, T. *Colour in Computer Graphics*. ITTI Computer graphics and Visualisation, Manchester Computing Centre, The University of Manchester, Manchester, England, December 1993.

- [102] LONGHURST, R. *Geometrical and Physical Optics*, third ed. Longman Group Limited, London, 1973.
- [103] LUDEKER, W., AND GUNTHER, K. Leaf reflectance: A stochastic model for analysing the blue shift. In *Pro. Symp. On Global Environmental Monitoring* (Victoria, BC, Canada, 1990), pp. 465–480.
- [104] MA, Q., NISHIMURA, A., PHU, P., AND KUGA, Y. Transmission, reflection and depolarization of an optical wave for a single leaf. *IEEE Transactions on Geoscience and Remote Sensing* 28, 5 (September 1990), 865–872.
- [105] MACADAM, D. *Color Measurements Theme and Variations*. Springer Verlag, Berlin, 1981.
- [106] MAIER, S., LUDEKER, W., AND GUNTHER, K. SLOP: A revised version of the stochastic model for leaf optical properties. In *Physical Measurements and Signatures In Remote Sensing* (Balkerna, Rotterdam, 1997), Guyot and P. Phulpin, Eds., pp. 327–331.
- [107] MARCHUK, G., MIKHAILOV, G., NAZARALIEV, M., DARBINJAN, M., KARGIN, B., AND ELEPOV, B. *The Monte Carlo Methods in Atmospheric Optics*. Springer Verlag, Berlin, 1980.
- [108] MARTIN, G., MYERS, D., AND VOGELMANN, T. Characterization of plant epidermal lens effects by a surface replica technique. *Journal of Experimental Botany* 42, 238 (May 1991), 581–587.
- [109] MAX, N., MOBLEY, C., KEATING, B., AND WU, E. Plane-parallel radiance transport for global illumination in vegetation. In *Rendering Techniques'97 (Proceedings of the Eight Eurographics Rendering Workshop)* (Etienne, June 1997), J. Dorsey and P. Slusallek, Eds., Springer-Verlag, pp. 239–250.
- [110] MCCLENDON, J. The micro-optics of leaves. i. patterns of reflection from the epidermis. *American Journal of Botany* 71, 10 (1984), 1391–1397.
- [111] MCCLENDON, J., AND FUKSHANSKY, L. On the interaction of absorption spectra of leaves - ii. the non-absorbed ray of the sieve effect and the mean optical pathlength in the remainder of the leaf. *Photochemistry and Photobiology* 51, 2 (1990), 211–216.
- [112] MECH, R. *Modeling and Simulation of the Interaction of Plants with the Environment using L-systems and their Extensions*. PhD thesis, Department of Computer Science, University of Calgary, November 1997.
- [113] MELANED, M. Optical properties of powders. Part I. optical absorption coefficients and the absolute value of the diffuse reflectance. *Journal of Applied Physics* 34 (1963), 560–570.
- [114] MEYER-ARENDE, J. *Introduction to Modern and Classical Optics*. Prentice-Hall, New Jersey, 1984.
- [115] MOBLEY, C. *Light and Water: Radiative Transfer in Natural Waters*. Academic Press, San Diego, 1994.
- [116] MYNEMI, R., ROSS, J., AND ASRAR, G. A review on the theory of photon transport in leaf canopies. *Agricultural and Forest Meteorology* 45 (1989), 1–153.
- [117] NICODEMUS, F., RICHMOND, J., HSIA, J., GINSBERG, I., AND LIMPERIS, T. Geometrical considerations and nomenclature for reflectance. In *Physics-Based Vision Principles and Practice: Radiometry* (Boston, 1992), L. Wolff, S. Shafer, and G. Healey, Eds., Jones and Bartlett Publishers, pp. 94–145.
- [118] NISHITA, T., SIRAI, T., TADAMURA, K., AND NAKAMAE, E. Display of the earth taking into account atmospheric scattering. In *SIGGRAPH Proceedings, Annual Conference Series* (August 1993), pp. 175–182.
- [119] NORMAN, A. *Soybean Physiology, Agronomy, and Utilization*. Academic Press, New York, N.Y., 1978.
- [120] OVERHEM, R., AND WAGNER, D. *Light and Color*. John Wiley & Sons, New York, N.Y., 1982.
- [121] PALMER, K., AND WILLIAMS, D. Optical properties of water in the near infrared. *Journal of the Optical Society of America* 64, 8 (August 1974), 1107–1110.

- [122] PHONG, B. Illumination for computer generated pictures. *Communications of ACM* 18, 6 (June 1975), 311–317.
- [123] POTTER, D., AND CLINE, M. Massive parallel computational simulations in light scattering. *Proceedings of the IEEE* 79, 4 (April 1991), 567–572.
- [124] PRUSINKIEWICZ, P., AND LINDENMAYER, A. *The Algorithmic Beauty of Plants*. Springer Verlag, New York, 1990.
- [125] ROSS, J., AND MARSHAK, A. Calculation of canopy bidirectional reflectance using the Monte Carlo method. *Remote Sensing of Environment* 24 (1988), 213–225.
- [126] ROSS, J., AND MARSHAK, A. Monte Carlo methods. In *Photon - Vegetation Interactions - Applications in Optical Remote Sensing and Ecology* (Berlin, 1991), R. Mynemi and J. Ross, Eds., Springer-Verlag, pp. 441–467. ch. 14.
- [127] RUHLE, W., AND WILD, A. The intensification of absorbance changes in leaves by light-dispersion. differences between high-light and low-light leaves. *Planta* 146 (1979), 551–557.
- [128] SALISBURY, F., AND ROSS, C. *Plant Physiology*, third ed. Wadsworth Publishing Company, Belmont, California, 1985.
- [129] SCHLICK, C. An inexpensive brdf model for physically-based rendering. *Proc. of European Association for Computer Graphics Conference and Exhibition - EUROGRAPHICS 13*, 3 (1994), 233–246.
- [130] SELIGER, H., AND MCELROY, W. *Light: Physical and Biological Action*. Academic Press, New York, 1966.
- [131] SHINYA, M., MORI, T., AND OSUMI, N. A system subdivision approach for large radiosity computation. *The Visual Computer* 14 (1998), 18–30.
- [132] SHIRLEY, P. Physically based lighting calculations for computer graphics: A modern perspective. In *Eurographics Workshop on Photosimulation, Realism and Physics in Computer Graphics* (Amsterdam, June 1990), K. Bouatouch and C. Bouville, Eds., Elsevier, pp. 67–81.
- [133] SHIRLEY, P. *Physically based lighting for computer graphics*. PhD thesis, Dept. of Computer Science, University of Illinois, November 1990.
- [134] SHIRLEY, P. Radiosity via ray tracing. In *Graphics Gems II* (1991), Ed. Academic Press, pp. 306–310.
- [135] SHIRLEY, P. Time complexity of Monte Carlo radiosity. In *Proceedings of the Annual Conference of the European Association for Computer Graphics - EUROGRAPHICS* (Amsterdam, 1991), F. Post and W. Barth, Eds., North-Holland, pp. 459–465.
- [136] SHIRLEY, P., BARANOSKI, G., CHO, B., DEFRANCESCO, A., GUPTA, V., JONES, B., KAMATH, R., KIM, J., KIM, K., LOOS, T., MA, H., MEYER, C., RUSINOV, D., SAMPSON, S., VOGL, G., WINNICKA, B., AND ZIMMERMAN, K. *The GG Library Reference Manual*. Department of Computer Science, Indiana University, Bloomington, Indiana, USA, 1993.
- [137] SHIRLEY, P., AND WANG, C. Distribution ray tracing: Theory and practice. In *Proceedings of the Third Eurographics Workshop on Rendering* (Bristol, England, 1992), pp. 200–209.
- [138] SIEGEL, R., AND HOWELL, J. *Thermal Radiation Heat Transfer*. MacGraw-Hill Kogakusha, Tokyo, 1972.
- [139] SILLION, F. A unified hierarchical algorithm for global illumination with scattering volumes and object clusters. *IEEE Transactions on Visualization and Computer Graphics* 1, 3 (1995), 240–254.
- [140] SMAIL, L. *Analytic Geometry and Calculus*. Appleton-Century-Crofts, New York, 1953.
- [141] SUITS, G. The calculation of the directional reflectance of a vegetative canopy. *Remote Sensing of Environment* 2 (1972), 117–125.

- [142] TANAKA, S. Estimation of sunlit leaf area in tobacco plant community by the Monte Carlo method. estimation on direct sunlight. In *Photosynthesis and Utilization of Solar Energy. Level III Exp 1968, J IBP/PP - Photosynthesis Level III Group* (Tokyo, 1969), pp. 76–79.
- [143] TODLER, K., AND HAMMER, C. PARC++: A parallel C++. *Software Practice and Experience* 25, 6 (June 1995), 623–636.
- [144] TUCKER, C., AND GARRAT, M. Leaf optical system modeled as a stochastic process. *Applied Optics* 16, 3 (1977), 635–642.
- [145] TURNER, G. *Introduction to Paint Chemistry*. Chapman and Hall, New York, 1967.
- [146] VEAH, E. *Robust Monte Carlo Methods for Light Transport Simulation*. PhD thesis, Stanford University, December 1997.
- [147] VERHOEF, W. Light scattering by leaf layers with application to reflectance canopy modeling: the sail model. *Remote Sensing of Environment* 16 (1984), 125–141.
- [148] VERHOEF, W. Earth observation modeling based on layer scattering matrices. *Remote Sensing of Environment* 17 (1985), 164–178.
- [149] VERNON, L., AND SEELY, G. *The Chlorophylls*. Academic Press, New York, 1966.
- [150] VOGELMANN, T. Plant tissue optics. *Annual Review of Plant Physiology and Plant Molecular Biology* 44 (1993), 231–251.
- [151] VOGELMANN, T., AND MARTIN, G. The functional significance of palisade tissue: penetration of directional versus diffuse light. *Plant, Cell and Environment* 16 (1993), 65–72.
- [152] WALTER-SHEA, E., NORMAN, J., AND BLAD, B. A two-pass solution to the rendering equation: A synthesis of ray tracing and radiosity methods. *Remote Sensing of Environment* 29 (1989), 161–174.
- [153] WARD, G. Measuring and modeling anisotropic reflection. *Computer Graphics (SIGGRAPH Proceedings)* (July 1992), 265–272.
- [154] WATT, A., AND WATT, M. *Advanced Animation and Rendering Techniques*. Addison-Wesley, New York, 1992.
- [155] WESTIN, S., ARVO, J., AND TORRANCE, K. Predicting reflectance from complex surfaces. *Computer Graphics (SIGGRAPH Proceedings)* 26, 2 (July 1992), 255–264.
- [156] WOOLLEY, J. Reflectance and transmittance of light by leaves. *Plant Physiology* 47 (1971), 656–662.
- [157] WOOLLEY, J. Refractive index of soybean leaf cell walls. *Plant Physiology* 55 (1975), 172–174.
- [158] YAMADA, N., AND FUJIMURA, S. A mathematical model of reflectance and transmittance of plant leaves as a function of chlorophyll pigment content. In *International Geoscience and Remote Sensing Symposium* (September 1988), pp. 833–834.
- [159] ZERLAUT, G., AND ANDERSON, T. Multiple-integrating sphere spectrophotometer for measuring absolute spectral reflectance and transmittance. *Applied Optics* 20, 21 (November 1981), 3797–3804.
- [160] ZSCHEILE, F., AND COMAR, C. Influence of preparative procedure on the purity of chlorophyll components as shown by absorption spectra. *Botanical Gazette* 102 (March 1941), 463–481.
- [161] ZSCHEILE, F., JR., J. W., BEADLE, B., AND ROACH, J. The preparation and absorption spectra of five pure carotenoids pigments. *Plant Physiology* 17, 3 (July 1942), 331–346.

Index

- abaxial epidermis, 36
- ABM, 51
- absorptance, 18
- absorption spectra, 37
- absorptivity, 20
- adaxial epidermis, 36
- AGR, 42
- angiosperms, 37

- BDF, 18
- Beer's law, 20
- bifacial leaves, 36
- Bouguer's law, 20
- BRDF, 18
- Brewster's angle, 73
- Brewster's law, 73
- brightness, 18
- BTDF, 18

- carotenoids, 37
- chromaticity coordinates, 60
- coherent component of reflected light, 15
- complex index of refraction, 15
- conductor, 15
- conifers, 37
- cumulative distribution function, 25
- cuticle, 35

- detour effect, 56
- dielectrics, 16
- diffraction, 73

- effective absorption coefficient, 55
- epicuticular wax, 36
- extinction coefficient, 15

- factor of intensification, 56
- ferns, 37
- four-flux theory, 42
- FSM, 61

- generalized plate model, 42
- goniophotometer, 29
- gymnosperms, 37

- Helmholtz Reciprocity Rule, 19
- hue, 29

- importance sampling, 23
- incoherent component of reflected light, 15
- interference, 73
- inversion procedure, 42

- K-M theory, 42

- Lambert's law of absorption, 20
- law of reflection, 16
- law of refraction, 16
- LEAFMOD, 46
- LFMOD1, 44
- LIBERTY, 46
- lightness, 29
- LOPEX, 55
- luminaires, 15
- luster, 29

- Markov chain, 44
- masking effect, 71
- measurement of appearance, 29
- mesophyll, 35
- mesophyll loop, 54
- Mie scattering, 38

- palisade cell, 36
- physically plausible, 19
- pigments, 37
- plate model, 41
- polarization, 73
- probability density function, 23
- Prospect, 42
- Pteridophytes, 37

- radiance, 18
- radiant energy, 18
- radiant intensity, 18
- radiant power, 18, 20
- random walk, 51
- ray geometrical path length, 55
- ray law, 21

Rayleigh scattering, 38
Raytran, 44
reflectance, 18
reflection, 15, 16
reflection haze, 29
refraction, 15
refractive index, 15
refractive-reflective scattering, 38
retroreflection, 38
Russian roulette, 74

SAIL, 42
saturation, 29
scattering probability function, 20
shadowing effect, 71
sieve effect, 56
SLOP, 45
solid angle, 18
spatial distribution of the propagated light, 29
spectral distribution of the propagated light, 29
spectrophotometer, 29
spongy cell, 36

transmission, 15
transmission haze, 29
transmittance, 18

unifacial leaves, 36

veinlet, 72
venation system, 71

W-S theory, 38
warping, 23
warping functions, 25